PHOTOCHEMICAL REACTION OF RENIERAMYCINS AND EVALUATION OF CYTOTOXICITY
AGAINST LUNG CANCER CELLS

Miss Suwimon Sinsook

จุฬาลงกรณ์มหาวิทยาลัย
CHULALONGKORN UNIVERSITY

A Thesis Submitted in Partial Fulfillment of the Requirements
for the Degree of Master of Science in Pharmaceutical Sciences and Technology
FACULTY OF PHARMACEUTICAL SCIENCES
Chulalongkorn University
Academic Year 2022

ปฏิกิริยาเคมีแสงของเรนิอีราไมซินและการประเมินความเป็นพิษต่อเซลล์มะเร็งปอด

น.ส.สุวิมล สินสุข

Thesis Title	PHOTOCHEMICAL REACTION OF RENIERAMYCINS AND EVALUATION OF CYTOTOXICITY AGAINST LUNG CANCER CELLS
By	Miss Suwimon Sinsook
Field of Study	Pharmaceutical Sciences and Technology
Thesis Advisor	Associate Professor SUPAKARN CHAMNI, Ph.D.

Accepted by the FACULTY OF PHARMACEUTICAL SCIENCES, Chulalongkorn University in Partial Fulfillment of the Requirement for the Master of Science

.... Dean of the FACULTY OF
PHARMACEUTICAL SCIENCES
(Professor PORNANONG ARAMWIT, Ph.D.)

THESIS COMMITTEE

.... Chairman
(Associate Professor BOONCHOO SRITULARAK, Ph.D.)

.... Thesis Advisor
(Associate Professor SUPAKARN CHAMNI, Ph.D.)

.... Examiner
(Associate Professor CHATCHAI CHAOTHAM, Ph.D.)

.... External Examiner
(KORNVIKA CHARUPANT, Ph.D.)

สุวิมล สินสุข : ปฏิกิริยาเคมีแสงของเรนิอีราไมซินและการประเมินความเป็นพิษต่อเซลล์มะเร็งปอด. (PHOTOCHEMICAL REACTION OF RENIERAMYCINS AND EVALUATION OF CYTOTOXICITY AGAINST LUNG CANCER CELLS) อ.ที่ปรึกษาหลัก : รศ. ดร.ศุภกาญจน์ ชำนิ

มะเร็งปอดเป็นสาเหตุของการเสียชีวิตมากกว่ามะเร็งชนิดอื่น ๆ ซึ่งผู้ป่วยมะเร็งปอดโดยส่วนใหญ่จะพบมะเร็งปอดชนิด เซลล์ไม่เล็ก (NSCLC) มะเร็งปอดเป็นโรคที่รักษายากเนื่องจากปัญหาการดื้อยา ดังนั้น ในปัจจุบันจึงมีความต้องการยาต้านมะเร็ง ปอดที่มีประสิทธิภาพพร้อมความปลอดภัยและเข้าถึงได้ง่าย Ecteinascidin 743 (Trabectedin หรือ Yondelis®) มีโครงสร้างที่ จัดอยู่ในกลุ่มเตตราไฮโดรไอโซควิโนลีนอัลคาลอยด์ที่ได้จากสิ่งมีชีวิตทางทะเล เป็นยาที่ได้รับการอนุมัติสำหรับการรักษาโรคมะเร็ง ปอดในมนุษย์ ในงานวิจัยนี้จึงศึกษากระบวนการกึ่งสังเคราะห์ของสารอนุพันธ์เรนิอีราไมซินชนิดใหม่ ๆ ให้มีโครงสร้างของคาร์บอน ตำแหน่งที่ 7, 8 และ 22 คล้ายกับยาดังกล่าว เพื่อการค้นพบและพัฒนาสารที่มีฤทธิ์เป็นพิษต่อเซลล์มะเร็งปอดชนิดเซลล์ไม่เล็ก กลุ่ม สารเรนิอีราไมซินสามารถแยกได้จาก *Xestospongia* sp. ซึ่งเป็นฟองน้ำสีน้ำเงินที่พบบริเวณเกาะสีชัง จังหวัดชลบุรี ประเทศไทย โดยมีเรนิอีราไมซิน เอ็ม เป็นอัลคาลอยด์หลักที่สกัดได้ และมีโครงสร้างหลักเป็นบิสเตตราไฮโดรไอโซควิโนลีนควิโนน โดยพบว่าเรนิอี ราไมซิน เอ็ม แสดงความเป็นพิษต่อเซลล์มะเร็งปอดชนิดเซลล์ไม่เล็ก ดังนั้นจึงทำการศึกษาการปรับเปลี่ยนโครงสร้างโดยเน้นที่การ ดัดแปลงของหมู่แทนที่คาร์บอนตำแหน่ง 7 และ 8 ของเรนิอีราไมซินจากธรรมชาติ คือ เรนิอีราไมซิน เอ็ม, เอ็น, และโอ ด้วย ปฏิกิริยาเคมีแสง ร่วมกับการศึกษาสภาวะการเกิดปฏิกิริยาภายใต้แหล่งกำเนิดแสง และตัวทำละลายต่าง ๆ ที่ให้ผลผลิตของหมู่ [1,3]-dioxole ที่คาร์บอนตำแหน่ง 7, 8 สูงที่สุด จากการทดลองพบว่าปฏิกิริยาที่ใช้แสงสีฟ้าในไดคลอโรมีเทนให้ร้อยละผลผลิตที่ดี ที่สุด ภายใต้ปฏิกิริยาเคมีแสงที่พัฒนาขึ้นนี้เรนิอีราไมซิน เอ็ม ให้ผลิตภัณฑ์เป็นเรนิอีราไมซิน ที และเรนิอีราไมซิน เอ็น และโอ ให้ ผลิตภัณฑ์เป็นเรนิอีราไมซิน ยู ซึ่งผลจากปฏิกิริยาเคมีแสงสนับสนุนการเปลี่ยนแปลงโครงสร้างทางเคมีของสารเรนิอีราไมซินตาม ธรรมชาติภายใต้สิ่งแวดล้อมใต้ทะเลที่แสงแดดส่องถึง นอกจากนี้ได้มีกระบวนการกึ่งสังเคราะห์อนุพันธ์เอสเทอของเรนิอีราไมซินที่มี หมู่ 4'-ไพริดีนคาร์บอนิลที่คาร์บอนตำแหน่ง 22 โดยใช้ปฏิกิริยาเอสเทอริฟิเคชัน และอนุพันธ์ใหม่ที่ได้จากปฏิกิริยาจากแสงและเอ สเทอริฟิเคชันที่มีทั้งหมู่ [1,3]-dioxole ที่คาร์บอนตำแหน่ง 7 และ 8 และ 4'-ไพริดีนคาร์บอนิลที่คาร์บอนตำแหน่ง 22 ในโครงสร้าง สารเรนิอีราไมซินจากธรรมชาติและอนุพันธ์ที่เตรียมได้รวมทั้งสิ้น 10 สาร ได้ถูกนำไปทดสอบฤทธิ์ความเป็นพิษต่อเซลล์มะเร็งปอด ชนิดเซลล์ไม่เล็ก ชนิด H292 และ H460 พบว่า อนุพันธ์ 22-*O*-(4'-pyridinecarbonyl) jorunnamycin A แสดงค่า IC_{50} ที่ 3.52 ± 0.62 µM และ 3.98 ± 0.38 µM เมื่อเทียบกับเซลล์ H292 และ H460 ตามลำดับ ซึ่งแสดงความเป็นพิษต่อเซลล์ได้ดีกว่าเรนิอีราไม ซิน เอ็ม ที่เป็นสารตั้งต้น 10 และ 8 เท่าตามลำดับ และอนุพันธ์ 22-*O*-(4'-pyridinecarbonyl) renieramycin T แสดงค่า IC_{50} ที่ 1.27 ± 0.20 µM และ 1.83 ± 0.83 µM เมื่อเทียบกับเซลล์ H292 และ H460 ตามลำดับ ซึ่งแสดงความเป็นพิษต่อเซลล์ได้ดีกว่ายา ต้านมะเร็งซิสพลาตินที่เป็นตัวควบคุมเชิงบวก 2 และ 3 เท่า ตามลำดับ ดังนั้น อนุพันธ์ใหม่ของสารเรนิอีราไมซินจึงเป็นที่น่าสนใจ เพื่อพัฒนาต่อไปเป็นสารต้านมะเร็งปอดในอนาคต

สาขาวิชา	เภสัชศาสตร์และเทคโนโลยี	ลายมือชื่อนิสิต ....
ปีการศึกษา	2565	ลายมือชื่อ อ.ที่ปรึกษาหลัก ....

6370009933 : MAJOR PHARMACEUTICAL SCIENCES AND TECHNOLOGY

KEYWORD: Xestospongia sp.; marine sponge; renieramycins; semi-synthesis; photochemical reaction; anti-cancer; non-small cell lung cancer (NSCLC)

Suwimon Sinsook : PHOTOCHEMICAL REACTION OF RENIERAMYCINS AND EVALUATION OF CYTOTOXICITY AGAINST LUNG CANCER CELLS. Advisor: Assoc. Prof. SUPAKARN CHAMNI, Ph.D.

Lung cancer causes more deaths than any other type of cancers, with the majority of patients diagnosed with non-small cell lung cancer (NSCLC). Lung cancer is a difficult disease to treat because of the drug resistant problem. Therefore, there is an immediate need for effective, safe, and easily accessible anti-lung cancer drug. Ecteinascidin 743 (Trabectedin or Yondelis®), a marine-derived tetrahydroisoquinoline alkaloid, is an approved drug for treating human lung cancer. This research was studied on the semi-syntheses of new renieramycins derivatives with similar structures to above drug for discovery and development of potent NSCLC cytotoxic agents. Renieramycins was extracted from *Xestospongia* sp., a blue sponge found at the vicinity of Si-Chang island, Chonburi, Thailand. Renieramycin M was reported as a major alkaloid possessing a bis-tetrahydroisoquinolinequinone as core structure. Regarding the previous report, renieramycin M shows cytotoxicity against NSCLC. Thus, structural modifications focusing on the transformation of substituents at carbon positions 7 and 8 of natural renieramycins including renieramycin M, N, and O were performed by photochemical reaction in conjugation with the reaction optimizations using various light sources and solvents to obtain the [1,3]-dioxole group at carbon positions 7 and 8, efficiently. The result showed that the photochemical reaction with blue light in dichloromethane furnished the highest yield. Under this optimized photochemical reaction, renieramycin M transformed to renieramycin T and renieramycin N and O produced renieramycin U. The results of photochemical reaction support chemical transformations of natural renieramycins under the ocean with sunlight exposure. Furthermore, semi-syntheses of the ester derivatives of renieranycins containing a 4'-pyridinecarbonyl substituent at carbon position 22, using an esterification reaction and new derivatives from the sequential esterification and photochemical reaction containing both 4'-pyridinecarbonyl substituent at carbon position 22 and [1,3]-dioxole group at carbon positions 7 and 8 were conducted. The series of natural renieramycins and derivatives totally 10 compounds were evaluated their cytotoxicity against H292 and H460 NSCLC cell lines. As the results, *22-O-*(4'-pyridinecarbonyl) jorunnamycin A exhibited IC_{50} at 3.52 ± 0.62 μM and 3.98 ± 0.38 μM against H292 and H460, respectively with 10 and 8 folds more potent than that of renieramycin M, mother compound. Besides, *22-O-*(4'-pyridinecarbonyl) renieramycin T showed IC_{50} at 1.27 ± 0.20 μM and 1.83 ± 0.83 μM against H292 and H460, respectively with 2 and 3 folds more potent than that of Cisplatin, a first-line chemotherapeutic drug. Hence, these new renieramycins derivatives are the promising candidates for further development an anti-lung cancer agent.

| Field of Study: | Pharmaceutical Sciences and Technology | Student's Signature .... |
| Academic Year: | 2022 | Advisor's Signature .... |

ACKNOWLEDGEMENTS

TABLE OF CONTENTS

LIST OF TABLES

LIST OF FIGURES

จุฬาลงกรณ์มหาวิทยาลัย

CHULALONGKORN UNIVERSITY

LIST OF ABBREVATIONS

NSCLC	Non-small-cell lung cancer
SCLC	Small cell lung cancer
CSCs	Cancer stem cells
H292	Human non-small-cell lung cancer cell line
H460	Human non-small-cell lung cancer cell line
QG56	Human lung carcinoma cell line
NCI-H460	Human lung carcinoma cell line
HCT116	Human colon carcinoma cell line
DLD1	Human colon carcinoma cell line
T47D	Human breast cancer cell line
MDA-MB-435	Human breast carcinoma cell line
AsPC1	Human pancreatic adenocarcinoma cell line
DU145	Human prostate carcinoma cell line
DNA	Deoxyribonucleic acid
EMT	Epithelial-mesenchymal transition
Mcl-1	Myeloid cell leukemia 1
Bcl-2	B-cell lymphoma 2
Sox2	SRY-Box Transcription Factor 2
STAT3	Signal transducer and activator of transcription 3
Nrf2	Nuclear factor erythroid 2-related factor 2
B16F10	Murine melanoma cell line
CD133^{+}	Prominin-1
GSK-3β	Glycogen synthase kinase-3 beta
ERK1/2	Extracellular signal-regulated protein kinases 1 and 2
MEK1	Mitogen-activated protein kinase

FAK/Akt	Focal adhesion kinase/serine-threonine protein kinase
AKT/c-Myc	Serine-threonine protein kinase/cellular myelocytomatosis oncogene
Nanog	Homeobox protein NANOG
Oct4	Octamer-binding transcription factor 4
MTT	3-(4,5-dimethylthiazol-2-yl)-2,5-diphenyltetrazolium bromide
DMSO	Dimethyl sulfoxide
RPMI	Roswell park memorial institute
FBS	Fetal bovine serum
IC_{50}	Half maximal inhibitory concentration
SD	Standard deviation
SAR	Structure-activity relationship
HAT	Hydrogen atom transfer
EtOAc	Ethyl acetate
DMAP	4-dimethylaminopyridine
EDCI	1-(3-dimethylamino- propyl)-3-ethylcarbodiimide hydrochloride
H_2	Hydrogen gas
Pd/C	Palladium on carbon
CH_2BrCl	Bromochloromethane
Cs_2CO_3	Cesium carbonate
DMF	Dimethylformamide
CH_2Cl_2	Dichloromethane
$CHCl_3$	Chloroform
THF	Tetrahydrofuran
WHO	World Health Organization
TLC	Thin-layer chromatography
UV	Ultraviolet
LED	Light emitting diode

VEGF	Vascular endothelial growth factor
OCH_2O	Methylenedioxy
$CDCl_3$	Deuterated chloroform
NMR	Nuclear magnetic resonance
^{1}H-NMR	Proton-1 nuclear magnetic resonance
^{13}C-NMR	Carbon-13 nuclear magnetic resonance
COSY	Homonuclear correlation spectroscopy
HSQC	Heteronuclear single quantum coherence spectroscopy
HMBCs	Heteronuclear multiple bond correlations spectroscopy
CD	Circular Dichroism
IR	Infrared
HR-MS	High-resolution mass spectrometry
HRESIMS	High resolution electrospray ionisation mass spectrometry
ECD	Electronic circular dichroism
δ	Chemical shift in NMR data
J	J-coupling in NMR data
C	Concentration
s	Singlet in NMR data
d	Doublet in NMR data
t	Triplet in NMR data
m	Multiplet in NMR data
dd	Doublet of doublet in NMR data
ddd	Doublet of doublet of doublet in NMR data
dq	Doublet of quartet in NMR data
dt	Doublet of triplet in NMR data
br	Broad in NMR data
qq	Quartet of quartet in NMR data

CHAPTER I

INTRODUCTION

1.1 Background and Rational

Bisisoquinolinequinone marine alkaloids, including renieramycins, saframycins, ecteinascidins, and jorunnamycins, have been identified as highly effective anticancer agents[1, 2]. Ecteinascidin 743, alternatively referred to as trabectedin, is a compound derived from the Caribbean tunicate, *Ecteinascidia turbinata*. In 2015, the United States Food and Drug Administration granted approval for its application in the treatment of advanced soft tissue sarcoma and ovarian carcinoma. Lurbinectedin (PM01183), a bistetrahydroisoquinoline analog, received approval in 2020 for the second-line treatment of metastatic small-cell lung cancer. Both trabectedin and lurbinectedin **(Figure 1)** action through the same mechanism involving DNA-binding interactions, specifically targeting the N2 position of guanine within the DNA minor groove leading to double-strand breaks[3-6]. Consequently, both compounds trigger apoptosis through the induction of double-strand breaks in the DNA[7, 8].
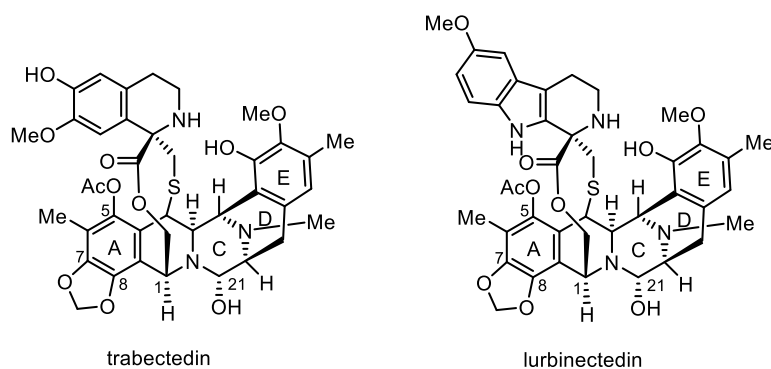
Figure 1 The structures of bistetrahydroisoquinoline natural products

Renieramycins, a group of compounds exhibiting structural similarities to trabectedin, were initially isolated from a variety of marine sponges including the genera *Reniera*[9, 10], *Cribrochalina*[11], and *Xestospongia*[12, 13]. Renieramycins belong to the bistetrahydroisoquinolinequinone family. Notably, they contain an angelate ester at the position 22. These marine alkaloids exhibit significant bioactivities encompassing antimicrobial[9] and antileishmanial[14] properties, in addition to anticancer activities[12, 13, 15-17]. Renieramycin M (**1**), N (**2**) and O (**3**) were successfully isolated in gram-scale quantities from the Thai sponge species, *Xestospongia* sp., located in the Si-Chang Island of Thailand **(Figure 2)**[13]. Renieramycin M demonstrates cytotoxicity against an array of human cancer cell lines, including colon carcinoma (HCT116 and DLD1), lung carcinoma (QG56 and NCI-H460), pancreatic adenocarcinoma (AsPC1), and ductal breast epithelial tumor (T47D)[12, 13, 15]. Moreover, renieramycin T (**4**) and U (**5**) were isolated from *Xestospongia* sp.[15], a renieramycin-ecteinascidin hybrid marine natural alkaloid, contains a [1,3]-dioxole ring fusing to the left-side carbon framework (ring A) of renieramycin, which is similar to the structure of trabectedin. Compounds **4** and **5** exhibited robust *in vitro* anticancer activity, specifically in non-small-cell lung carcinoma (NSCLC)[15]. Bistetrahydro isoquinolinequinone alkaloids have been reported to exert their cytotoxic mechanisms on non-small-cell lung carcinoma (NSCLC) cells through a variety of pathways. These include the sensitization of cells resistant to anoikis[18], the modulation of lung cancer stem cell (CSC) markers[19-21], and the suppression of the

epithelial-mesenchymal transition (EMT)[22]. Additionally, these alkaloids induce

apoptosis in lung cancer cells through several mechanisms involving degradation of

the myeloid cell leukemia 1 (Mcl-1) protein[23], p53-dependent pathways[24, 25], and

mitochondria-dependent pathways[26].
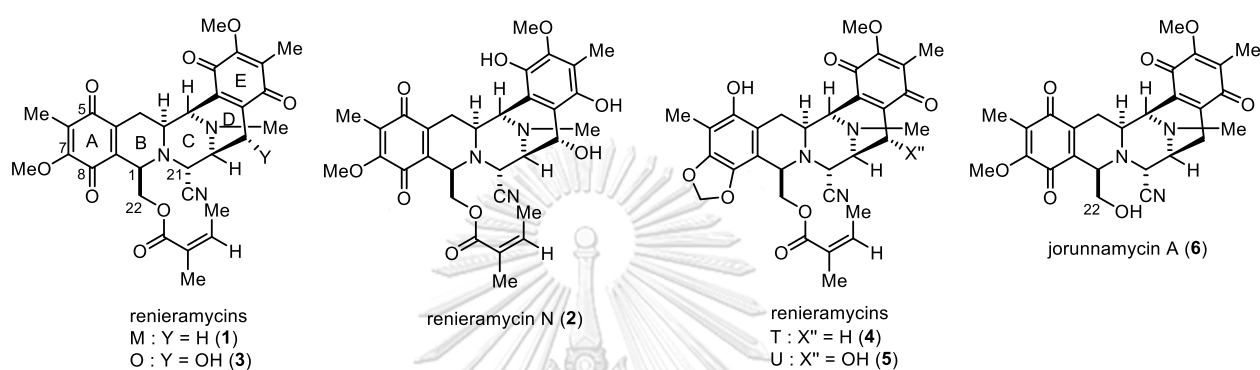
Figure 2 The structures of natural tetrahydroisoquinolinequinone

Based on literature relating to the structural modification of renieramycins, it

has been found that the presence of a leaving group, such as hydroxyl group (—OH)

and cyanoyl group (—CN), at the C-21 position is pivotal for the cytotoxicity[27].

Furthermore, the structure-activity relationship (SAR) study on renieramycin focusing

on side chain modification has shown that the introduction of a nitrogen-heterocyclic

ester, such as a 4'-pyridinecarbonyl ester, can significantly improve cytotoxicity

(Figure 3). In alignment with our previous investigations into side chains at the C-22

position, the semi-synthetic derivatives of jorunnamycin A (**6**), possessing a 4'-

pyridinecarbonyl ester group (**7**), displayed enhanced cytotoxicity relative to their

parent compounds against human colon carcinoma (HCT116), breast carcinoma

(MDA-MB-435), and human NSCLC (H292 and H460) cell lines[28, 29]. In addition, the

incorporation of a 4'-pyridinecarbonyl ester at the C-5 position has been achieved through the modification of hydroquinone 5-*O*-(4'-pyridinecarbonyl) of renieramycin M (**8**), derived from natural **1** via a two-step hydrogenation and selective esterification process. Compound **8** was observed to demonstrate inhibitory effects on NSCLC cell lines, with IC_{50} values in the nanomolar range[16]. Moreover, modifications to the ecteinascidin-renieramycin hybrid have been conducted on the left-hand system (A ring) by transforming the *p*-quinoline of **1** into a methylenedioxy-bridged phenol of **4** via an ambient light-induced intramolecular photoredox reaction[30].

22-*O*-(4'-pyridinecarbonyl)
jorunnamycin A (**7**)

hydroquinone 5-*O*-(4'-pyridinecarbonyl)
renieramycin M (**8**)
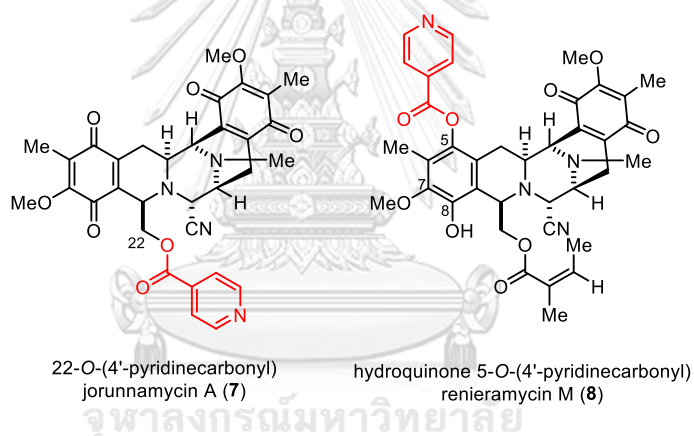
Figure 3 The structures of 4'-pyridinecarbonyl ester derivatives of renieramycins

In order to gain insights into the structure-activity relationship (SAR) of renieramycin-ecteinascidin hybrid compounds, this study aimed to investigate suitable conditions for the photochemical reaction to construct [1,3]-dioxole ring fusing to the left-side carbon framework (ring A) of renieramycin in conjugation with developing the 4'-pyridinecarbonyl substituted derivatives of renieramycin-type derivatives. These derivatives hold promise for potential drug development

endeavors. The semi-syntheses of renieramycin-type derivatives involved photochemical reactions and esterification, starting from natural compounds **1** or **6**. Subsequently, the *in vitro* cytotoxicity against NSCLC H292 and H460 cell lines was evaluated using the 3-(4,5-dimethylthiazol-2-yl)-2,5-diphenyltetrazolium bromide (MTT) assay.

1.2 Objectives of Study

1. To study photochemical reactions for the modification of renieramycins.

2. To evaluate cytotoxicity of renieramycins derivatives against the non-small-cell lung cancer cells.

1.3 Hypothesis of Study

1. Derivatives of renieramycins containing [1,3]-dioxole groups can be synthesized by photochemical reactions of renieramycins.

2. Derivatives of renieramycins containing [1,3]-dioxole groups show potent cytotoxicity against the non-small-cell lung cancer cells.

1.4 Benefits of Study

1. The photochemical reactions that can modify the structure of renieramycins.

2. New derivatives of renieramycins show cytotoxicity against non-small-cell lung cancer cells.

1.5 Research Design

```
┌─────────────────────────────────────────────────────┐
│      1. Structural modifications of renieramycins     │
└─────────────────────────────────────────────────────┘
                          │
                          ▼
┌─────────────────────────────────────────────────────┐
│  (a) Photochemical reaction at carbon positions 7 and 8 │
│  (b) Esterification at carbon positions 5 or 22       │
└─────────────────────────────────────────────────────┘
            │                              │
            ▼                              ▼
┌─────────────────────┐        ┌─────────────────────────┐
│ Natural renieramycins│        │ Renieramycins derivatives│
└─────────────────────┘        └─────────────────────────┘
            │                              │
            └──────────────┬───────────────┘
                           ▼
        ┌─────────────────────────────────────┐
        │  Purification by column chromatography │
        └─────────────────────────────────────┘
                           │
                           ▼
```

Structure determination by ^{1}H-NMR, ^{13}C-NMR

High-resolution mass spectroscopic methods

2. Cytotoxic evaluation of renieramycins derivatives

MTT assay: non-small-cell lung cancer

(NSCLC) cell lines H292 and H460

Evaluation of Inhibitory Concentration (IC$_{50}$)

Figure 4 Research design

CHAPTER II

LITERATURE REVIEW

2.1 Natural Source of Renieramycins

Renieramycins belong to the tetrahydoisoquinolinequinone marine alkaloid family that was isolated from the Thai blue sponge (*Xestospongia* sp.). The blue sponge is classified in phylum Porifera, kingdom Animalia, that found in the ocean around Thailand, Philippines, Australia, Indonesia, Malaysia[31]. In Thailand, *Xestospongia* sp. was observed at Si-Chang island, the Gulf of Thailand and the Andaman Sea. The blue sponge habitat is generally relied on the adhesion of the rock, sand, and coral reefs[13]. It has been reported that when the sponge has wound, renieramycins is produced as the secondary metabolites at the high concentrations[32]. The blue sea sponge (*Xestospongia* sp.) is the food for the nudibranch (*Jorunna funebris*). After digestion, renieramycins are detected in various nudibranch's organs such as the mantle tissue and foot muscles[32]. Renieramycin M (**1**) is the major alkaloid isolated from the sponge *Xestospongia* sp. (**Figure 5**). The structure of this compound consists of the two units of tetrahydroisoquinoline-quinone. This compound exhibited potent cytotoxicity against several human cancer cell lines including breast cancer, colon cancer, lung cancer, pancreatic cancer and prostate cancer[16]. Therefore, compound **1** plays a key role as drug lead and serves as a chemical template for structure-activity relationship studies in both chemistry and pharmacology aspects.

The macroscopic characterizations of the blue sea sponge include bluish-gray color when it alive, clumpy surface, small many porous, thick body, oval oxeas, and many open tubular oscula[13].

Xestospongia sp.[33]
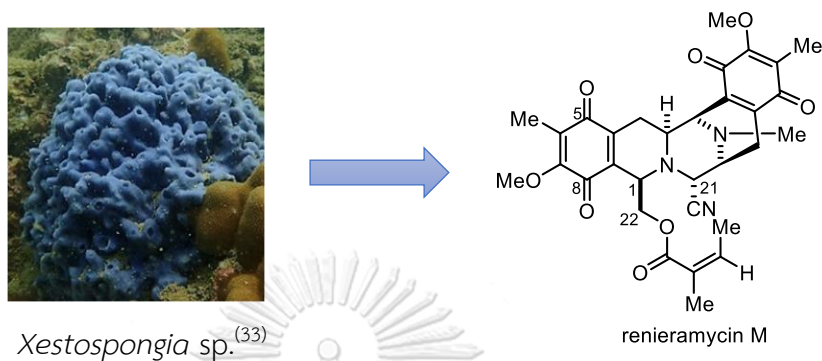
renieramycin M

Figure 5 Thai blue sponge (*Xestospongia* sp.) and structure of renieramycin M

2.2 Chemical Structure of Renieramycins

The core chemical structure of renieramycins is a bistetrahydroisoquinoline-quinone including 5 rings. The ring A and ring B are a tetrahydroisoquinolinequinone unit, as same as ring D and ring E. These two units are connected by ring C, which is a six membered heterocycle. Structure of renieramycin A-Y were reported and classified based on their characteristic structures at ring A, B, D and E involving tetrahydroisoquinoline, tetrahydroisoquinolinequinone, and hydroquinone **(Figure 6)**[1]. In general, ring A and ring E have quinone moiety, which is a reactive functional group prone to the reduction. The carbon at position 22 has an ester substituent called the angelate group.
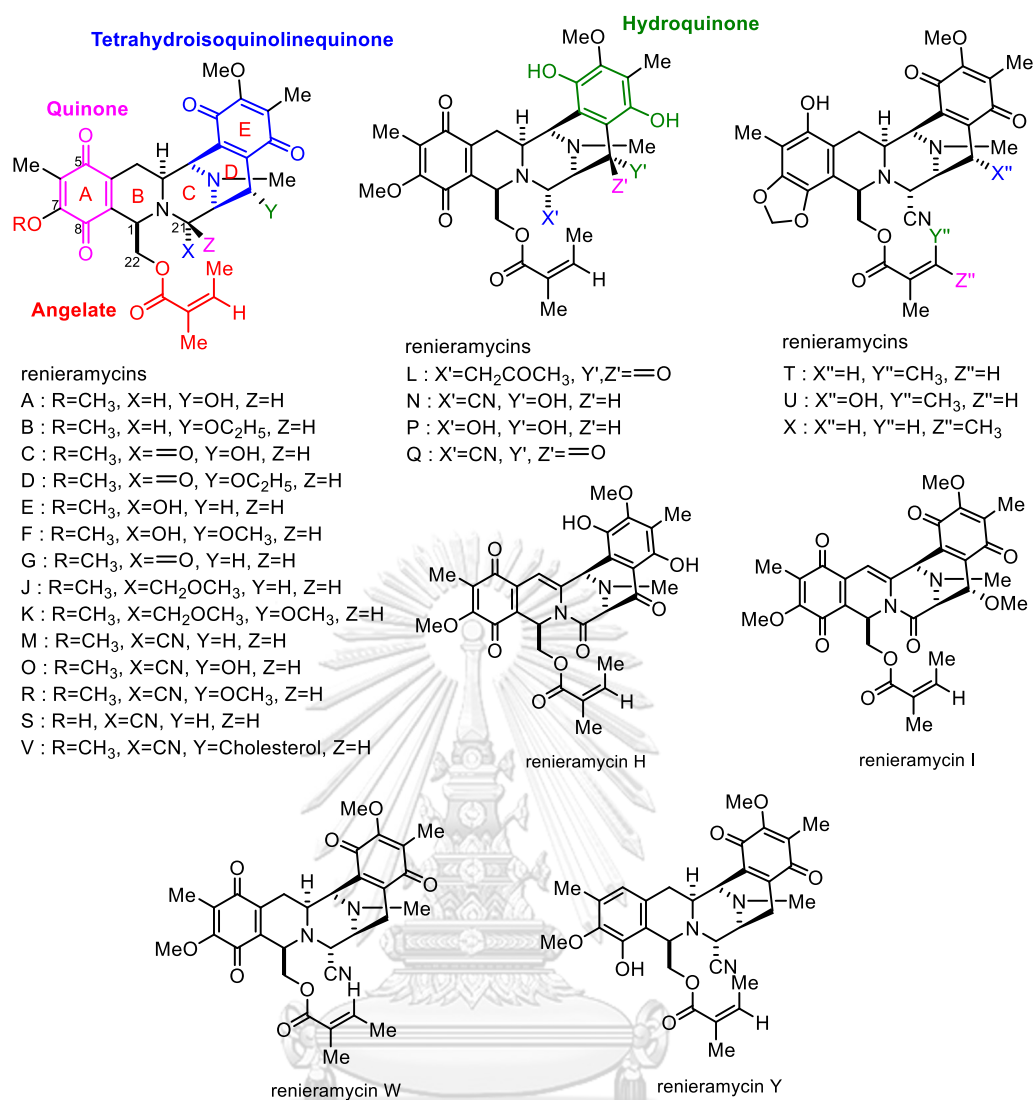
Figure 6 Structure of renieramycins[1]

2.3 Chemical Modification of Renieramycin M

Renieramycins show structurally similar to saframycins and ecteinascidin 743, which is the approved anticancer drug[33]. The distinct differences between the chemical structures of renieramycins and ecteinascidin-743 are a [1,3]-dioxole ring at carbon positions 7 and 8 along with substituent at carbon positions 21 and 22 **(Figure 7)**. The carbon at position 1 of ecteinascidin 743 contains cyclic ester, while renieramycins has liner ester as an angelate group. Besides, the carbon at position 5

of ecteinascidin 743 comprises of acetyl ester group, whereas renieramycins has quinone group. The modification of renieramycin M were reported with the improvement of cytotoxic potency against several cancer cell lines[29, 34]. The transformation involved the elimination of angelate ester to deliver the hydroxyl group (—OH) of primary alcohol at the carbon position 22 and reinstalled the newly additional ester by esterification with corresponding carboxylic acid, acid chloride, and acid anhydride (Figure 8)[27]. On the other option, reduction of a quinone group on rings A and E to obtain hydroquinone followed by esterification was recently reported[16]. Interestingly, the renieramycin M derivatives having 4'-pyridinecarbonyl group at the carbon position 22 and acetyl and *n*-propanoyl groups at the carbon position 5 (Table 1) displayed the stronger cytotoxicity than that of renieramycin M (1) against the H292 and H460 non-small-cell lung cancer cell lines[16, 29]. Moreover, at carbon position 21, ecteinascidin 743 has hydroxyl group while renieramycin M (1) has cyanide group. The carbon at position 21 can form carbinolamine, which is the point of DNA alkylation[15, 27]. The cyanide group at carbon position 21 of renieramycin M (1) can be transformed into a hydroxyl group by reacting with silver nitrate via oxidation reactions[27].
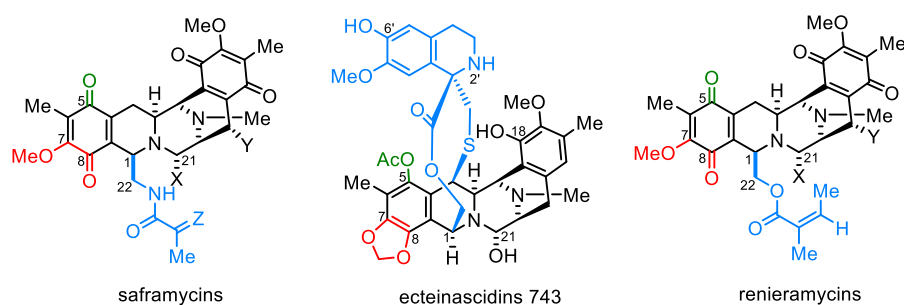
Figure 7 Structural comparison of saframycins, ecteinascidin 743 and renieramycins[1]
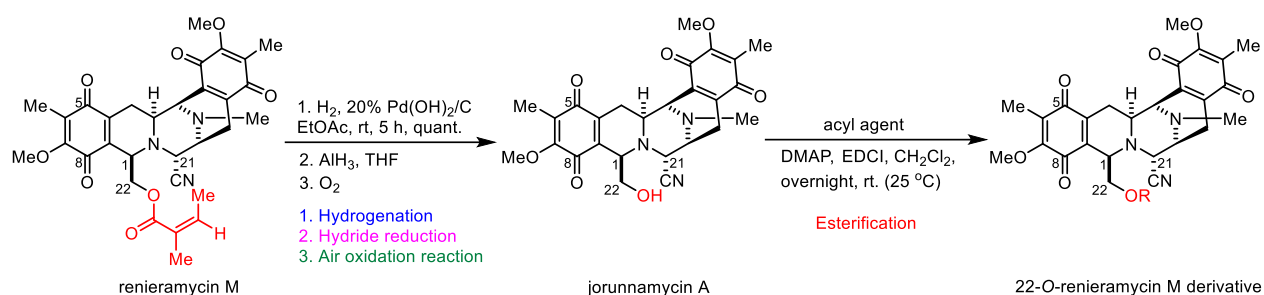
Figure 8 Semi-synthesis of renieramycins derivative from renieramycin M[27]

Table 1 Cytotoxicity of potent renieramycin M derivatives against H292 and H460 non-small-cell lung cancer cell lines[16, 29]

Structure	Cytotoxicity IC$_{50}$ ± SD (nM)		Structure	Cytotoxicity IC$_{50}$ ± SD (nM)	
	H292	H460		H292	H460
1. renieramycin M	24 ± 1	6.5 ± 0.4	2. 22-*O*-(4'-pyridinecarbonyl) renieramycin M	1.1 ± 0.1	1.6 ± 0.3
3. hydroquinone 5-*O*-(acetyl) renieramycin M	3.0 ± 0.6	3.6 ± 0.4	4. hydroquinone 5-*O*-(*n*-propanol) renieramycin M	2.3 ± 0.4	5.1 ± 0.5

Therefore, it is interesting to modify the renieramycin M (**1**) structure to contain the [1,3]-dioxole ring by using specific reaction such as photochemical reaction, which was recently reported **(Figure 9)**[35, 36]. The synthesis of [1,3]-dioxole

was succeeded by using the photo-induced ring-closing reaction. The photochemical reaction and mechanism were revealed and applied to the total synthesis of ecteinascidins and renieramycin T (**4**) marine natural products[35]. Based on the reported data, synthesis of [1,3]-dioxole using the photo-induced ring-closing reaction with one-pot acetylation gave the improved reaction yield **(Figure 9 [1])**[35]. In addition, using tetrahydrofuran (THF) as a solvent under photochemical reaction with blue light showed the optimum yields **(Figure 9 [2] and [3])**[36]. Moreover, the synthesized of ecteinascidin 743 from cyanosafracin B was investigated via intermediate **18**, a quinone compound, that underwent reduction with hydrogenation (under 1 atmosphere of H_2, utilizing Pd/C catalyst). This reduction yielded an unstable hydroquinone, which was subsequently reacted with bromochloromethane (CH_2BrCl) and cesium carbonate (Cs_2CO_3) in the presence of dimethylformamide (DMF) as a solvent. This reaction led to the formation of compound **19**[37], where a [1,3]-dioxole ring was introduced at carbon positions 7 and 8 of ring A. Continuing with investigations, compound **20** was reduced using a Pd/C catalyst (at a concentration of 10%) and immediately treated with a combination of CH_2BrCl and Cs_2CO_3 in DMF. This treatment facilitated the formation of a five-membered ring, producing compound **21** with a yield of 44%[38] **(Figure 10)**.
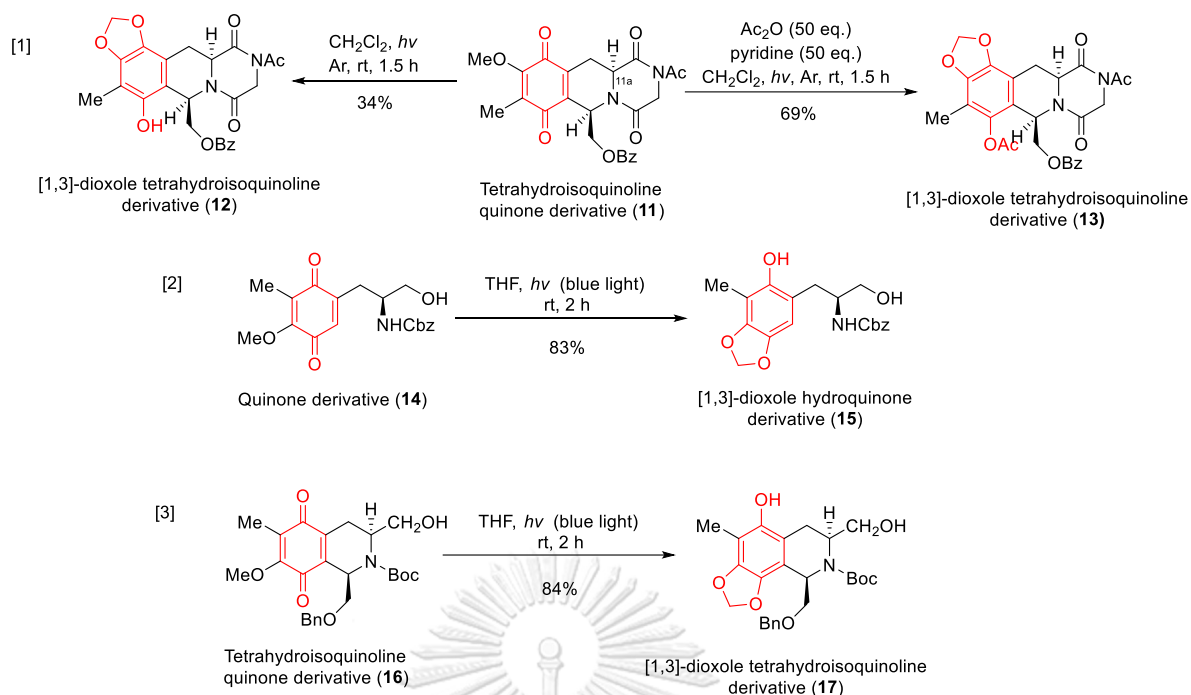
Figure 9 Synthesis of [1,3]-dioxole ring by photo-induced ring-closing reaction of quinone moiety[35, 36]
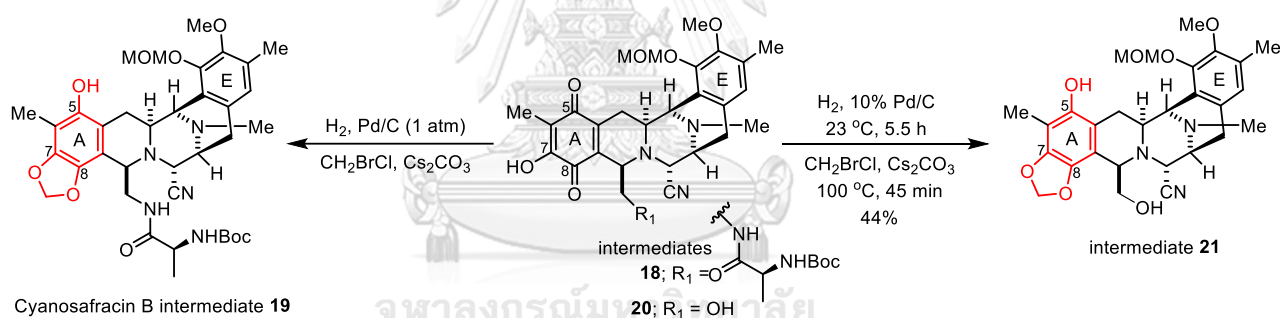
Figure 10 Synthesis of [1,3]-dioxole ring by hydrogenation of the quinone group[37, 38]

Recently, Yokoya and his research team reported on the photoredox reactions of compounds in the 1,2,3,4-tetrahydroisoquinoline group, achieving 5-hydroxy-tetrahydroisoquinol [1,3]-dioxoles in excellent yields[39]. They also investigated the photoredox reactions of natural products such as saframycin A and renieramycin M. The photoredox reaction was successfully employed to convert renieramycin M into renieramycin T in a highly efficient manner **(Figure 11)**. When

renieramycin M was exposed to an 18 W fluorescent light at 25 °C in dichloromethane (CH_2Cl_2) at a concentration of 0.4 mM, around the time of 10 hours, renieramycin T was obtained in a yield of 64%. Additionally, a minor amount of renieramycin S was produced in a yield of 6%. The complete consumption of the starting material necessitated a relatively lengthy reaction time of 10 hours. However, by employing a xenon lamp (300 W), switching to dichloroethane as the solvent, or adjusting the concentration of the starting material to 2 or 4 mM, the reaction time significantly decreased to a range of 3 to 8 hours[39]. This research serves as an exemplary model for investigating favorable conditions to achieve high yields in photoredox reactions and for converting the quinone group into a closed-ring structure, specifically the [1,3]-dioxole ring. It provides valuable insights for future studies in these areas, paving the way for advancements in yield optimization and ring-closing transformations involving quinone compounds.
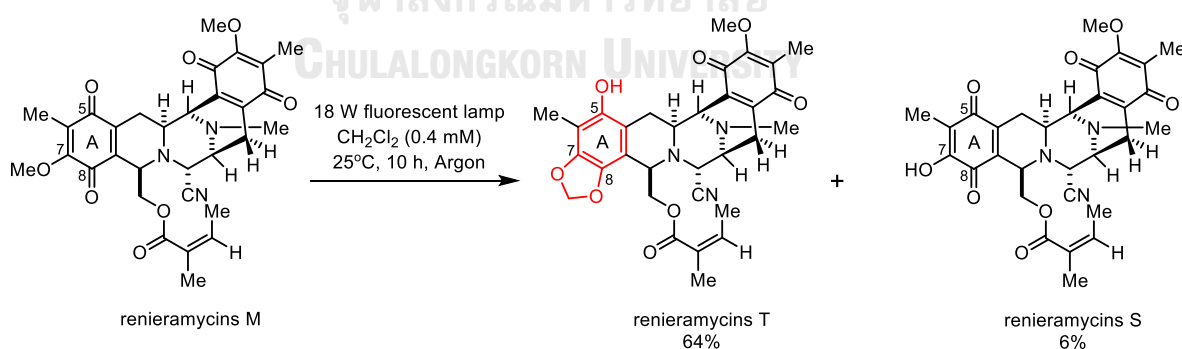
Figure 11 Synthesis of [1,3]-dioxole ring by photoredox reaction of the quinone moiety[39]

2.4 Anticancer Activity of Renieramycins

Renieramycins exhibited cytotoxicity against many types of cancer cells, including colon, lung, prostate, breast, pancreatic, and non-small-cell lung cancers[16]. Renieramycins derivatives were developed as the new anticancer agents regarding DNA damage via free radicals generation from quinone moiety[16]. It was found that renieramycin M caused the death of cancer cells via the necrosis rather than apoptosis pathway, which may result in greater undesirable toxicity of the compound[40]. Measuring with dihydroethidium fluorescence probe specific to free radical species to identify the formation of superoxide anion free radicals causing the death of cancer cells through necrosis pathway. Interestingly, 5-*O*-acetylhydroquinone renieramycin M was found to reduce the necrosis pathway, while continuing to cause cancer cell death via the apoptosis pathway, with the decrease of Bcl-2 and Mcl-1 in the intrinsic pathway[28, 41].

Natural renieramycins from *Xestospongia* sp. showed cytotoxicity against human carcinoma including colon (HCT116, DLD1), lung (QG56, NCI-H460) and prostate (DU145) **(Table 2)**. The most potent cytotoxic agents against these cancer cell lines are renieramycin E, renieramycin N and remieramycin M, respectively. Therefore, it is interesting to use these three compounds as the lead compounds for the structure-activity relationship study[12, 13, 27].

Table 2 Cytotoxicity of renieramycins[12, 13, 27]

Compounds	Human cancer cell line (IC$_{50}$ in µM)				
	Colon carcinoma		Lung carcinoma		Prostate carcinoma
	HCT116	DLD1	QG56	NCI-H460	DU145
Renieramycin O	0.028	n.d.	0.040	n.d.	n.d.
Renieramycin Q	0.059	n.d.	0.071	n.d.	n.d.
Renieramycin R	0.023	n.d.	0.029	n.d.	n.d.
Renieramycin S	0.015	n.d.	0.026	n.d.	n.d.
Renieramycin M	0.0079	0.0096	0.019	0.0059	n.d.
Renieramycin N	0.0056	0.0057	0.011	0.0067	n.d.
Renieramycin E	0.00038	n.d.	0.001	n.d.	0.00038
Renieramycin J	0.73	n.d.	0.51	n.d.	0.37

n.d. refers to not determined.

Renieramycin M was modified into a variety of new derivatives, which were of significant biological activity at carbon positions 5 and 22, with both positions being studied with the alkyl, aromatic, heterocyclic, and amino groups[16, 33]. Furthermore, it was found that 22-*O*-(*N*-Boc-L-glycine) ester of renieramycin M obstructed the migration and invasion processes in human lung cancer cells by restraining the FAK/Akt-mediated signal, which subsequently led to the inhibition of the epithelial-to-mesenchymal transition (EMT)[22]. Moreover, hydroquinone 5-*O*-cinnamoyl ester of renieramycin M impeded cancer stem cells (CSCs) in H460 cells by obstructing the AKT/c-Myc signaling pathway leading to a decrease in the expression of the stem cell

transcription factors, namely Nanog, Oct4, and Sox2. Besides, it also inhibited the Akt-

regulated c-Myc pathway in other types of lung cancer cells[42] **(Figure 12)**.
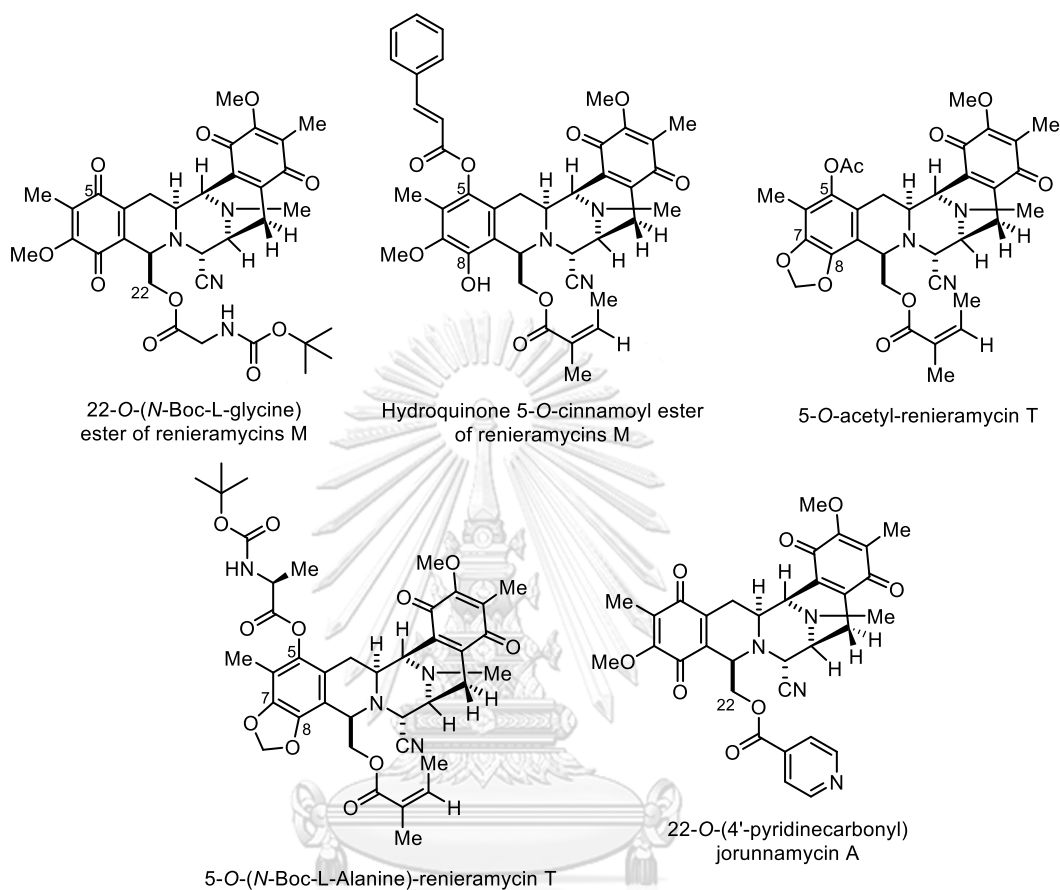
Figure 12 The chemical structures of renieramycin M and renieramycin T derivatives [20-22, 42]

Renieramycin T, a renieramycin-ecteinascidin hybrid compound primarily

targeted and harmed lung cancer cells, leaving normal lung epithelial cells mostly

unaffected. It expedites the breakdown of the Mcl-1, a known protein to regulate the

survival and advancement of cancer[17]. Then, an inflammation-related tumor model

was created by using the supernatant of RAW264.7 cells to stimulate B16F10 mouse

melanoma cells. Renieramycin T was found to inhibit the adhesion of B16F10 cells to

fibronectin-coated substrate, as well as their migration and invasion through the Matrigel in dose dependent manner[43]. Moreover, renieramycin T diminished the phosphorylation of STAT3 and reduced the expression of Nrf2, causing the inhibition of the migration and invasion of B16F10 cancer cells[43]. In addition, renieramycin T was synthesized into various new derivatives with ester substituents at carbon position 5 **(Figure 12)**. The series of renieramycin T derivatives showed to trigger apoptosis and reduce the expression of cancer stem cell (CSC) markers in H292 cells. 5-*O*-acetyl renieramycin T enhanced cisplatin-induced apoptosis and reduced the count of cisplatin-induced CD133$^+$ cells[20]. This compelling evidence suggests that 5-*O*-acetyl renieramycin T could be a potential contender as a sensitizer in cancer chemotherapy, potentially diminishing resistance and inhibiting tumor growth[20]. Next, 5-*O*-N-Boc-L-alaninoyl renieramycin T exhibited a strong capacity to induce apoptosis and suppress CSCs in lung cancer cells. Furthermore, 5-*O*-N-Boc-L-alaninoyl renieramycin T showed the ability to perform allosteric inhibition of the Akt protein. Given the crucial role Akt plays in cancer cell survival and stemness characteristics, these findings suggest that 5-*O*-N-Boc-L-alaninoyl renieramycin T may hold promise as a potential treatment for CSC and Akt-driven cancers[21].

The study investigating the anticancer effects of jorunnamycin A, a bistetrahydroisoquinolinequinone having free alcohol at carbon position 22, revealed that it specifically suppressed stem-like characteristics in lung CSC-enriched spheroids. This suppression occurred through the inhibition of the GSK-3β/β-catenin

signaling pathway, resulting in the downregulation of key transcription factors, namely Nanog, Oct-4, and Sox2[44]. Moreover, jorunnamycin A demonstrated its anticancer activity by sensitizing CSC-enriched lung cancer cells to cisplatin-induced apoptosis. This sensitization is achieved through the upregulation of the tumor suppressor protein p53 and a decrease in the expression of the anti-apoptotic protein Bcl-2[44]. In addition, the study on the derivatives of jorunnamycin A concerning reveals that the network pharmacology approach was utilized to initially identify the targets of 22-O-(4'-pyridinecarbonyl) jorunnamycin A in NSCLC. The *in-silico* analysis revealed 78 potential targets of 22-O-(4'-pyridinecarbonyl) jorunnamycin A against NSCLC[45]. Given that inadequate apoptotic cell death leads to unsatisfactory clinical outcomes, understanding the underlying mechanisms is crucial for new drug development. Besides, 22-O-(4'-pyridinecarbonyl) jorunnamycin A possessed significant apoptotic-inducing properties. Through a combination of cell-based assays and bioinformatic analysis, ERK1/2 and MEK1 were identified as molecular targets of 22-O-(4'-pyridinecarbonyl) jorunnamycin A, which play a crucial role in mediating apoptosis in NSCLC[45].

2.5 Lung Cancer

2.5.1. Lung Cancer Metastasis

Based on data from the International Agency for Research on Cancer, it was projected that approximately 1.8 million cancer-related deaths and 2.2 million new cancer cases would occur globally across 36 countries in 2020[46]. Lung cancer,

affecting nearly one-quarter of the global population, continues to result in more fatalities than the four leading cancer types including brain, prostate, colorectal, and breast cancers combined. It holds the highest incidence rate (11.7% of total cases) among all cancer types and ranks second in terms of mortality (18% of total cancer deaths) for both men and women[46, 47]. The high mortality rate associated with lung cancer can be attributed to its metastatic nature, with approximately 90% of deaths resulting from the spread of the tumor beyond its original site[48]. Lung cancer is categorized into two main histological classes: non-small cell lung cancer (NSCLC) and small cell lung cancer (constituting approximately 15% of cases). These classes exhibit distinct biological behaviors. NSCLC can be further divided into adenocarcinoma, large cell carcinoma, and squamous cell carcinoma, each with its unique patterns of growth and spread. NSCLC comprises over 80% of all lung cancer cases, especially among patients with advanced or metastatic disease, which generally carries a grim prognosis[49]. Regrettably, a significant portion approximately 57% of lung cancer patients are diagnosed at an advanced stage or with metastasis (stage IV disease), resulting in a low survival rate of only 5% at the 5-year mark following diagnosis[47]. The metastasis of NSCLC is influenced by several factors, including the histological subtype detected at the time of diagnosis, as well as the age and sex of the patient[50]. Metastasis in lung cancer tends to occur frequently in various sites, including the bone, brain, liver, and adrenal gland[51]. Extensive evidence indicates that lung cancer cells possess the ability to survive in hypoxic

conditions, evade immune responses, and migrate from the primary tumor site, ultimately increasing the likelihood of metastasis[52]. Despite significant progress in the development of advanced treatment regimens, there is still no known curative therapy for advanced-stage metastatic lung cancer.

2.5.2. Treatment Options for Lung Cancer and Advanced-stage NSCLC

The management and treatment of clinical cases of lung cancer typically involve a combination of surgery, radiotherapy, chemotherapy, and targeted therapy. These treatment modalities can be administered individually or in combination, and the selection of specific options depends on factors such as the type of cancer cells, the stage of cancer, and the overall performance status of the patient[53]. Surgery is the primary treatment modality for early-stage cancers (stage I and II) and is considered the only curative therapy. Approximately 25% of patients with lung cancer are eligible for surgical resection at the time of diagnosis[54]. For patients with unresectable tumors, radiotherapy is often the treatment of choice. While surgery can be curative for early-stage disease, most patients require additional chemotherapy even after the removal of visible cancerous tissue during surgery. Although surgery and radiotherapy are considered standard options for early-stage NSCLC, the therapeutic effectiveness of radiotherapy is limited for patients with distant metastasis. Presently, one in three NSCLC patients have advanced-stage tumors (stage IV disease) that are not amenable to surgical eradication. For these patients, systemic chemotherapy remains the primary approach for palliative

treatment, aimed at prolonging life and improving quality of life[55, 56]. Chemotherapy serves as the fundamental cornerstone for patients at all stages of NSCLC, ranging from early resectable tumors to advanced metastatic stages, where chemotherapy remains the sole treatment option. The current first-line therapy for stage IV NSCLC patients involves platinum-based chemotherapy as a single cytotoxic agent, resulting in a median survival of 6.5 months. However, combining cisplatin or carboplatin with taxanes or vinca alkaloids in doublet regimens extends survival to around 10 months[57]. Furthermore, combination chemotherapy incorporating targeted therapy such as monoclonal VEGF or pemetrexed has demonstrated an overall survival benefit of up to 12 months. This combination therapy is approved as the first-line treatment for stage IIIB and IV non-squamous NSCLC[58, 59]. Additionally, several approved second-line therapies, including docetaxel (Taxotere), pemetrexed, erlotinib, and gefitinib, have been licensed for the treatment of all types of non-small cell lung cancer. The combination of one of these agents has shown improved tolerability in phase II and randomized clinical trials conducted on patients with metastatic cancer. However, the development of acquired or intrinsic resistance poses limitations to the therapeutic success in cancer patients[60, 61]. In addition, radiation therapy itself can have an impact on cancer cells by potentially inducing distant metastasis, promoting tumor migration, and enhancing the invasive capabilities of the cancer cells[62, 63]. In contrast, NSCLC cells exhibit lower sensitivity to radiation therapy and are less responsive to current treatment modalities

compared to SCLC cells. However, pretreatment with chemotherapy has shown the ability to enhance the sensitivity of cancer cells to radiotherapy, while the use of radiotherapy alone does not significantly impact the median survival rate. The current range of chemotherapeutic drugs for NSCLC does not sufficiently demonstrate cytotoxic agent activity in suppressing migration and invasion associated with metastasis[64]. Despite advancements in the development of advanced treatments, there are still significant challenges in terms of side effects and overall survival rates, particularly when it comes to the poor responses observed with the current standard treatments, except in cases of localized tumors. Therefore, there is an urgent need to develop more effective and better-tolerated chemotherapeutic treatments to address these issues.

2.6 Rationale and Significance

According to the World Health Organization (WHO) in 2018, lung cancer is the major cause of death among other type of cancers[65]. Lung cancer is a disease in which the lung cells are abnormal, may have abnormal functioning, uncontrolled cell proliferation, and may spread the cancer cells to other parts of the body[66]. Lung cancer was classified into two main classes: small cell lung cancer (SCLC), which accounts for 10 to 15% of lung cancer cases, and non-small-cell lung cancer (NSCLC), which accounts for 80 to 85% of lung cancer cases[67]. The cause of lung cancer mainly involves breathing carcinogens from smoking cigarettes and tobacco, asbestos, radon gas, diesel exhaust fumes, and air pollution. Lung cancer especially

non-small-cell lung cancer is a major health problem for people around the world. Importantly, lung cancer is a disease that difficult to cure. Thus, effective treatment with safe and easily accessible is the current need[68].

To date, marine derived tetrahydroisoquinoline alkaloid such as ecteinascidin 743 (Trabectedin or Yondelis®)[69] are approved for lung cancer treatment in human. Therefore, this research work is interested to modify the structure of renieramycins to obtain new derivatives having partial chemical structure similar to ecteinacidin 743 including [1,3]-dioxole ring at ring A using the photochemical reaction and ester side chain at carbon position 22. The obtaining renieramycin-type derivatives were further evaluated their cytotoxicity against the highly metastatic H292 and H460 NSCLC cells.
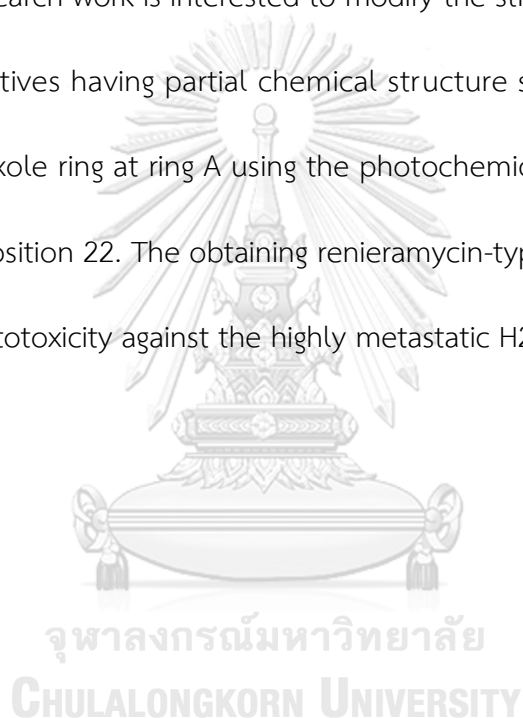
CHAPTER III

METHODOLOGY

3.1 Introduction to the Semi-Synthesis of Renieramycins Derivatives

Renieramycins, members of the bistetrahydoisoquinolinequinone marine alkaloid family, were isolated from the Thai blue sponge (*Xestospongia* sp.). This sponge species was classified under the phylum Porifera in the kingdom Animalia and was found in the oceanic regions surrounding Thailand, Philippines, Australia, Indonesia, and Malaysia[31]. Among the compounds found in the sponge, renieramycin M stands out as a major alkaloid with notable cytotoxicity against various human cancer cell lines, including breast, colon, lung, pancreatic, and prostate cancers[16]. Due to its potent activity, renieramycin M holds significant promise as a lead compound in drug development and serves as a valuable chemical template for structure-activity relationship studies in the fields of chemistry and pharmacology.

Currently, marine-derived tetrahydroisoquinoline alkaloids, such as ecteinascidin 743 (Trabectedin or Yondelis®), have gained approval for the treatment of lung cancer in humans[69]. Hence, this research aims to modify the structure of renieramycins to obtain new derivatives that bear partial chemical motifs resemblance to ecteinascidin 743, including the incorporation of a [1,3]-dioxole group through photochemical reactions, as well as ester side chains at carbon positions 5 and 22 by esterification. Subsequently, the cytotoxicity of these derivatives was

evaluated against highly metastatic non-small-cell lung cancer cells, namely H292 and H460.

3.2 Materials

3.2.1. General Experimental Procedures

All reagents used in this study were purchased from Tokyo Chemical Industry (TCI), Tokyo, Japan. Glassware utilized in the experiments was thoroughly dried in an oven. Photochemical reactions were conducted using a commercially available LED light (4 W LED Filament GLS Blue light 220-240 V EVE) and an 18 W fluorescent white light (100 V, HATAYA, Japan) sources. Thin-layer chromatography (TLC) analysis was performed on 60-F254 aluminum silica gel plates (Merck), and the resulting chromatograms were visualized under UV light at wavelengths of 254 and 365 nm. Flash column chromatography purification was accomplished using (60, 230-400 mesh) silica gel, employing ethyl acetate and hexane as the mobile phase.

Nuclear magnetic resonance (NMR) spectra, including ^{1}H and ^{13}C, were recorded at 400 MHz and 100 MHz, respectively, using a Bruker ADVANCE NEO 400 MHz NMR spectrometer. Deuterated chloroform ($CDCl_3$) served as the internal standard, with chemical shifts referenced to 77.0 ppm for ^{13}C and 7.27 ppm for ^{1}H spectra. Infrared (IR) spectra were acquired using a Perkin Frontier Fourier Transform Infrared Spectrometer. High-resolution mass spectrometry (HR-MS) measurements were conducted on an A microTOF Bruker Daltonics mass spectrometer. Optical rotations were measured using a JASCO P-2000 polarimeter equipped with a 1 mL

cell and a 1 dm path length. Electronic circular dichroism (ECD) spectra were obtained using a JASCO J-815 CD spectrometer.

3.2.2. Extraction and Isolation

Under the auspices of the Aquatic Resources Research Institute, Chulalongkorn University, and with approval from the Department of Fisheries, Ministry of Agriculture and Cooperatives, Thailand (0510.2/8234, Date 28 October 2019), specimens of the Thai blue sponge (*Xestospongia* sp.) were collected via SCUBA diving at Si-chang Island in the Gulf of Thailand, at a depth of 3-5 meters. The freshly obtained blue sponge was subsequently macerated and subjected to a pre-treatment step involving a 10% potassium cyanide solution in phosphate buffer solution at pH 7. The resulting mixture was filtered and concentrated under reduced pressure. To isolate the desired compounds, namely renieramycin M (**1**), renieramycin N (**2**)[13], and renieramycin O (**3**)[12], the treated sponge extract underwent extraction using hexane and ethyl acetate solvents. The subsequent purification process employed silica gel column chromatography, with an eluent composed of a mixture of hexane and ethyl acetate. Moreover, compound **1** was further transformed into jorunnamycin A (**6**) via a series of reactions involving hydrogenation, hydride reduction, and air oxidation[27, 28].

3.3 Screening of Photochemical Reaction Conditions using Renieramycin M as a Model Study

Renieramycin M (**1**) was utilized as the starting material for the reactions. A solution of compound **1** (15 mg, 0.03 mmol) was prepared in a selected solvent (20 mL) such as dichloromethane (CH_2Cl_2), chloroform ($CHCl_3$), or tetrahydrofuran (THF). The reaction mixture was vigorously stirred under a light source, either blue light (4 W LED) or white light (18 W fluorescent), for 24 hours at room temperature in a nitrogen atmosphere. The progress of the reaction was monitored by TLC, using ethyl acetate:hexane (1:1 v/v) as the mobile phase. Once the reaction reached completion, the solvent was evaporated under reduced pressure. The resulting crude product was subsequently purified by flash column chromatography, employing silica gel as the stationary phase and a mixture of ethyl acetate and hexane as the mobile phase, yielding the desired products **(Figure 13)**.

renieramycins M (**1**)   renieramycins T (**4**)
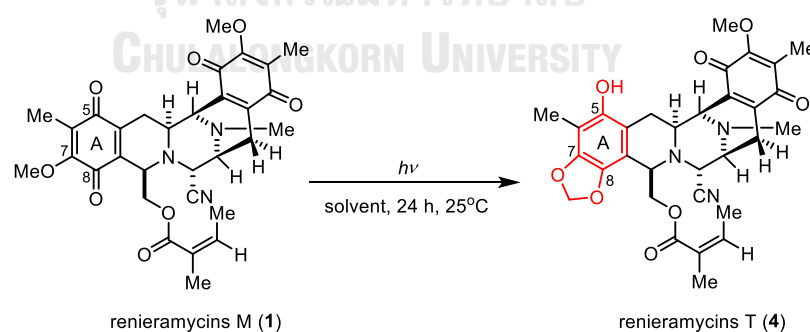
Figure 13 Transformation of renieramycin M to renieramycin T by photochemical reaction

For the photochemical reaction, screening of chemical reaction conditions are studies including solvents, and light **(Table 3)** to find the most suitable conditions.

Table 3 Screening of photochemical reaction conditions

Entry	Starting material	Light	Solvent
1	renieramycin M	White (18 W)	CH_2Cl_2
2	renieramycin M	White (18 W)	$CHCl_3$
3	renieramycin M	White (18 W)	THF
4	renieramycin M	Blue (4 W)	CH_2Cl_2
5	renieramycin M	Blue (4 W)	$CHCl_3$
6	renieramycin M	Blue (4 W)	THF

3.4 Photochemical Reaction of Natural Renieramycins

The appropriate conditions for photochemical reaction were finalized. Then, the natural renieramycins are employed into the photochemical reaction using renieramycin O (**3**) **(Figure 14)** and renieramycin N (**2**) **(Figure 15)** (40 mg, 0.07 mmol) with suitable light and solvent. Then use the same research protocol as renieramycin M (**1**).
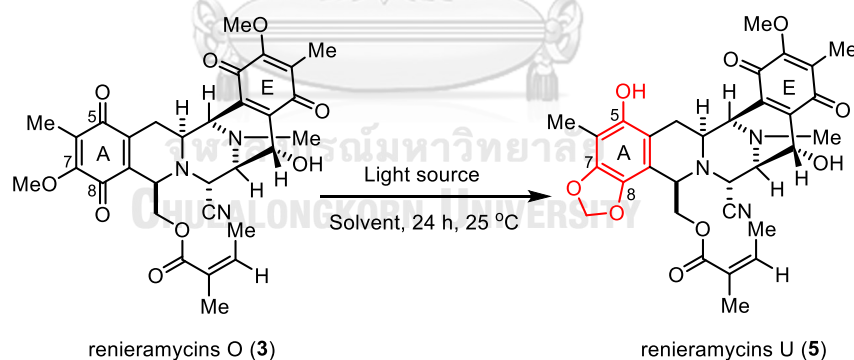
Figure 14 Semi-synthesis of natural renieramycin O by photochemical reaction
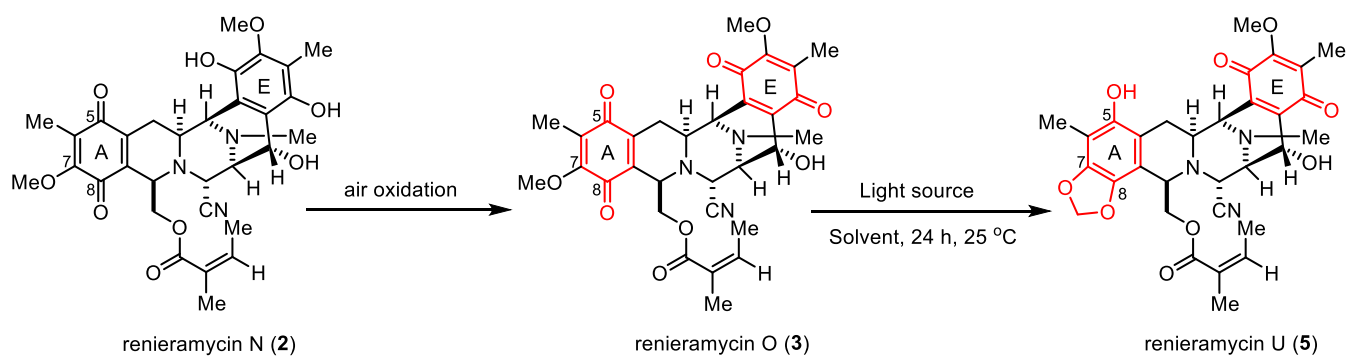
Figure 15 Semi-synthesis of natural renieramycin N by photochemical reaction

3.5 Procedure for Semi–Synthesis of 22-*O*-(4'-pyridinecarbonyl) renieramycin T

Jorunnamycin A (**6**) (25 mg, 0.05 mmol, 1 equiv) in dry dichloromethane (CH$_2$Cl$_2$) (10 mL) was added to an oven–dried round–bottomed flask. Then, 4-dimethylaminopyridine (DMAP) (31 mg, 0.25 mmol, 5 equiv), 1-(3-dimethylamino-propyl)-3-ethylcarbodiimide hydrochloride (EDCI) (49 mg, 0.25 mmol, 5 equiv), and isonicotinoyl chloride hydrochloride (45 mg, 0.25 mmol, 5 equiv) were added into the reaction. The reaction mixture was stirred for 24 hours at room temperature under nitrogen atmosphere and monitored by TLC using a mixture solvent of ethyl acetate: hexane (1:1 v/v) as a mobile phase. After completion, the reaction was concentrated under reduced pressure. Next, the resultant crude product was purified by flash column chromatography using silica gel as stationary phase and the mixed solvent of ethyl acetate and hexane as mobile phase to provide the yellow product of 22-*O*-(4'-pyridinecarbonyl) jorunnamycin A (**7**). After that, compound **7** (6 mg, 0.01 mmol) in CH$_2$Cl$_2$ (15 mL) was irradiated under suitable light at room temperature under a nitrogen atmosphere for 24 hours. The reaction mixture was monitored by TLC and purified to obtain 22-*O*-(4'-pyridinecarbonyl) renieramycin T (**10**) **(Figure 16)**. Furthermore, the purified product is characterized by ^{1}H-NMR, ^{13}C-NMR, high-resolution mass spectroscopic (HR-MS), CD spectroscopy and Optical rotation methods.
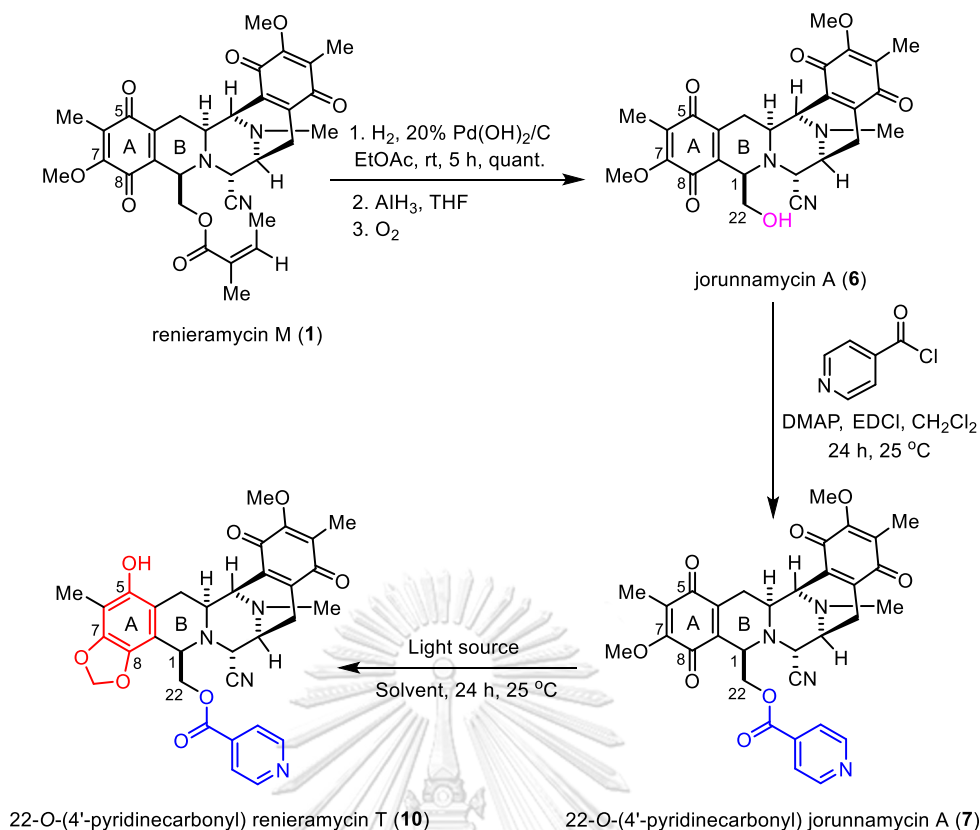
Figure 16 Semi-synthesis of renieramycins derivative by esterification and photochemical reaction

3.6 Cytotoxic Evaluations against NSCLC cell lines of Renieramycins Derivatives

The *in vitro* cytotoxicity of compounds **1-10 (Figure 17)** was assessed against

H292 and H460 non-small-cell lung carcinoma (NSCLC) cell lines using the 3-(4,5-

dimethylthiazol-2-yl)-2,5-diphenyltetrazolium bromide (MTT) colorimetric assay.

Cisplatin and doxorubicin served as positive controls, while 0.2% dimethyl sulfoxide

(DMSO) from Merck Millipore (Billerica, Massachusetts, USA) or Sigma-Aldrich was

used as the negative control. The H292 and H460 NSCLC cell lines were obtained

from the American Type Culture Collection (ATCC, Manassas, Virginia, USA). Roswell

Park Memorial Institute (RPMI) 1640 medium, fetal bovine serum (FBS), L-glutamine,

penicillin/streptomycin solution, and Albumax I were procured from Gibco

(Gaithersburg, Massachusetts, USA).

renieramycins
M: Y = H (**1**)
O: Y = OH (**3**)

renieramycin N (**2**)

renieramycins
T: X" = H (**4**)
U: X" = OH (**5**)

jorunnamycin A (**6**)

22-*O*-(4'-pyridinecarbonyl)
jorunnamycin A (**7**)

hydroquinone 5-*O*-(4'-pyridinecarbonyl)
renieramycin M (**8**)

5-*O*-(4'-pyridinecarbonyl)
renieramycin T (**9**)

22-*O*-(4'-pyridinecarbonyl)
renieramycin T (**10**)
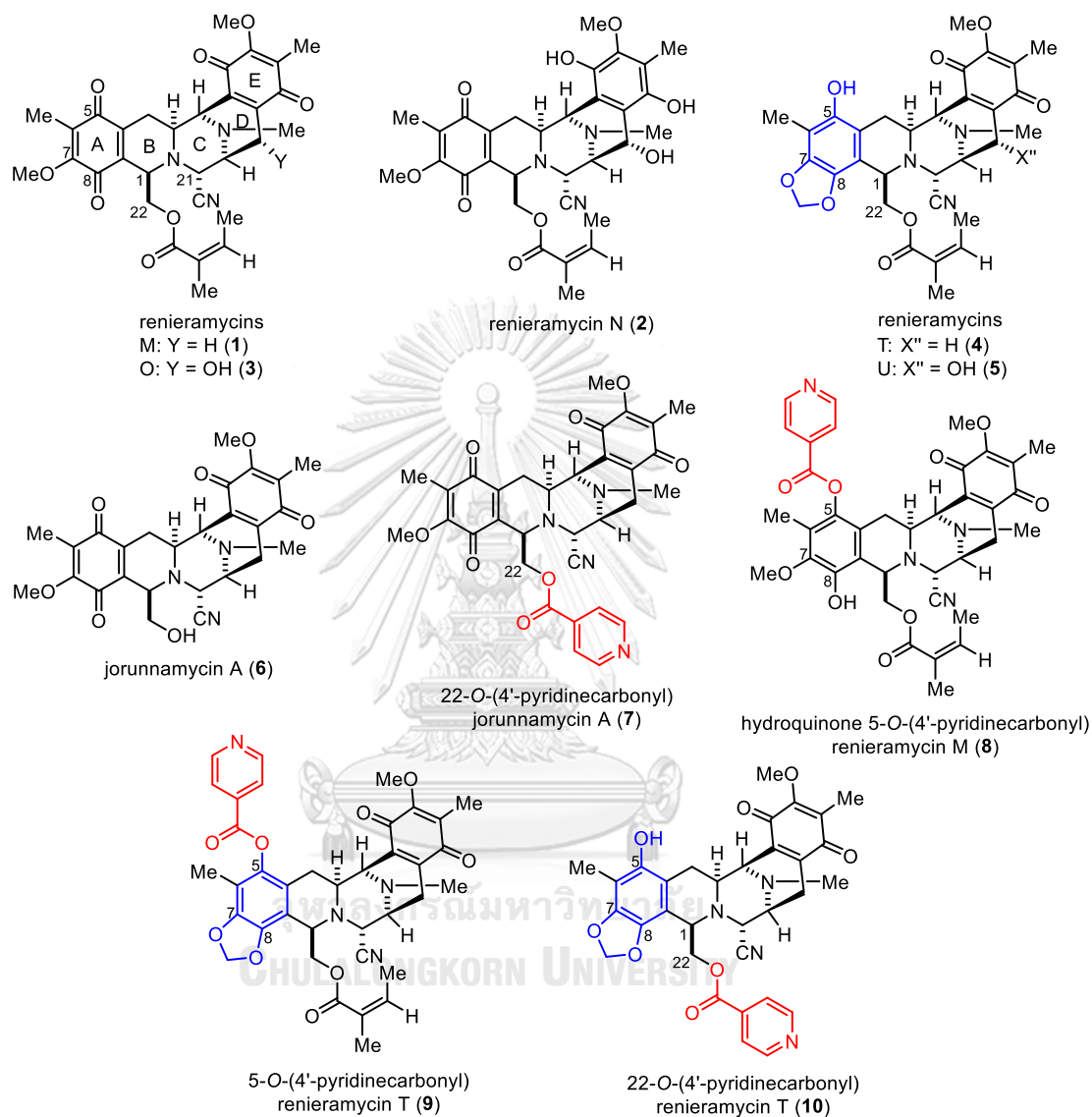
Figure 17 Renieramycins-type derivatives for in vitro evaluation of cytotoxicity

The non-small-cell lung carcinoma H292 and H460 cell lines were cultured in

RPMI 1640 medium supplemented with 10% FBS, 2 mM L-glutamine, and 100

units/mL of penicillin/streptomycin, maintained at 37 °C under 5% CO_2. Cells were

trypsinized and seeded at a density of 5000 cells/well in 96-well plates and

incubated with RPMI media for 24 hours. Each test compound was prepared as a 10 mM stock solution in DMSO and further diluted to serial concentrations ranging from 1-250 nM, ensuring a DMSO concentration of less than 0.2% v/v. After treat with various concentrations of each compound for 72 hours, cells were incubated with 0.5 mg/mL of MTT for 2 hours. The resulting formazan salt was solubilized using 100 μL of DMSO, and the absorbance of the formazan product was measured at 570 nm using a spectrophotometric microtiter plate reader (Perkin Elmer Victor 3 1420 Multilabel Plate Counter). The experiment was performed with three replicate wells and at least five concentrations of the tested compounds. Cell viability was analyzed using GraphPad Prism software (version 5) by calculating the percentage of non-treated control cells and determining the mean half maximal inhibitory concentration (IC_{50}) values.

$$\% \text{ Cell viability} = \frac{\text{Absorbance at 570 nm (sample)}}{\text{Absorbance at 570 nm (control)}} \times 100$$

Figure 18 Equation for calculating percent cell viability

3.7 Data Analysis and Statistics

The results of the effective inhibitory concentrations (IC_{50}) are shown in mean ± standard deviation (SD).

CHAPTER IV

RESULTS AND DISCUSSION

4.1 Screening of Photochemical Reaction Conditions using Renieramycin M as a Model Study

Renieramycins M (**1**) were isolated from the Thai blue sponge *Xestospongia* sp. The starting material **1** dissolved in different solvents consisting of CH_2Cl_2, $CHCl_3$ and THF (20 mL) under the light source of white light (18 W fluorescent) or blue light (4 W LED) for 24 hours to obtain renieramycin T (**4**) as a product. Then, compound **4** was elucidated structure by spectroscopic techniques. Regarding the optimal conditions of the photochemical reaction **(Table 4)**, it was found that utilizing dichloromethane (CH_2Cl_2) as the solvent under a 4 W LED (blue light) source resulted in the highest yield by achieving 81% of a yellow amorphous powder of the product **4 (Figure 19)**. Therefore, this condition was selected for photochemical reaction of other renieramucins.

Table 4 Optimization of photochemical conditions of renieramycins M

Entry	Starting Material	Lamp[a]	Solvent	Renieramycins Product	Isolated yield (%)
1	1	18 W	CH_2Cl_2	4	64
2	1	18 W	$CHCl_3$	4	46
3	1	18 W	THF	4	47
4	1	4 W	CH_2Cl_2	4	81
5	1	4 W	$CHCl_3$	4	51
6	1	4 W	THF	4	54

[a]18 W refers to white light fluorescent lamp and 4 W refers to blue light LED lamp.
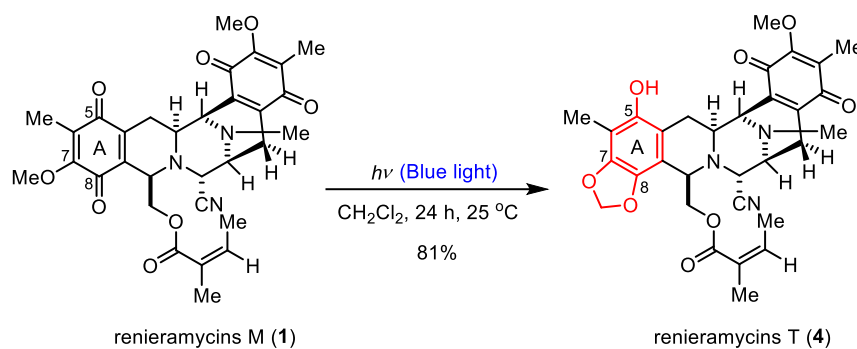
Figure 19 Modification of renieramycin M to renieramycin T by photochemical reaction

4.1.1. Reaction mechanism of photochemical reaction

A plausible mechanism explaining the formation of the compound **IV** with a [1,3]-dioxole ring for the photochemical reaction has been described in **Figure 20**. Light induces the n$\rightarrow\pi^*$ transition in quinone **I** that is capable of generating a quinol diradical, **II**. This can facilitate a 1,6-hydrogen atom transfer (HAT) between the alkoxyl radical at carbon position 5 and the methoxyl radical at carbon position 7, leading to compound **III**. Subsequently, a biradical formation takes place, culminating in a recombination to yield compound **IV**, which exhibits a [1,3]-dioxole ring at carbon positions 7 and 8 on the A-ring.
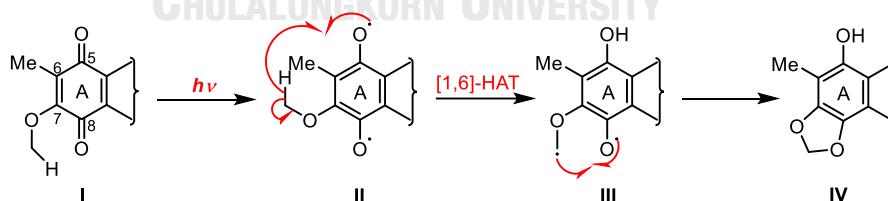
Figure 20 Proposed mechanism for photochemical reaction of quinone[27, 70]

4.1.2. Physical and spectroscopic data of Compound 4
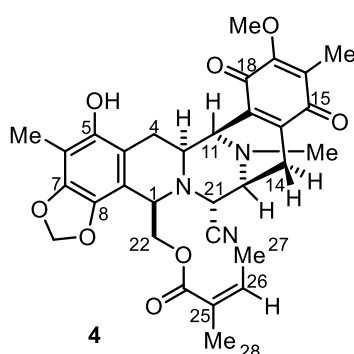
renieramycin T (**4**): The compound **4** was synthesized from **1** (15 mg, 0.03 mmol) in dry CH_2Cl_2 (20 mL) under 4 W LED lamp (Blue light) to obtain **4** as a yellow amorphous powder at 81%; ^1H NMR data, see **Table 5**.

The compound **4** was measured ^1H NMR for preliminary structural identification regarding the additional [1,3]-dioxole ring substituents. The known natural renieramycins **1** and **4** were compared their spectroscopic data **(Table 5)**. The key characteristic chemical shifts (δ) involve methylenedioxy motif (OCH_2O) or [1,3]-dioxole ring at carbon positions 7 and 8, showing a chemical shift at 5.85 and 5.92 ppm for ^1H NMR spectrum. Furthermore, upon comparing the spectroscopic data of product **4** with the relevant literature reports of the starting material **1**, it was observed that the methoxy group ($-OCH_3$) at carbon position 7, with a chemical shift of 4.02 ppm in the starting material **1**[71], was absent in the NMR spectrum of product **4**. Conversely, the hydroxy group (–OH) at carbon position 5 was detected in the ^1H NMR of compound **4**, with a chemical shift of 4.46 ppm. The spectroscopic data obtained from the experimental results and the related literature reports exhibited a high degree of similarity, confirming that the synthesized product is indeed the same compound.

Table 5 ^{1}H NMR (400 MHz) spectral data of compound **1** and **4** in $CDCl_3$[71]

Proton No.	Reported data (**1**) δ_H in ppm (*J* in Hz)	Reported data (**4**) δ_H in ppm (*J* in Hz)	Experimental data (**4**) δ_H in ppm (*J* in Hz)
1	3.99 (m)	4.16 (dd, 5, 4)	4.16 (1H, overlapped)
3	3.11 (dt, 11, 3)	3.24 (ddd, 12, 3, 2)	3.25 (1H, br d, 11.6)
4	α 2.89 (dd, 17, 8)	α 2.87 (dd, 15, 2)	α 2.87 (1H, br d, 15.2)
	β 1.36 (ddd, 17, 11, 3)	β 1.67 (dd, 15, 12)	β 1.67 (1H, overlapped)
11	4.01 (dd, 3, 2)	4.00 (dd, 3, 1)	4.01 (1H, overlapped)
13	3.40 (ddd, 8, 3, 2)	3.37 (ddd, 7, 2, 1)	3.38 (1H, d, 6.8)
14	α 2.76 (dd, 21, 8)	α 2.75 (dd, 21, 7)	α 2.77 (1H, dd, 17.2, 6.8)
	β 2.30 (d, 21)	β 2.30 (d, 21)	β 2.33 (1H, overlapped)
21	4.07 (d, 3)	4.11 (d, 2)	4.11 (1H, d, 2.4)
22	α 4.10 (dd, 12, 3)	α 3.99 (dd, 11, 5)	α 3.98 (1H, overlapped)
	β 4.53 (dd, 12, 3)	β 4.41 (dd, 11, 4)	β 4.42 (1H, dd, 11.2, 3.6)
26	5.96 (qq, 7, 2)	6.00 (qq, 7, 2)	6.00 (1H, qq, 7.2, 1.5)
27-CH$_3$	1.82 (dq, 7, 2)	1.85 (dq, 7, 2)	1.85 (3H, dq, 7.2, 1.5)
28-CH$_3$	1.58 (dq, 2, 2)	1.69 (dq, 2, 2)	1.69 (3H, s)
6-CH$_3$	1.94 (s)	2.11 (s)	2.11 (3H, s)
16-CH$_3$	1.90 (s)	1.94 (s)	1.94 (3H, s)
7-OCH$_3$	4.02 (s)		
17-OCH$_3$	3.99 (s)	3.98 (s)	3.99 (3H, s)
OCH$_2$O		5.85 (d, 2)	5.85 (1H, s)
		5.92 (d, 2)	5.92 (1H, s)
N-CH$_3$	2.28 (s)	2.29 (s)	2.29 (3H, s)
5-OH		4.55 (br s)	4.46 (1H, br s)

4.2 Photochemical Reaction of Natural Renieramycins

Natural renieramycin N (**2**) and O (**3**) also were isolated from *Xestospongia* sp. After that, compounds **2** and **3** were irradiated under blue light (4 W LED) in CH_2Cl_2 as a solvent for overnight to give the same product as a yellow amorphous powder of renieramycin U (**5**) at 55% and 48% yield, respectively **(Figure 21)**. Compound **2** was oxidized by air at the hydroquinone ring E changing to the quinone group of **3** **(Figure 22)**. Next, the photochemical of **3** produced **5** significantly. Then, chemical structure compound **5** was elucidated by ^{1}H-NMR and ^{13}C-NMR spectroscopy, high-resolution mass spectroscopy (HR-MS), circular dichroism (CD), and optical rotation methods.
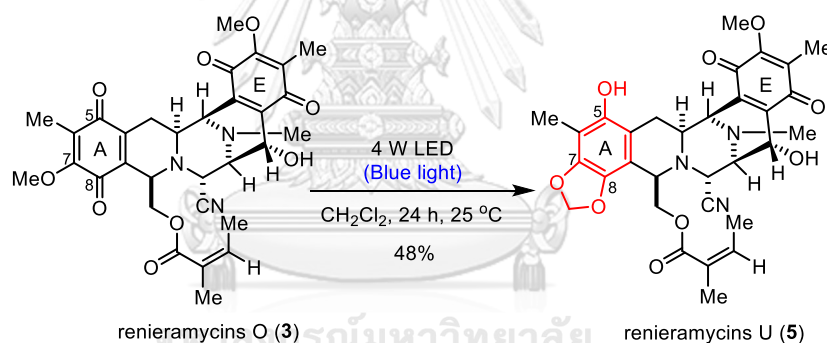
Figure 21 Photochemical reaction-based semi-synthesis of natural renieramycin O
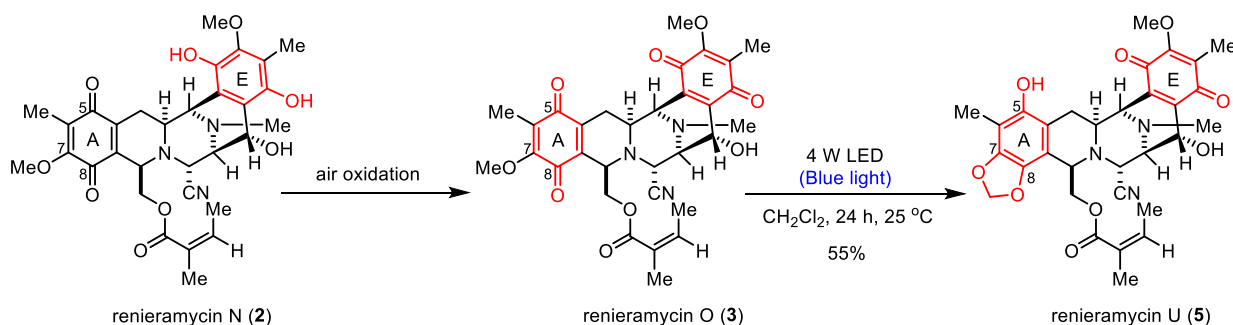
Figure 22 Transformation of air-oxidation and photochemical reaction of renieramycin N into renieramycin U

4.2.1. Reaction mechanism of oxidation reaction

The air oxidation reaction of hydroquinone (**I**) at the ring E occurred **(Figure 23)**, as previously reported[12, 13, 16, 27], due to the transformation of the unstable 1,4-hydroquinone into a more stable 1,4-quinone moiety. The potential mechanism of air oxidation involves the conversion of **I** to the semiquinone radical intermediate (**II**) and subsequently to **III**. This process entailed atom loss or electron donation to oxygen to enhance the stability of the molecule, where compound **I** acted as the reducing agent by donating electrons and oxygen (O_2) served as the oxidizing agent, accepting electrons in the air.
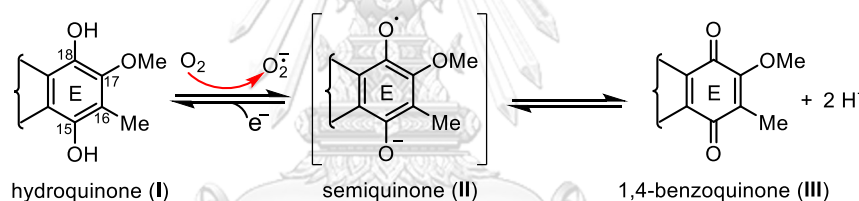
Figure 23 Suggested mechanism for the air oxidation process of hydroquinone[72]

4.2.2. Physical and spectroscopic data of Compound 5

5
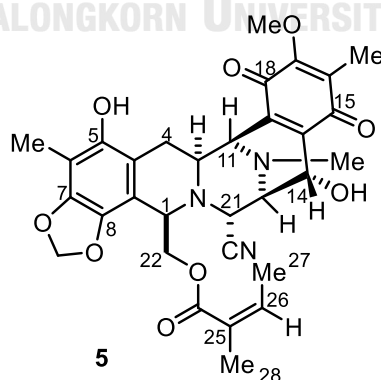
renieramycin U (**5**): The compound **5** was synthesized from **3** (40 mg, 0.07 mmol) in dry CH_2Cl_2 (20 mL) under 4 W LED lamp (blue light) to obtain **5** as a yellow

amorphous powder at 48% yield; $[\alpha]_D^{25}$ −5.4 (*c* 0.71, CHCl$_3$) (lit. $[\alpha]_D^{23}$ −51.3 (*c* 0.07, CHCl$_3$)[15]; IR (ATR) ν_{max} 3384 (br), 2926, 1714, 1651, 1455, 1230, 1147, 1093, 1045, 759 cm^{-1}; ECD $\Delta\varepsilon$ (*c* 240.02 μM, methanol, 20 $^{\circ}$C) −0.5 (296), −5.5 (280), −12.7 (273), +5.9 (264), +5.0 (260), −10.5 (245), +18.2 (230), +26.2 (219), +6.3 (214), +13.9 (209), +7.6 (198) nm; ^{1}H and ^{13}C NMR data, see **Table 6** and **7**; HRESIMS *m/z* 592.2290 ([M+H]$^+$, calculated for C$_{31}$H$_{34}$N$_3$O$_9$, 592.2290).

The circular dichroism (CD) spectroscopy results of compound (**5**) were compared to those of compounds renieramycin U and renieramycin T, which have the [1,3]-dioxole ring, as described in the previous report[15]. The analysis revealed that the obtained data exhibited a consistent spectral pattern.

For preliminary structural identification of compound **5**, focused on its additional [1,3]-dioxole substituent, ^{1}H NMR and ^{13}C NMR measurements were performed. Spectroscopic data from the synthesized compound were then matched with previously published data corresponding to the naturally occurring renieramycins **2**, **3**, and **5** (**Table 6** and **7**). The characteristic chemical shifts (δ) of of compound **5** the proton and carbon signals of the methylenedioxy ring (OCH$_2$O) or [1,3]-dioxole ring at carbon positions 7 and 8, which observed at 5.88 and 5.95 ppm, and 101.2 ppm, respectively. A noteworthy observation emerged when the spectroscopic data of product **5** was compared with the literature for starting materials **2** and **3**[13]. The methoxy group (–OCH$_3$) at carbon position 7, which initially

manifested a chemical shift of 3.94 ppm (^{1}H NMR) and 58.3 ppm (^{13}C NMR) in starting material **2**[13], and a chemical shift of 4.03 ppm (^{1}H NMR) and 61.1 ppm (^{13}C NMR) in starting material **3**[13], was found to be absent in the NMR spectrum of the synthesized product **5**. In contrast, the presence of a hydroxy group (–OH) at carbon position 5 was validated in the ^{1}H NMR of compound **5**, with a chemical shift of 3.52 ppm. The collected spectroscopic data, drawn from both experimental results and related literature, displayed a considerable degree of concordance. This consistency solidifies the assertion that the synthesized product is indeed identical to the corresponded natural compound.

Table 6 ^{1}H NMR (400 MHz) spectral data of compound **2** in pyridine-d$_5$, **3** and **5** in CDCl$_3$[13, 15]

Proton No.	Reported data (**2**) δ_H in ppm (J in Hz)	Reported data (**3**) δ_H in ppm (J in Hz)	Reported data (**5**) δ_H in ppm (J in Hz)	Experimental data (**5**) δ_H in ppm (J in Hz)
1	4.37 (1H, ddd, 2.6, 2.6, 2.0)	3.98 (1H, m)	4.14 (1H, dd, 5.2, 3.4)	4.16 (1H, dd, 4.9, 3.2)
3	3.44 (1H, ddd, 11.2, 2.6, 2.6)	3.05 (1H, ddd, 11.6, 3.3, 2.3)	3.19 (1H, ddd, 11.6, 2.4, 2.4)	3.22 (1H, dt, 12.1, 2.3)
4	α 3.60 (1H, dd, 17.8, 2.6) β 2.20 (1H, ddd, 17.8, 11.2, 2.6)	α 2.87 (1H, dd, 17.2, 2.3), β 1.27 (1H, ddd, 17.2, 11.6, 2.6)	α 2.86 (1H, dd, 15.3, 2.4), β 1.54 (1H, dd, 15.3, 11.6)	α 2.88 (1H, dd, 15.0, 2.3) β 1.62 (1H, overlapped)
11	4.74 (1H, d, 2)	4.09 (1H, dd, 3.3, 1.3)	4.08 (1H, dd, 2.4, 0.5)	4.11 (1H, br d, 2.3)
13	3.96 (1H, dd, 2.6, 2.0)	3.42 (1H, br s)	3.39 (1H, dd, 2.7, 0.5)	3.43 (1H, dd, 7.0, 2.4)
14	β 5.18 (1H, s)	4.37 (1H, s)	4.37 (1H, d, 1.2)	4.39 (1H, br d, 7.0)
21	4.94 (1H, d, 2.6)	4.23 (1H, d, 2.6)	4.22 (1H, d, 2.7)	4.24 (1H, dd, 7.0, 2.4)
22	α 4.58 (1H, dd, 11.6, 2.6) β 4.51 (1H, dd, 11.6, 2.0)	α 4.53 (1H, dd, 11.6, 3.0), β 4.09 (1H, dd, 11.1, 3.4)	α 3.96 (1H, dd, 11.3, 5.2), β 4.41 (1H, dd, 11.3, 3.4)	α 3.96 (1H, dd, 11.3, 5.2) β 4.43 (1H, dd, 11.3, 3.2)

Table 6 (Cont.) ^{1}H NMR (400 MHz) spectral data of compound **2** in pyridine-d_5, **3** and **5** in $CDCl_3$[13, 15]

Proton No.	Reported data (**2**) δ_H in ppm (J in Hz)	Reported data (**3**) δ_H in ppm (J in Hz)	Reported data (**5**) δ_H in ppm (J in Hz)	Experimental data (**5**) δ_H in ppm (J in Hz)
26	5.70 (1H, qq, 7.3, 1.3)	5.98 (1H, qq, 7.3, 1.7)	6.02 (1H, qq, 7.3, 1.5)	6.04 (1H, qq, 7.0, 1.0)
27-CH$_3$	1.74 (3H, dq, 7.3, 1.7)	1.82 (3H, dq, 7.3, 1.3)	1.85 (3H, dq, 7.3, 1.5)	1.91 (3H, dq, 7.0, 1.0)
28-CH$_3$	1.44 (3H, dq, 1.7, 1.3)	1.57 (3H, dq, 1.7, 1.3)	1.69 (3H, dq, 1.5, 1.5)	1.71 (3H, s)
6-CH$_3$	1.92 (3H, s)	1.94 (3H, s)	2.10 (3H, s)	2.13 (3H, s)
16-CH$_3$	2.40 (3H, s)	1.92 (3H, s)	1.95 (3H, s)	1.98 (3H, s)
7-OCH$_3$	3.94 (3H, s)	4.03 (3H, s)		
17-OCH$_3$	3.74 (3H, s)	4.02 (3H, s)	4.04 (3H, s)	4.06 (3H, s)
OCH$_2$O			5.89 (1H, d, 1.2) 5.92 (1H, d, 1.2)	5.88 (1H, s) 5.95 (1H, s)
N-CH$_3$	2.70 (3H, s)	2.46 (3H, s)	2.46 (3H, s)	2.49 (3H, s)
OH	10.68, 9.30, 7.60 (each 1H, br s, OH)	3.52 (1H, br s)	3.49 (1H, d, 2.1, 14-OH) 4.26 (1H, br s, 5-OH)	3.52 (1H, br s, 14-OH)

Table 7 ^{13}C NMR (100 MHz) spectral data of compound **2** in pyridine-d_5, **3** and **5** in $CDCl_3$[13, 15]

Carbon No.	Reported data (**2**) δ_C in ppm	Reported data (**3**) δ_C in ppm	Reported data (**5**) δ_C in ppm	Experimental data (**5**) δ_C in ppm
1	54.4	56.4	56.6	56.6
3	53.1	53.4	55.6	55.5
4	22.9	25.3	26.7	26.7
5	183.6	185.4	140.7	141.0
6	124.9	128.6	112.0	112.0
7	153.8	155.6	144.7	144.7
8	179.1	180.8	140.3	140.0
9	133.9	135.7	112.0	112.0

Table 7 (Cont.) ^{13}C NMR (100 MHz) spectral data of compound **2** in pyridine-d_5, **3** and **5** in $CDCl_3$[13, 15]

Carbon No.	Reported data (**2**) δ_C in ppm	Reported data (**3**) δ_C in ppm	Reported data (**5**) δ_C in ppm	Experimental data (**5**) δ_C in ppm
10	140.3	141.1	119.4	119.4
11	54.6	55.0	55.8	55.8
13	63.1	62.4	62.7	62.7
14	62.0	62.0	62.2	62.3
15	145.2	187.8	188.1	188.0
16	115.7	128.4	128.9	129.0
17	144.2	155.8	155.8	155.8
18	139.4	182.8	183.0	183.0
19	115.9	135.3	136.0	136.0
20	114.7	141.0	140.7	140.7
21	55.2	56.4	57.7	57.6
22	60.5	62.1	64.7	64.6
24	164.8	166.5	167.1	167.1
25	125.4	126.2	126.7	126.7
26	136.5	140.6	139.9	140.0
27-CH_3	13.1	15.7	15.7	15.8
28-CH_3	17.7	20.3	20.5	20.5
6-CH_3	6.3	8.7	8.7	8.8
16-CH_3	7.3	8.4	8.5	8.5
7-OCH_3	58.3	61.1		
17-OCH_3	57.7	61.1	61.0	61.1
OCH_2O			101.1	101.2
N-CH_3	40.8	42.4	42.4	42.4
21-CN	117.8	116.3	116.9	116.9

4.3 The Result of Semi–Synthesis of 22-*O*-(4'-pyridinecarbonyl) renieramycin T

Jorunnamycin A (**6**) was prepared in 3 steps from compound **1** under hydrogenation, hydride reduction, and air oxidation [33]. Next, compound **6**, DMAP, EDCI, and isonicotinoyl chloride hydrochloride were dissolved in CH_2Cl_2 (10 mL) to provide the yellow product of 22-*O*-(4'-pyridinecarbonyl) jorunnamycin A (**7**) in 72% yield under the reported protocol[29]. After that, compound **7** in CH_2Cl_2 (15 mL) was irradiated under 4 W LED lamp (blue light) for 24 hours to obtain a yellow powder product of 22-*O*-(4'-pyridinecarbonyl) renieramycin T (**10**) in 83% yield **(Figure 24)**. Then, compound **10** was elucidated chemical structure by full spectroscopic analyses. In this step, the hydroxyl group (—OH) at carbon position 22 of compound **6** underwent a transformation into a 4'-pyridinecarbonyl group, resulting in compound **7**. This was achieved via an esterification reaction, using EDCI as a coupling reagent and DMAP as a nucleophilic base catalyst. Subsequently, the carbon positions 7 and 8 of compound **7** are converted into a [1,3]-dioxole ring via a photochemical reaction, utilizing blue light. This step yielded product **10**, which possesses a [1,3]-dioxole ring on ring A at carbon positions 7 and 8. Furthermore, carbon position 22 features a 4'-pyridinecarbonyl group, rendering it a novel derivative of renieramycins.
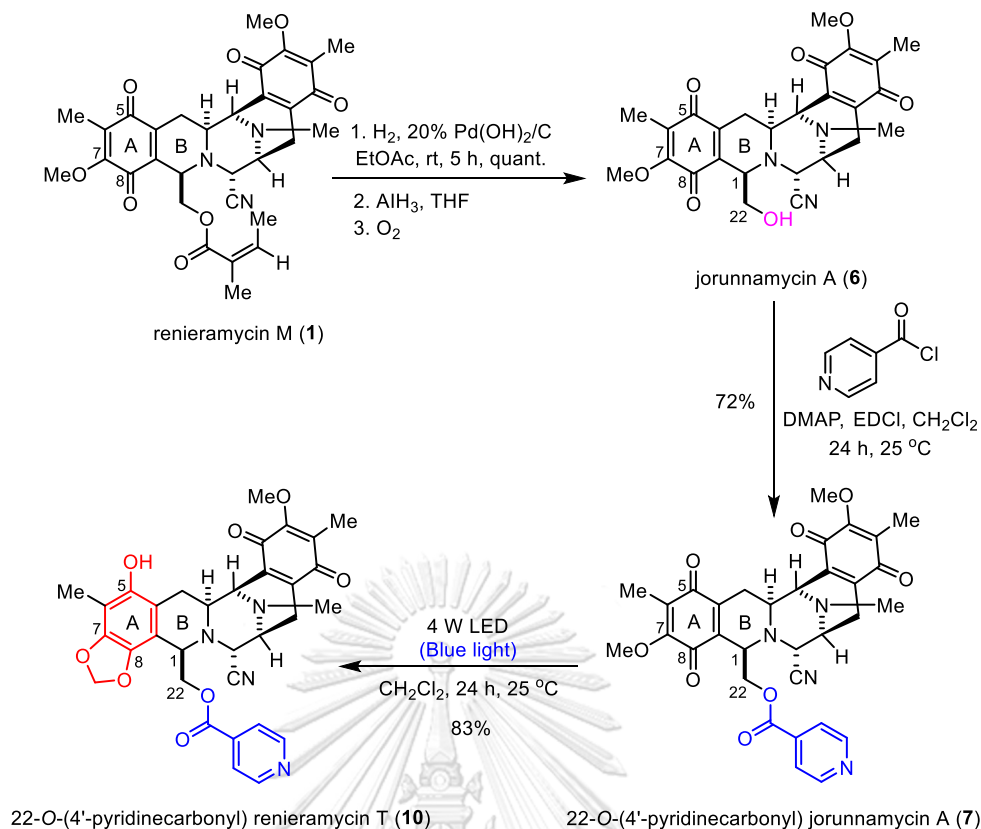
Figure 24 The semi-synthesis of renieramycin derivatives through a process involving esterification and photochemical reactions

4.3.1. Reaction mechanism of esterification reaction

Acid chlorides, also known as acyl chlorides, readily undergo a reaction with water, resulting in the formation of carboxylic acids. This reaction is markedly accelerated when involving hydroxides (OH), attributable to their heightened nucleophilic strength[73]. The mechanism of the reaction encompasses a nucleophilic addition of water (H_2O), subsequently followed by a proton transfer which culminates in the formation of a geminal diol. However, geminal diols exhibit instability and, as a consequence, one of the oxygen atoms expels the chloride ion (Cl^-), ultimately yielding a carboxylic acid as illustrated in **Figure 25 [2]**. When the reaction involves a hydroxide ion (OH^-), the process entails fewer steps and

progresses at an increased rate, due to the superior nucleophilic properties of the

hydroxide ion, as shown in **Figure 25 [1]**[73].

The Steglich esterification protocol implemented leveraged 1-ethyl-3-(3-

dimethylaminopropyl) carbodiimide (EDCI) coupling of compound **6**, with 4-

dimethylaminopyridine (DMAP) functioning as a nucleophilic base catalyst[74]. This

coupling mechanism is depicted in **Figure 25**. In the initial stage, DMAP functions as a

nucleophile and carries out the deprotonation of the carboxylic acid, leading to the

formation of a carboxylate ion (**II**), and concurrently imparting a positive charge to

DMAP (**I**). Subsequently, the compound (**II**) orchestrates a nucleophilic attack on the

carbodiimide core of EDC, culminating in the formation of an intermediate (**III**) bearing

a negative charge. Following this, DMAP-H$^+$ (**I**) steps in to protonate the intermediate

(**III**) substance, yielding intermediate (**IV**) that possesses a neutral charge. Upon

accepting a proton, it assumes the role of an electrophile to instigate a reaction with

DMAP, resulting in the formation of intermediate (**V**). Thereafter, compound **V**

undergoes a process of electron delocalization within its structure, facilitating the

displacement of the urea leaving group from **V**. In the terminal phase, the alcohol

component participates by directing its attack towards the carbonyl center of

intermediate **VI**. The compound **VII** structure experiences electron delocalization,

expelling DMAP[75], and ultimately producing an ester **VIII** with R_1 and R_2 substituents,

as demonstrated in **Figure 25** of compound **7**. This process using isonicotinoyl chloride as an acylating agent of esterification.
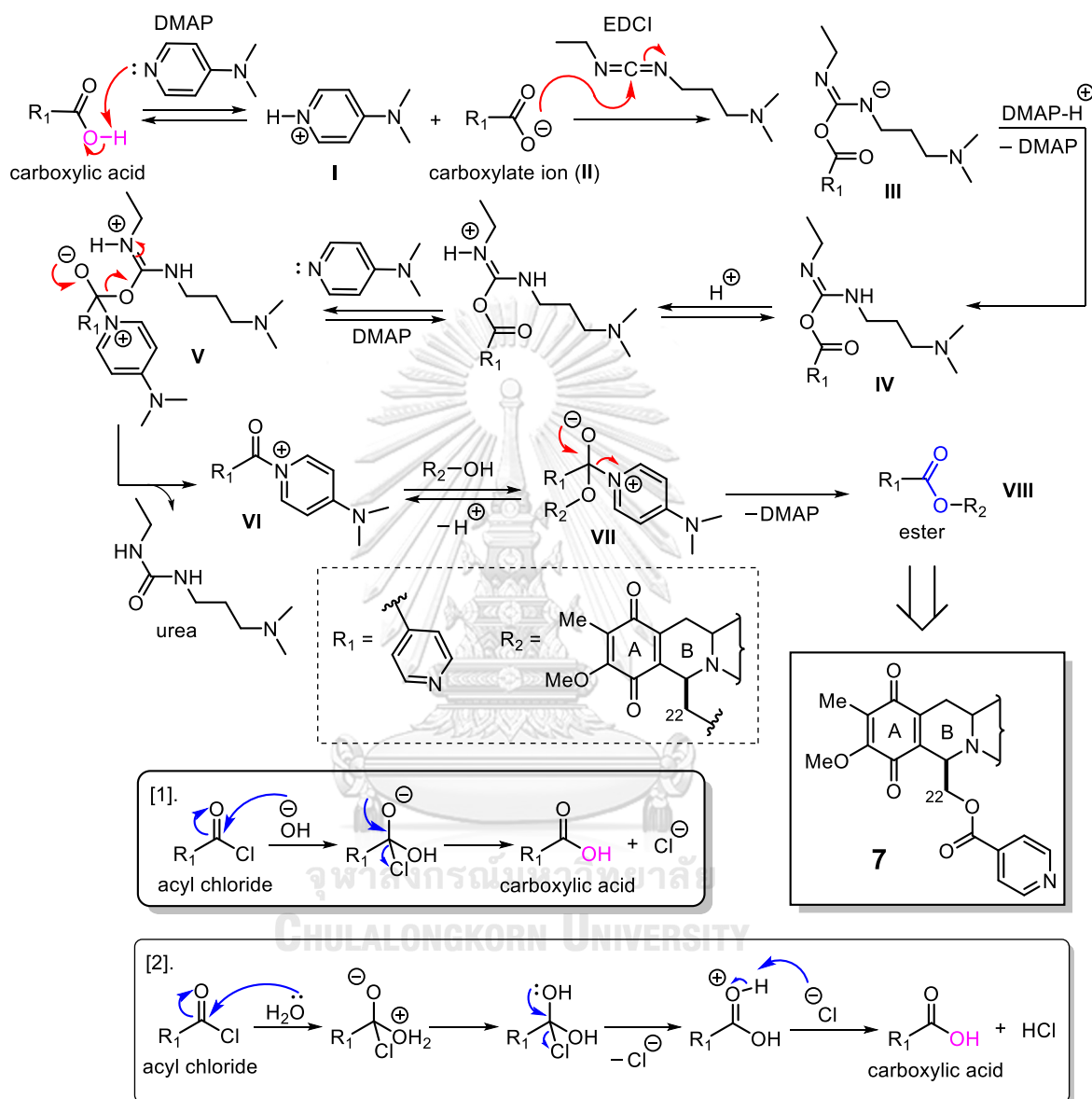
Figure 25 Proposed mechanism for esterification reaction of renieramycin ester[73-75]

4.3.2. Physical and spectroscopic data of Compound 7

7
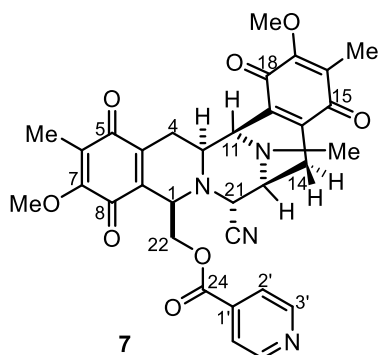
22-O-(4'-pyridinecarbonyl) jorunnamycin A (**7**): The compound **7** was synthesized regarding the reported procedure[29] using **6** (25 mg, 0.05 mmol, 1 equiv), DMAP (31 mg, 0.25 mmol, 5 equiv), EDCI (49 mg, 0.25 mmol, 5 equiv) and isonicotinoyl chloride hydrochloride (45 mg, 0.25 mmol, 5 equiv) in dry CH_2Cl_2 (10 mL) to obtain **7** as a yellow amorphous powder at 72% yield; ^1H and ^{13}C NMR data, see **Table 8** and **9**.

Structural identification focusing on the appended 4'-pyridinecarbonyl substituents by both ^1H NMR and ^{13}C NMR measurements were conducted on compound **7**. The spectroscopic data generated from this investigation were subsequently matched with previously reported data corresponding to jorunnamycin A (**6**) and renieramycin derivatives of compound **7**, as illustrated in **Tables 8** and **9**[28, 44]. The data revealed chemical shifts attributable to the 4'-pyridinecarbonyl group at carbon position 22. These chemical shifts (δ) presented at 7.47 ppm (2'-H, 6'-H) and 8.68 ppm (3'-H, 5'-H) in the ^1H NMR spectrum, and at 122.7 ppm (C-2', C-6'), 136.7

ppm (C-1'), 150.2 ppm (C-3', C-5'), and 164.0 ppm (C=O) in the ^{13}C NMR spectrum of

compound **7**.

Table 8 ^{1}H NMR (400 MHz) spectral data of compound **6** and **7** in CDCl$_3$[28, 44]

Proton No.	Reported data (**6**) δ_H in ppm (*J* in Hz)	Reported data (**7**) δ_H in ppm (*J* in Hz)	Experimental data (**7**) δ_H in ppm (*J* in Hz)
1	3.89 (d, 2.4)	4.10 (2H, m)	4.09 (2H, s)
3	3.17 (ddd, 11.2, 2.6, 2.4)	3.10 (1H, ddd, 11.6, 3.1, 2.4)	3.10 (1H, d, 11.2)
4	α 2.92 (dd, 17.6, 2.4) β 1.40 (ddd, 17.6, 11.2, 2.4)	α 2.92 (1H, dd, 17.4, 2.4) β 1.25 (H, ddd, 17.4, 11.6, 2.4)	α 2.92 (1H, d, 17.2) β 1.24 (1H, overlapped)
11	4.07 (d, 2.6)	3.95 (1H, br d, 2.2)	3.95 (1H, s)
13	3.42 (d, 2.4)	3.40 (1H, ddd, 7.6, 1.8, 0.6)	3.40 (1H, d, 7.2)
14	α 2.82 (dd, 20.8, 7.2) β 2.27 (d, 20.8)	α 2.71 (1H, dd, 20.9, 7.6) β 2.32 (1H, d, 20.9)	α 2.71 (1H, dd, 20.8, 7.2) β 2.34 (1H, d, 20.8)
21	4.15 (d, 2.4)	4.10 (2H, m)	4.09 (2H, s)
22	α 3.71 (dd, 11.2, 3.2) β 3.48 (dd, 11.2, 3.2)	α 4.99 (1H, dd, 11.7, 2.9) β 4.17 (1H, dd, 11.7, 2.1)	α 4.99 (1H, br d, 11.2) β 4.16 (1H, d, 11.2)
6-CH$_3$	1.93 (s)	2.00 (3H, s)	1.99 (3H, s)
16-CH$_3$	1.93 (s)	1.74 (3H, s)	1.73 (3H, s)
7-OCH$_3$	3.98 (s)	4.04 (3H, s)	4.04 (3H, s)
17-OCH$_3$	4.03 (s)	3.76 (3H, s)	3.76 (3H, s)
N-CH$_3$	2.30 (s)	2.23 (3H, s)	2.23 (3H, s)
2'-H, 6'-H		8.62 (2H, d, 8.3)	7.47 (2H, d, 4.4)
3'-H, 5'-H		7.44 (2H, d, 8.3)	8.68 (2H, d, 4.4)

Table 9 ^{13}C NMR (100 MHz) spectral data of compound **6** and **7** in CDCl$_3$[28, 44, 76]

Carbon No.	Reported data (**6**) δ_C in ppm	Reported data (**7**) δ_C in ppm	Experimental data (**7**) δ_C in ppm
1	58.0, CH	56.6	56.5
3	54.3, CH	54.3	54.3
4	25.3, CH$_2$	25.5	25.5
5	185.4, C=O	185.4	185.4
6	128.9, C	128.8	128.9
7	155.5, C	155.6	155.6
8	181.4, C=O	181.1	181.1
9	136.0, C	135.2	135.1
10	141.7, C	142.1	142.1
11	54.1, CH	54.1	54.1
12	41.5, N-CH$_3$	41.4	41.4
13	54.4, CH	54.5	54.4
14	21.6, CH$_2$	21.0	21.0
15	186.2, C=O	185.9	185.9
16	128.6, C	128.2	128.1
17	155.4, C	154.9	154.9
18	182.2, C=O	182.1	182.1
19	135.6, C	134.6	134.5
20	141.7, C	142.1	142.1
21	59.0, CH	58.4	58.4
22	64.1, CH$_2$	62.8	62.9
24		164.1	164.0
6-CH$_3$	8.7, CH$_3$	8.9	8.9
16-CH$_3$	8.7, CH$_3$	8.7	8.7
7-OCH$_3$	61.0, OCH$_3$	61.2	60.9
17-OCH$_3$	61.1, OCH$_3$	60.9	61.2

Table 9 (Cont.) ^{13}C NMR spectral data of compound **6** and **7** in CDCl$_3$

Carbon No.	Reported data (**6**)[44] δ_C in ppm	Reported data (**7**)[28] δ_C in ppm	Experimental data (**7**) δ_C in ppm
21-CN	116.8, CN	116.8	116.8
C-1'		136.2	136.7
C-2', C-6'		150.7	122.7
C-3', C-5'		122.5	150.2

4.3.3. Physical and spectroscopic data of Compound 10

10
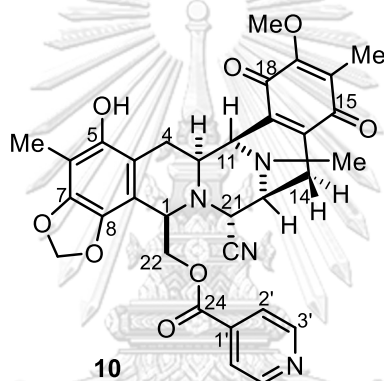
22-O-(4'-pyridinecarbonyl) renieramycin T (**10**): The compound **10** was synthesized from **7** (6 mg, 0.01 mmol) in dry CH$_2$Cl$_2$ (15 mL) under 4 W LED lamp (Blue light) to obtain **10** as a yellow amorphous powder at 83% yield; $[\alpha]_D^{25}$ −20.4 (*c* 0.37, CHCl$_3$); IR (ATR) ν_{max} 3279 (br), 2923, 1731, 1651, 1615, 1409, 1374, 1277, 1260, 1233, 1091, 1026, 953, 703 cm^{-1}; ECD $\Delta\varepsilon$ (*c* 247.24 μM, methanol, 20 °C) −8.1 (345), −6.5 (307), +7.3 (285), +11.5 (282), +2.0 (264), −3.9 (252), −5.5 (242), +0.3 (228), −10.9 (210) nm; ^{1}H and ^{13}C NMR data, see **Table 10** and **11**; HRESIMS *m/z* 599.2134 ([M+H]$^+$, calculated for C$_{32}$H$_{31}$N$_4$O$_8$, 599.2136).

The circular dichroism (CD) spectroscopy outcomes of compound **10** were juxtaposed with those of renieramycin M and renieramycin T, compound **10** possessing a structurally akin configuration to renieramycin M and featuring the [1,3]-dioxole ring analogous to renieramycin T, as elucidated in the preceding publication[13, 15, 71]. Scrutiny of the results disclosed that the acquired data demonstrated a coherent spectral pattern.

The structural identification compound **10** was measured ^{1}H and ^{13}C NMR spectroscopic techniques regarding the additional [1,3]-dioxole ring and 4'-pyridinecarbonyl substituents. The known compound of natural jorunnamycin A (**6**), renieramycin derivatives **7** and the novel renieramycin derivatives (**10**) were compared their spectroscopic data **(Table 10** and **11)**. The key characteristic chemical shifts (δ) involve methylenedioxy ring (OCH$_2$O) or [1,3]-dioxole ring at carbon positions 7 and 8, showing a chemical shift at 5.85 and 5.92 ppm for ^{1}H NMR spectrum and chemical shift at 101.2 ppm for ^{13}C NMR spectrum of compound **10**, and involve 4'-pyridinecarbonyl group at carbon positions 22, showing a chemical shift at 7.56 ppm (2'-H, 6'-H) and 8.71 ppm (3'-H, 5'-H) for ^{1}H NMR spectrum and chemical shift at 123.1 ppm (C-2', C-6'), 137.7 ppm (C-1'), 149.8 ppm (C-3', C-5') and 164.2 ppm (C=O) for ^{13}C NMR spectrum of compound **10**.

Table 10 ^{1}H NMR (400 MHz) spectral data of compound **6**, **7** and **10** in CDCl$_3$[44]

Proton No.	Reported data (**6**) δ_H in ppm (J in Hz)	Experimental data (**7**) δ_H in ppm (J in Hz)	Experimental data (**10**) δ_H in ppm (J in Hz)
1	3.89 (d, 2.4)	4.09 (2H, s)	3.96 (1H, d, 3.2)
3	3.17 (ddd, 11.2, 2.6, 2.4)	3.10 (1H, d, 11.2)	3.24 (1H, dt, 12.1, 2.6)
4	α 2.92 (dd, 17.6, 2.4) β 1.40 (ddd, 17.6, 11.2, 2.4)	α 2.92 (1H, d, 17.2) β 1.24 (1H, overlapped)	α 2.89 (1H, dd, 15.1, 1.8) β 1.55 (1H, dd, 15.1, 12.1)
11	4.07 (d, 2.6)	3.95 (1H, s)	4.07 (1H, d, 2.6)
12	2.30 (s)	2.23 (3H, s)	2.26 (3H, s)
13	3.42 (d, 2.4)	3.40 (1H, d, 7.2)	3.38 (1H, br d, 7.6)
14	α 2.82 (dd, 20.8, 7.2) β 2.27 (d, 20.8)	α 2.71 (1H, dd, 20.8, 7.2) β 2.34 (1H, d, 20.8)	α 2.70 (1H, dd, 20.8, 7.6) β 2.29 (1H, dd, 20.8, 1.4)
21	4.15 (d, 2.4)	4.09 (2H, s)	4.24 (1H, overlapped)
22	α 3.71 (dd, 11.2, 3.2) β 3.48 (dd, 11.2, 3.2)	α 4.99 (1H, br d, 11.2) β 4.16 (1H, d, 11.2)	α 4.83 (1H, dd, 11.2, 3.2) β 4.20 (1H, dd, 11.2, 3.2)
6-CH$_3$	1.93 (s)	1.99 (3H, s)	1.79 (3H, s)
16-CH$_3$	1.93 (s)	1.73 (3H, s)	2.16 (3H, s)
7-OCH$_3$	3.98 (s)	4.04 (3H, s)	
17-OCH$_3$	4.03 (s)	3.76 (3H, s)	3.80 (3H, s)
OCH$_2$O			5.85 (1H, s) 5.92 (1H, s)
2'-H, 6'-H		7.47 (2H, d, 4.4)	7.56 (2H, dd, 4.6, 1.4)
3'-H, 5'-H		8.68 (2H, d, 4.4)	8.71 (2H, dd, 4.6, 1.4)

Table 11 ^{13}C NMR (100 MHz) spectral data of compound **6**, **7** and **10** in CDCl$_3$[44]

Carbon No.	Reported data (**6**) δ_C in ppm	Experimental data (**7**) δ_C in ppm	Experimental data (**10**) δ_C in ppm
1	58.0, CH	56.5	54.7
3	54.3, CH	54.3	56.1
4	25.3, CH$_2$	25.5	27.0
5	185.4, C=O	185.4	141.8

Table 11 (Cont.) ^{13}C NMR (100 MHz) spectral data of compound **6**, **7** and **10** in CDCl$_3$

Carbon No.	Reported data (**6**)[44] δ_C in ppm	Experimental data (**7**) δ_C in ppm	Experimental data (**10**) δ_C in ppm
6	128.9, C	128.9	113.2
7	155.5, C	155.6	136.8
8	181.4, C=O	181.1	144.8
9	136.0, C	135.1	111.8
10	141.7, C	142.1	111.8
11	54.1, CH	54.1	59.2
12	41.5, N-CH$_3$	41.4	41.4
13	54.4, CH	54.4	54.7
14	21.6, CH$_2$	21.0	21.1
15	186.2, C=O	185.9	186.1
16	128.6, C	128.1	128.6
17	155.4, C	154.9	155.1
18	182.2, C=O	182.1	182.5
19	135.6, C	134.5	135.3
20	141.7, C	142.1	145.2
21	59.0, CH	58.4	56.9
22	64.1, CH$_2$	62.9	64.4
24		164.0	164.2
6-CH$_3$	8.7, CH$_3$	8.9	8.9
16-CH$_3$	8.7, CH$_3$	8.7	8.8
7-OCH$_3$	61.0, OCH$_3$	60.9	
17-OCH$_3$	61.1, OCH$_3$	61.2	60.9
21-CN	116.8, CN	116.8	117.2
OCH$_2$O			101.2
C-1'		136.7	137.7
C-2', C-6'		122.7	123.1
C-3', C-5'		150.2	149.8

The pivotal heteronuclear multiple bond correlations (HMBCs) established links between the carbons and protons of compound **10**. These included clear associations between the methylene proton at the [1,3]-dioxole ring and the quaternary aromatic carbons at C-7 and C-8, confirming the fused ring structure at ring A in compound **10 (Figure 26)**. In addition, compound **10** demonstrated notable HMBCs between the C-24 carbonyl carbon and both the C-22 methylene protons and the C-2' pyridine proton. Furthermore, correlations were observed between C-5' pyridine proton and C-1' pyridine carbon. The C-2' pyridine proton exhibited correlations with the C-3' pyridine carbon. Similarly, the C-22 methylene protons were found to be correlated with the C-9 quaternary carbon. Moreover, correlations were found between the C-14 methylene protons and the C-15 carbonyl carbon. Finally, the C-16 methyl protons demonstrated associations with the C-15 carbonyl carbon on ring E.
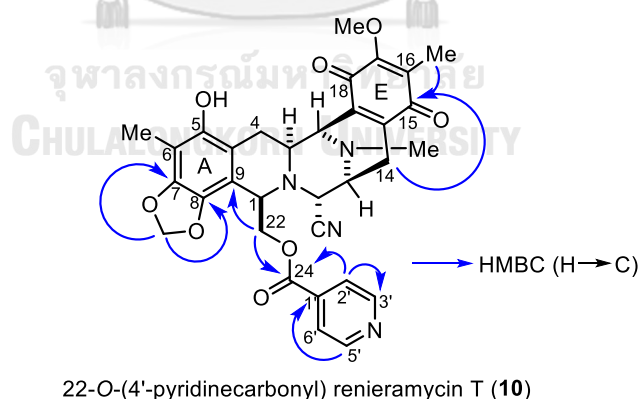

22-*O*-(4'-pyridinecarbonyl) renieramycin T (**10**)

Figure 26 HMBCs (blue arrows) for 22-*O*-(4'-pyridinecarbonyl) renieramycin T (**10**)

4.4 Cytotoxicity evaluation of compounds 1—10 against NSCLC cell lines

The cytotoxicity evaluation of compounds **1—10**, including natural renieramycins and their derivatives, was assessed against human NSCLC cell lines, specifically H292 and H460, using the MTT assay **(Table 12)**. The benchmark controls for these evaluations were established anticancer drugs, doxorubicin and cisplatin. A significant portion of the tested compounds demonstrated considerable inhibitory activity at nanomolar concentrations against both cell lines. Notably, renieramycin M (**1**), renieramycin N (**2**), and renieramycin O (**3**) were synthesized via a photochemical reaction. The results indicated that renieramycin T (**4**) and renieramycin U (**5**), which possess an additional [1,3]-dioxole ring at carbon positions 7 and 8, exhibit a diminished inhibitory effect on cancer cells in comparison to their parent compounds. Subsequently, jorunnamycin A (**6**) underwent an esterification reaction to yield 22-*O*-(4'-pyridinecarbonyl) jorunnamycin A (**7**). The transformation of the hydroxyl (—OH) group to a 4'-pyridinecarbonyl group at carbon position 22 resulted in a remarkable 30—40 folds increase in anticancer activity. It demonstrated the most effective inhibitory activity of **7** with IC_{50} values of 3.52 ± 0.62 and 3.98 ± 0.38 nM against H292 and H460 cell lines, respectively. Following this, the methoxy (—OCH$_3$) and carbonyl (C=O) groups at positions 7 and 8 were converted to a [1,3]-dioxole ring using a photochemical reaction. This process produced 22-*O*-(4'-pyridinecarbonyl) renieramycin T (**10**), which, contrary to expectations, displayed a decreased inhibitory

activity against cancer cells and showed IC_{50} at 1.27 ± 0.20 µM and 1.83 ± 0.83 µM against H292 and H460, respectively with 2 and 3 folds more potent than that of cisplatin.

For evaluation of the effect of 4'-pyridinecarbonyl group at position 5, compound **9** displayed the IC_{50} value of 35 nM against both NSCLC cell lines and had similar activity to substrate **1**, together with hydroquinone **8**. Besides, compound **9** showed an increased 2-fold inhibition effect compared to parent **4**. All evaluated compounds demonstrated superior cytotoxicity compared to cisplatin. In comparison to doxorubicin, the renieramycin-type compounds **1**, **7**, **8**, and **9** displayed enhanced anticancer activity, surpassing the performance of the standard anticancer drugs used as positive controls. The structure–cytotoxicity relationship data of 4'-pyridinecarbonyl substituent at various positions of renieramycins frameworks found that the corresponding ester at position 22, together with quinone at ring A revealed more significant cytotoxicity than not only ester substituent at C-5, but also [1,3]–dioxole bridge at ring A, based on IC_{50} value followed the order **7** > **8** = **9** > **10**. Therefore, the position of the substituent has a significant impact on the ability to suppress cancer cell lines.

Table 12 Cytotoxicity of natural renieramycins and renieramycins derivatives against NSCLC cell lines

Entry	Compound	5-*O*-substituents	22-*O*-substituents	IC$_{50}$ ± S.D. (nM)	
				H292	H460
1	**1**	5-carbonyl	angeloyl	35.36 ± 4.51	33.86 ± 2.16
2	**2**	5-carbonyl	angeloyl	170.03 ± 10.07	104.36 ± 22.02
3	**3**	5-carbonyl	angeloyl	111.74 ± 12.94	99.74 ± 0.13
4	**4**	OH	angeloyl	72.64 ± 2.55	83.32 ± 4.72
5	**5**	OH	angeloyl	183.37 ± 37.04	167.97 ± 3.53
6	**6**	5-carbonyl	OH	97.85 ± 6.75	157.53 ± 6.65
7	**7**	5-carbonyl	4-pyridinecarbonyl	3.52 ± 0.62	3.98 ± 0.38
8	**8**	4-pyridinecarbonyl	angeloyl	33.79 ± 0.40	35.77 ± 2.11
9	**9**	4-pyridinecarbonyl	angeloyl	35.27 ± 1.09	34.77 ± 2.19
10	**10**	OH	4-pyridinecarbonyl	1.27 ± 0.20 μM	1.83 ± 0.83 μM
11	Cisplatin	-	-	4.23 ± 0.40 μM	3.86 ± 0.46 μM
12	Doxorubicin	-	-	37.54 ± 4.41	43.37 ± 5.60

จุฬาลงกรณ์มหาวิทยาลัย
CHULALONGKORN UNIVERSITY

CHAPTER V
CONCLUSION

Based on the study of the photochemical reactions of renieramycin M (**1**) using white and blue light sources with three solvents, namely CHCl$_3$, CH$_2$Cl$_2$, and THF, which were capable of dissolving **1**, the initial experiments using white light resulted in a moderate percent yield. Subsequently, further investigation using blue light revealed a significant increase in the percent yield by approximately 1.1-1.3 folds. Therefore, CH$_2$Cl$_2$, which provided the highest percent yield, was selected as the optimal solvent for the semi-synthesis of natural renieramycins and renieramycin derivatives under subsequent blue light irradiation. In the semi-synthesis of natural renieramycins, which include renieramycin N (**2**) and renieramycin O (**3**), under these optimized conditions, it was found that the percent yield was still not as high as when using compound **1** as the starting material. Additionally, when compound **2** was subjected to photochemical reactions, it led to an air oxidation reaction, resulting in the formation of a mixed product between **3** and renieramycin U (**5**).

In the semi-synthesis of new derivatives of renieramycins, the initial step involved jorunnamycin A (**6**) as the starting material, which could be prepared from **1**. Subsequently, compound **6** underwent esterification to yield the product 22-*O*-(4'-pyridinecarbonyl) jorunnamycin A (**7**). This compound was further subjected to a photochemical reaction, resulting in the formation of the product 22-*O*-(4'-pyridinecarbonyl) renieramycin T (**10**).

Based on previous research reports, it has been identified that positions 5 and 22 are crucial for the activity of renieramycins[16, 29, 33]. In this study, we tested the potency of both starting materials and derived compounds in cytotoxicity against non-small-cell lung cancer cells, specifically H292 and H460 cell lines. Our findings indicate that when ring A is quinone and a substituent at position 22 is a 4'-pyridinecarbonyl group, the resulting compounds exhibit the most potent IC_{50} values and demonstrate referring the highest inhibition of lung cancer. Furthermore, we observed that hydroquinone 5-O-(4'-pyridinecarbonyl) renieramycin M (**8**) and 5-O-(4'-pyridinecarbonyl) renieramycin T (**9**) have similar inhibitory effects on lung cancer cells. All tested compound outperforming the cisplatin, and the derivatives of compounds **1**, **7**, **8**, and **9** surpassing the performance of doxorubicin anticancer drugs. Therefore, renieramycin derivatives are intriguing candidates for the development of future anticancer drugs.

APPENDIX

KBSC-RT-2-Pro-F(8-12) 1H-NMR (400 MHz) in CDCl3
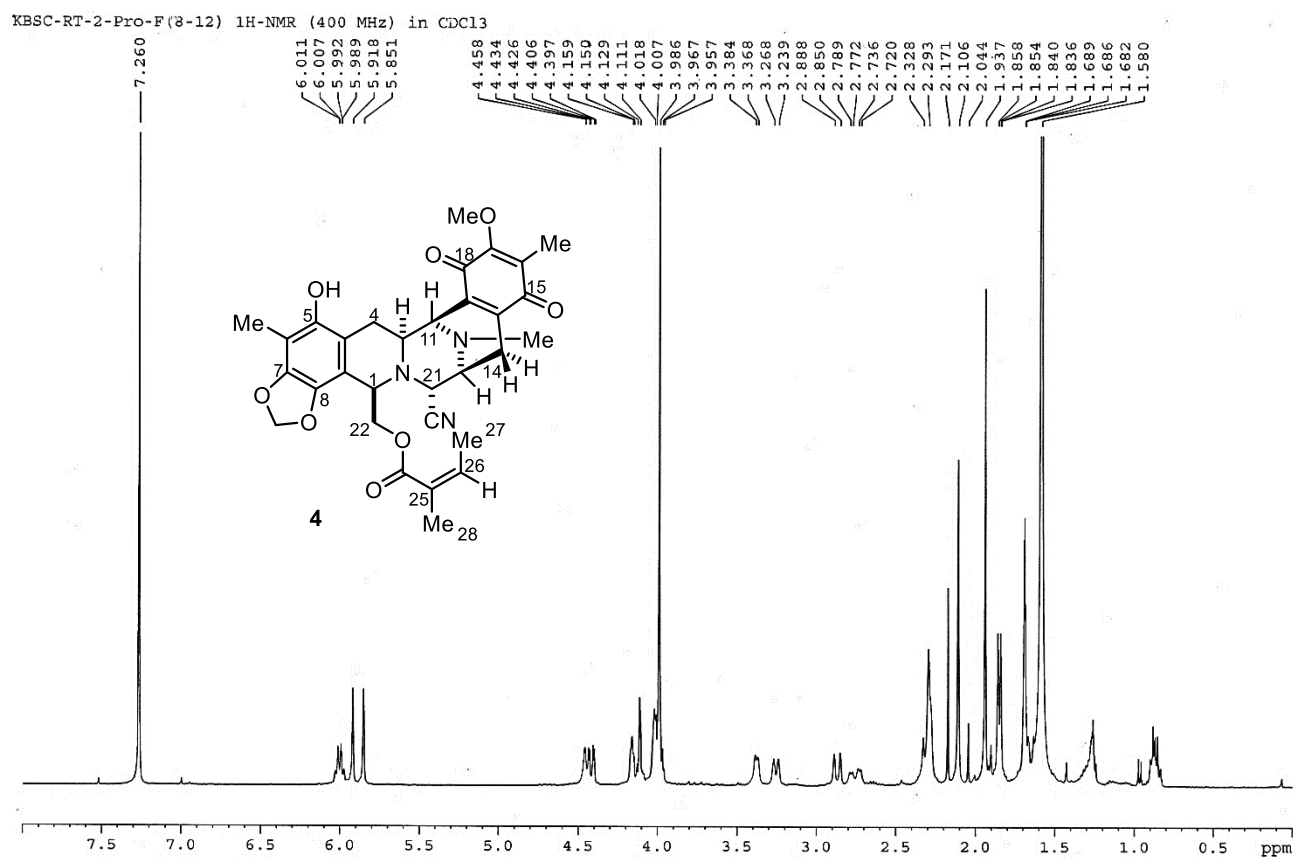
Figure 27 ^{1}H NMR (400 MHz) spectrum of **4** in CDCl$_3$

จุฬาลงกรณ์มหาวิทยาลัย

CHULALONGKORN UNIVERSITY

SSSC-renieramycin U 1H-NMR (400 MHz) in CDCl3
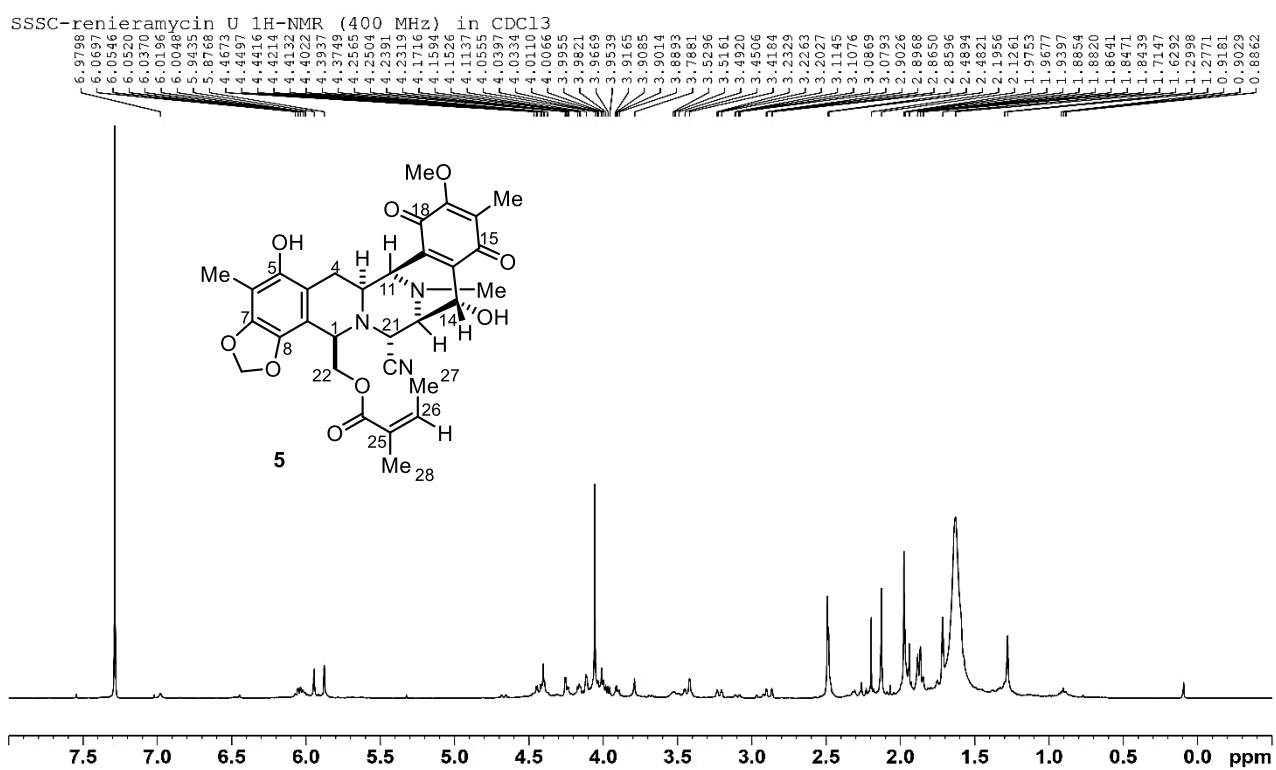
Figure 28 ^{1}H NMR (400 MHz) spectrum of **5** in CDCl$_3$

SSSC-renieramycin U 13C-NMR (100 MHz) in CDCl3
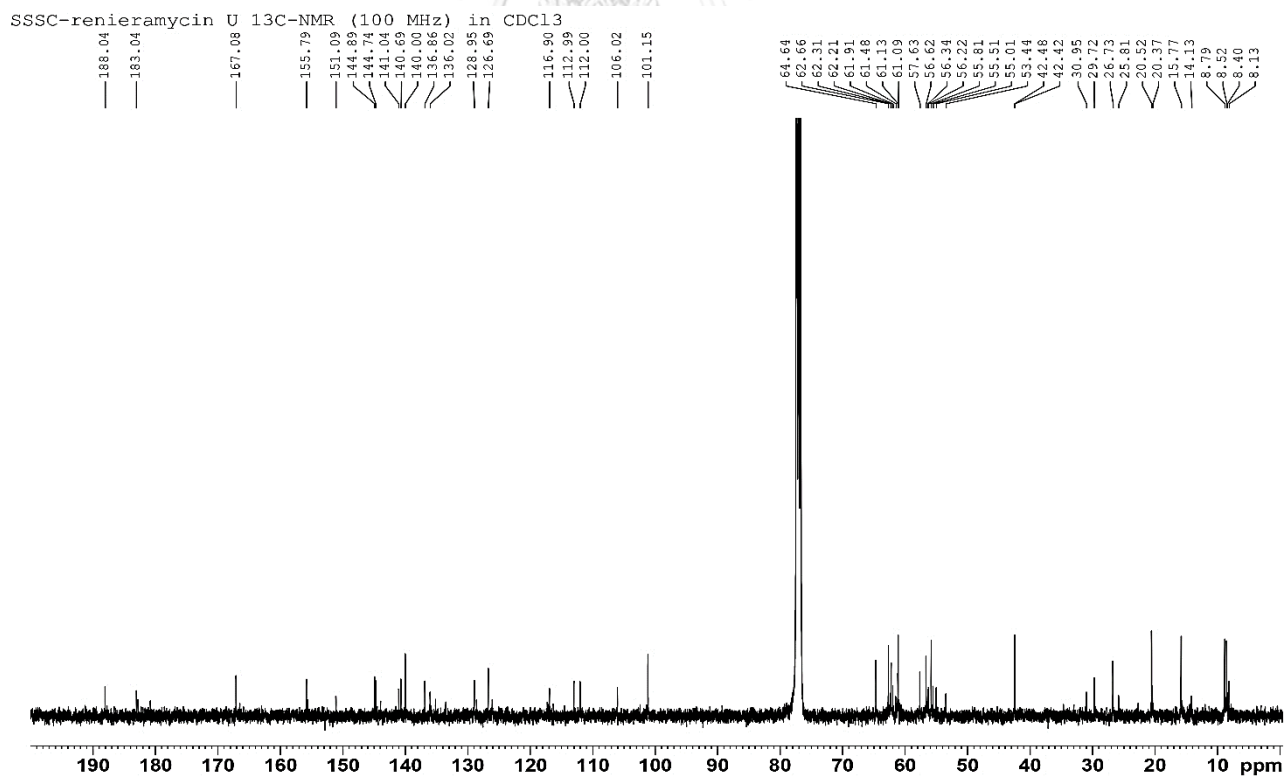
Figure 29 ^{13}C NMR (100 MHz) spectrum of **5** in CDCl$_3$
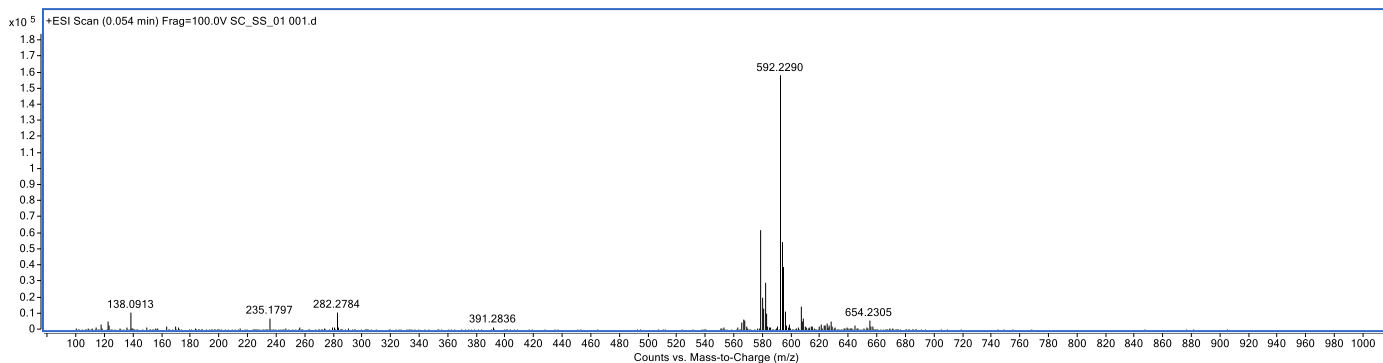
Figure 30 Mass spectrum of **5**
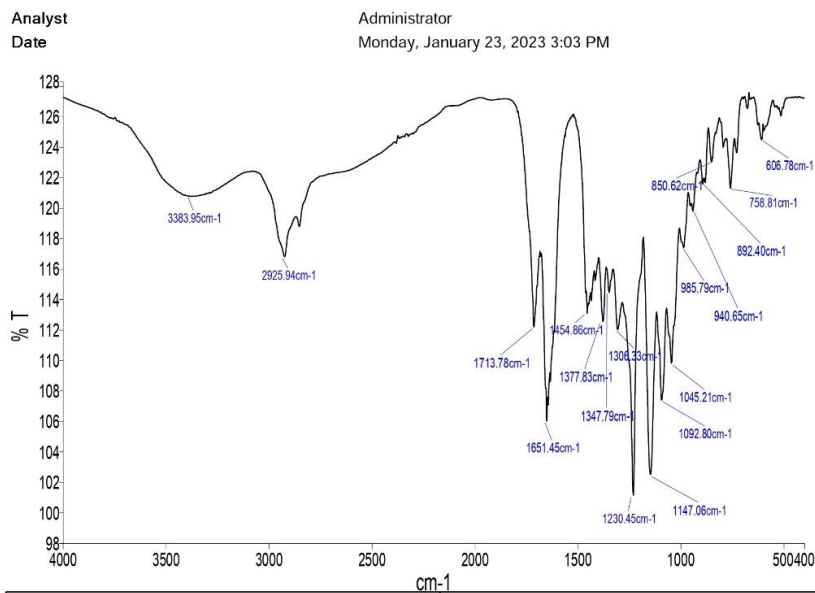
Figure 31 IR spectrum of **5**

1,3-dioxole-RO

[Data Information]
Creation Date   22/12/2565 13:36

[Measurement Information]
Instrument Name   P-2000
Model Name   P-2000
Serial No.   B204761232
Polarizer   Dichrom
Faraday Cell   Flint Glass

Accessory   PTC-262
Accessory S/N   C098461481
  Temperature   25.00 C
  Control Sonsor   Holder
  Monitor Sensor   Holder
  Start Mode   Keep target temperature +/-0.10 C
while 5 seconds
Light Source   Na
Monitor wavelength 589 nm
D.I.T.   10 sec
No. of cycle   5
Cycle interval   0 sec
Temp. Monitor   Holder
Temp. Corr. Factor   0 at 25 C
Aperture(S)   8.0mm
Aperture(L)   Auto
Mode   Specific O.R.
Path Length   10 mm
Concentration   10 w/v%
Water content of sample   0 %
Factor   1

[Comment]
Sample name   Kobusin
Comment
Username   Rivai
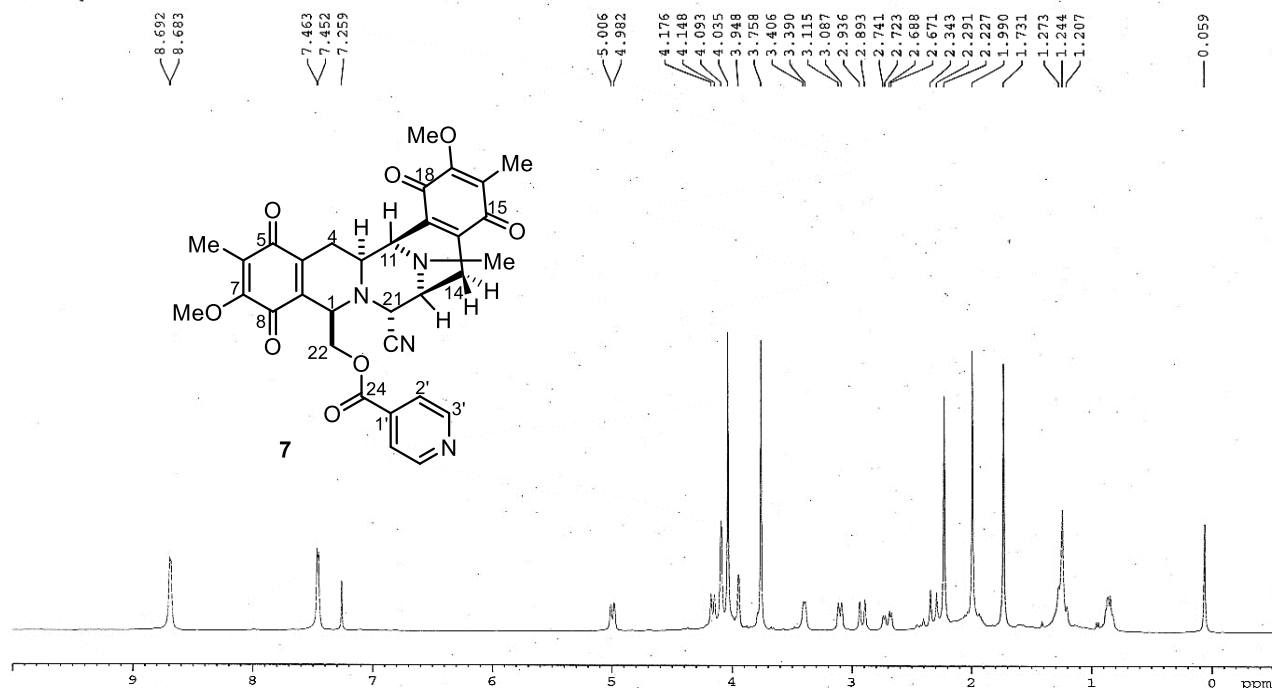Division
Organization   CU

		No.	Sample No.	Mode	Calc. Data	Temperature(C)	Blank	Measurement Date
1		1	1,3-dioxole-RN-1	Specific O.R.	-12.7000	24.99	0.0007	22/12/2565 13:30
2		2	1,3-dioxole-RN-2	Specific O.R.	-16.7000	24.99	0.0007	22/12/2565 13:30
3		3	1,3-dioxole-RN-3	Specific O.R.	-14.7000	25.00	0.0007	22/12/2565 13:30
4		4	1,3-dioxole-RN-4	Specific O.R.	-14.2000	25.00	0.0007	22/12/2565 13:31
5		5	1,3-dioxole-RN-5	Specific O.R.	-32.7000	25.00	0.0007	22/12/2565 13:31
6		6	Avg.					
7		7	S.D					
8		8	C.V					
9	*	9	1,3-dioxole-RO-1	Specific O.R.	-3.0141	25.00	0.0007	22/12/2565 13:35
10	*	10	1,3-dioxole-RO-2	Specific O.R.	-2.3099	25.00	0.0007	22/12/2565 13:35
11	*	11	1,3-dioxole-RO-3	Specific O.R.	-2.3099	25.00	0.0007	22/12/2565 13:36
12	*	12	1,3-dioxole-RO-4	Specific O.R.	-4.5634	25.00	0.0007	22/12/2565 13:36
13	*	13	1,3-dioxole-RO-5	Specific O.R.	-14.7042	25.00	0.0007	22/12/2565 13:36
14	*	14	Avg.		-5.3803			
15		15	S.D		5.2929			
16		16·	C.V		98.3750			

Figure 32 Optical rotation report of 5

Ester-4PyJA 1H-NMR 400 MHz in CDCl3

8.692
8.683
7.463
7.452
7.259
5.006
4.982
4.176
4.148
4.093
4.035
3.948
3.758
3.406
3.390
3.115
3.087
2.936
2.893
2.741
2.723
2.688
2.671
2.343
2.291
2.227
1.990
1.731
1.273
1.244
1.207
0.059

Figure 33 ^{1}H NMR (400 MHz) spectrum of **7** in CDCl$_3$

Ester-4PyJA 13C-NMR 100 MHz in CDCl3

185.86
185.37
182.09
181.08
163.95
155.59
154.90
150.22
142.06
136.70
135.11
134.52
128.86
128.13
122.70
116.78
77.32
77.00
76.68
62.88
61.19
60.91
58.36
56.45
54.44
54.26
54.08
41.38
25.50
21.00
8.87
8.68
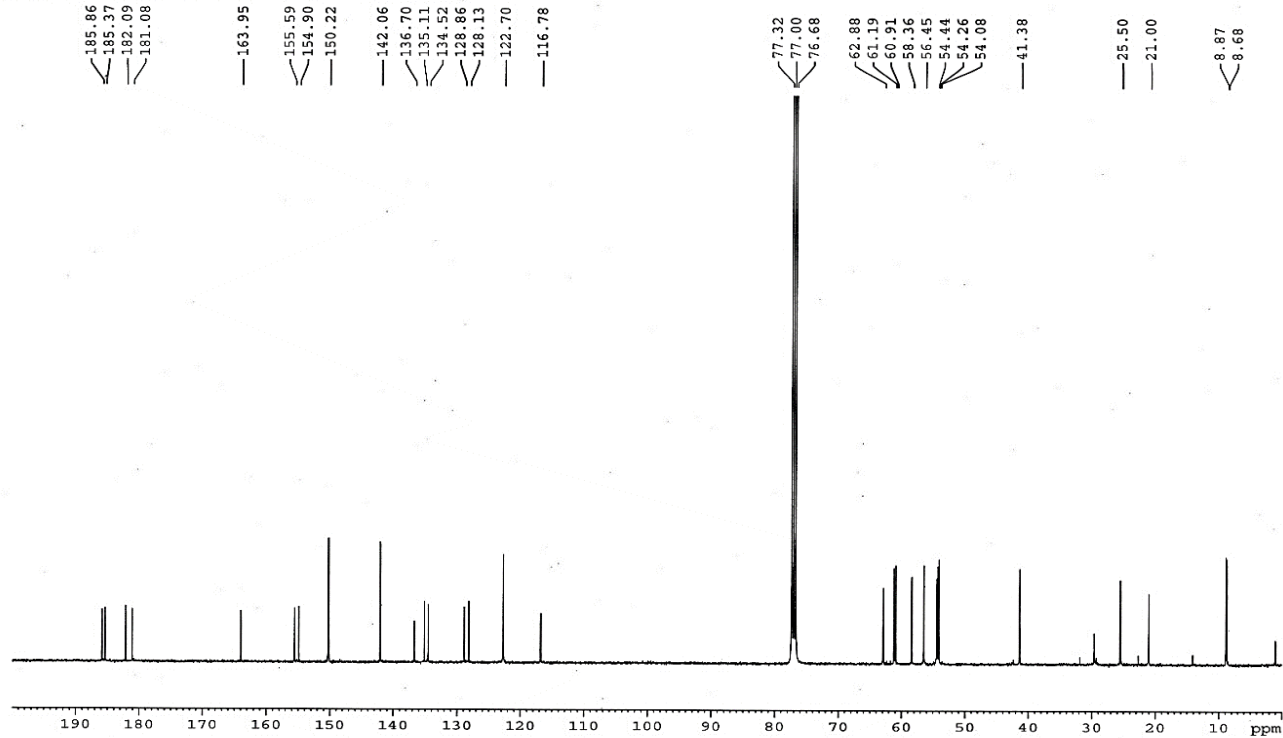
Figure 34 ^{13}C NMR (100 MHz) spectrum of **7** in CDCl$_3$

Ester-4PyJA 4 1 D:\Supakarn\data\root\nmr

Ester-4PyJA COSY in CDCl3
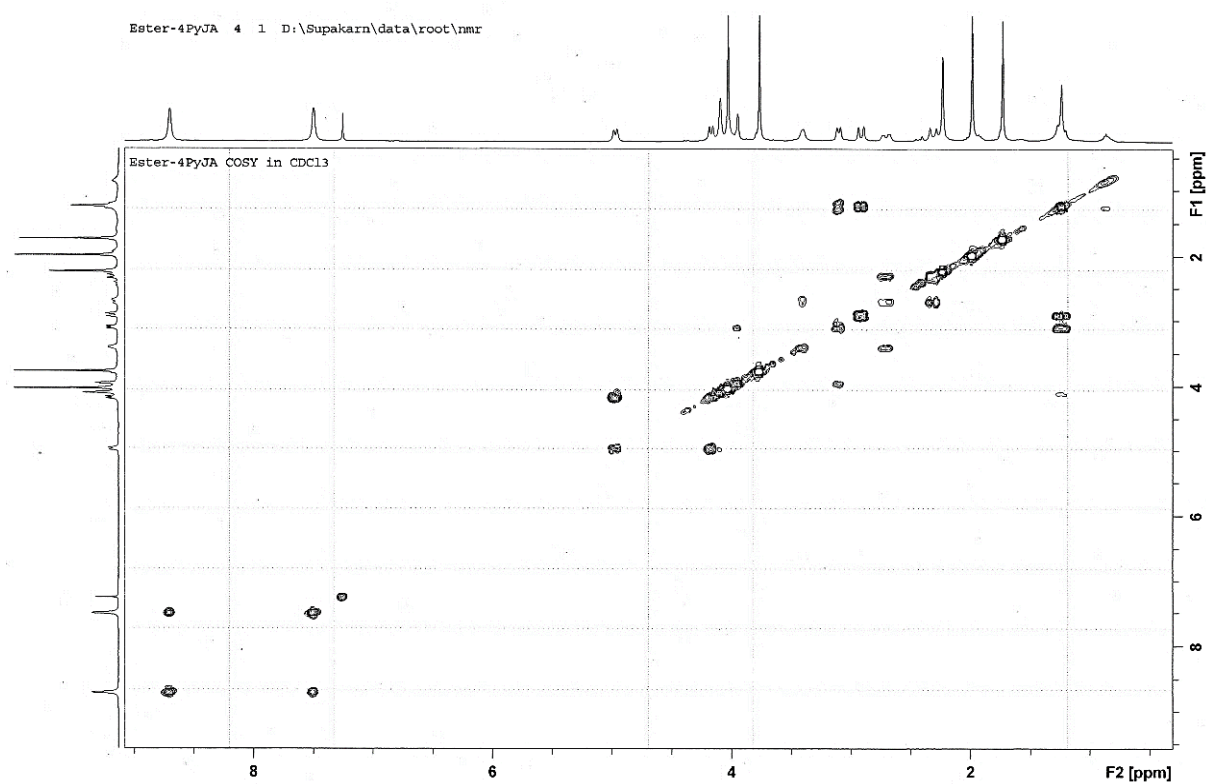
Figure 35 COSY (400 MHz) spectrum of **7** in CDCl₃

Ester-4PyJA 5 1 D:\Supakarn\data\root\nmr

Ester-4PyJA HSQC in CDCl3
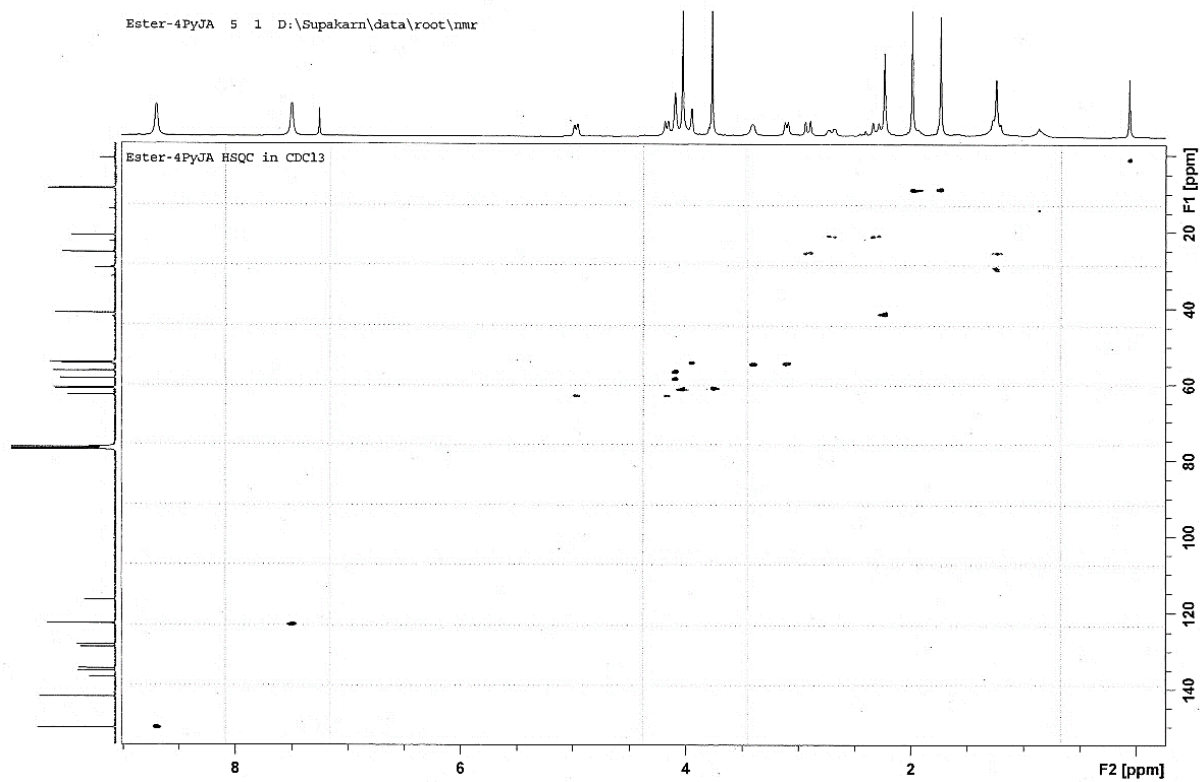
Figure 36 HSQC (400 MHz) spectrum of **7** in CDCl₃

Ester-4PyJA 6 1 D:\Supakarn\data\root\nmr

Ester-4PyJA HMBC in CDCl3
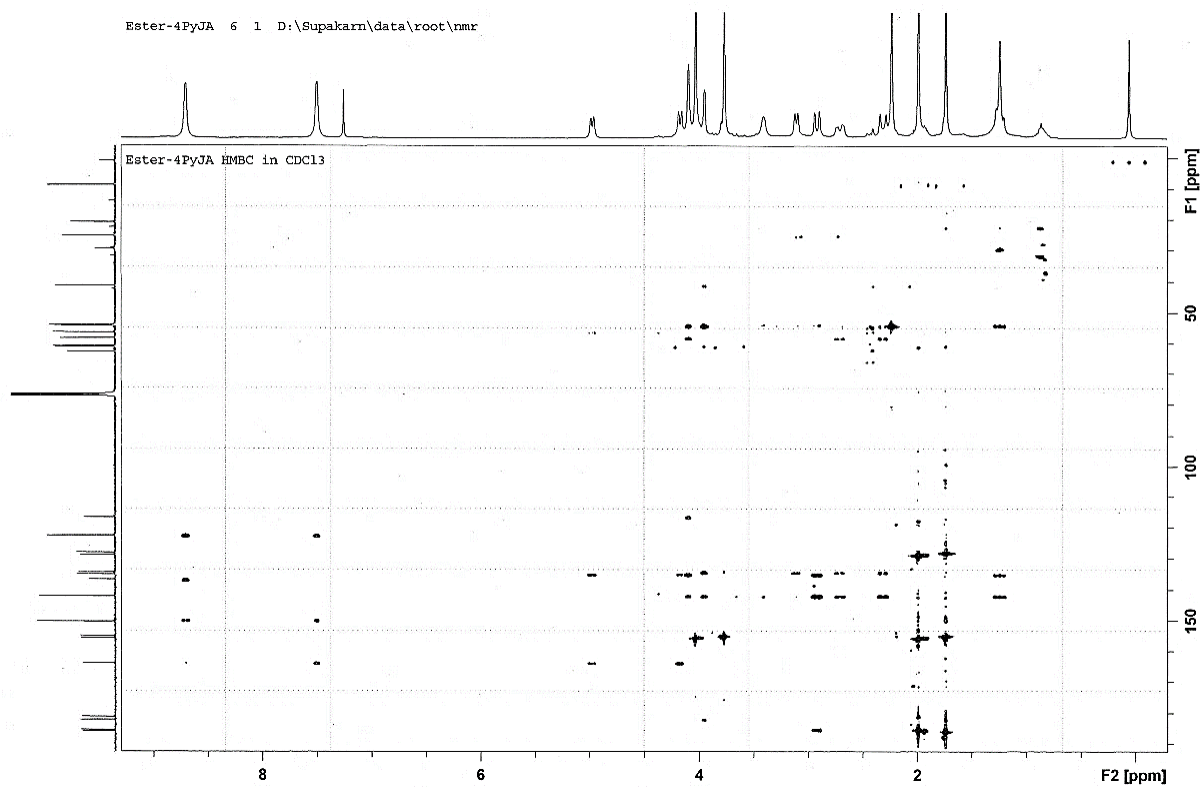
Figure 37 HMBC (400 MHz) spectrum of **7** in CDCl₃

จุฬาลงกรณ์มหาวิทยาลัย

CHULALONGKORN UNIVERSITY

Photoreaction isonicotinoylF(2) 1H-NMR (400 MHz) in CDCl3

8.718
8.714
8.706
8.703

7.567
7.564
7.556
7.552
7.260

5.906
5.860
5.298
4.846
4.839
4.819
4.811
4.239
4.232
4.223
4.215
4.195
4.187
4.167
4.146
4.128
4.110
4.097
4.093
4.070
4.065
3.961
3.395
3.376
3.258
3.227
2.906
2.872
2.739
2.720
2.687
2.668
2.327
2.324
2.271
2.256
2.155
2.096
2.043
1.789
1.579
1.548
1.542
1.511
1.275
1.251
1.239
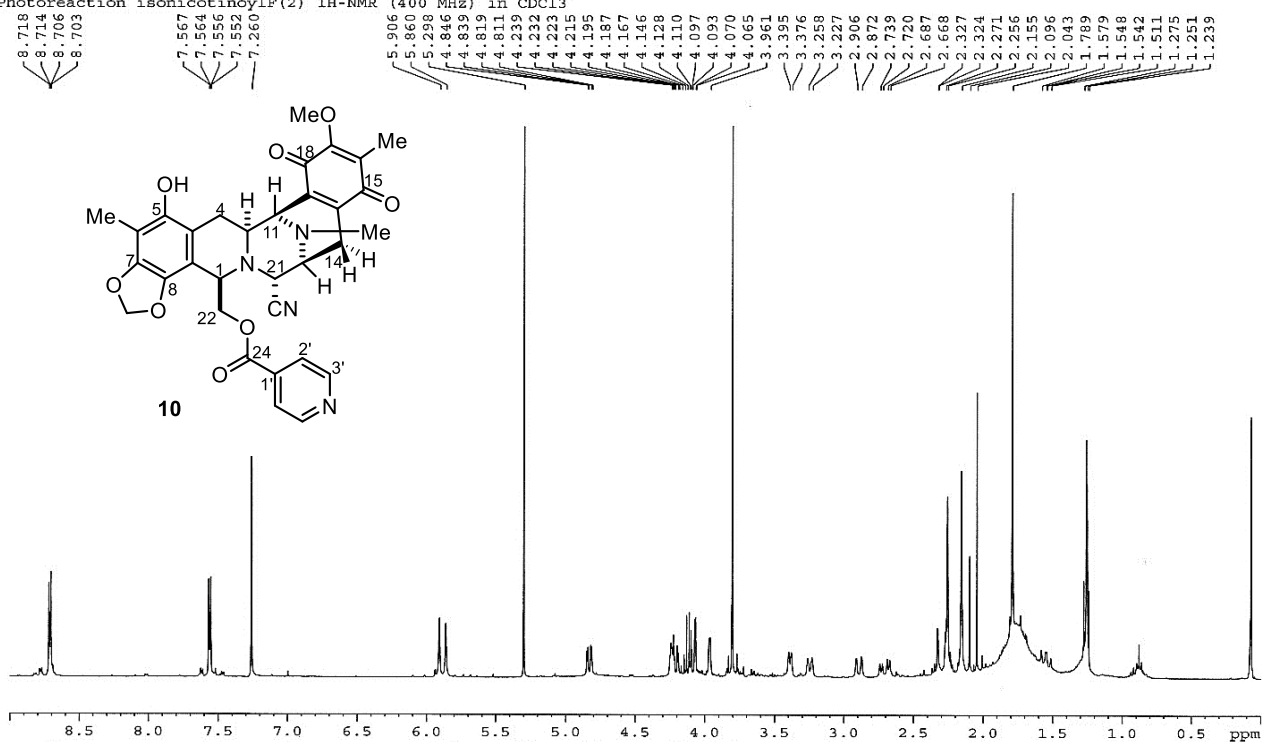
Figure 38 ^{1}H NMR (400 MHz) spectrum of **10** in CDCl$_3$

Photoreaction isonicotinoylF(2) 13C-NMR (100 MHz) in CDCl3

186.06
182.49

164.15

155.10

149.82
145.16
144.84
141.79
136.68
135.34

128.62

123.05

117.19
113.15
111.83

106.49

101.15

77.32
77.20
77.00
76.68

64.35
60.92
59.17
56.93
56.08
54.74
54.67

41.39

31.91
30.93
29.68
27.02

21.13

14.11

8.91
8.78

1.01
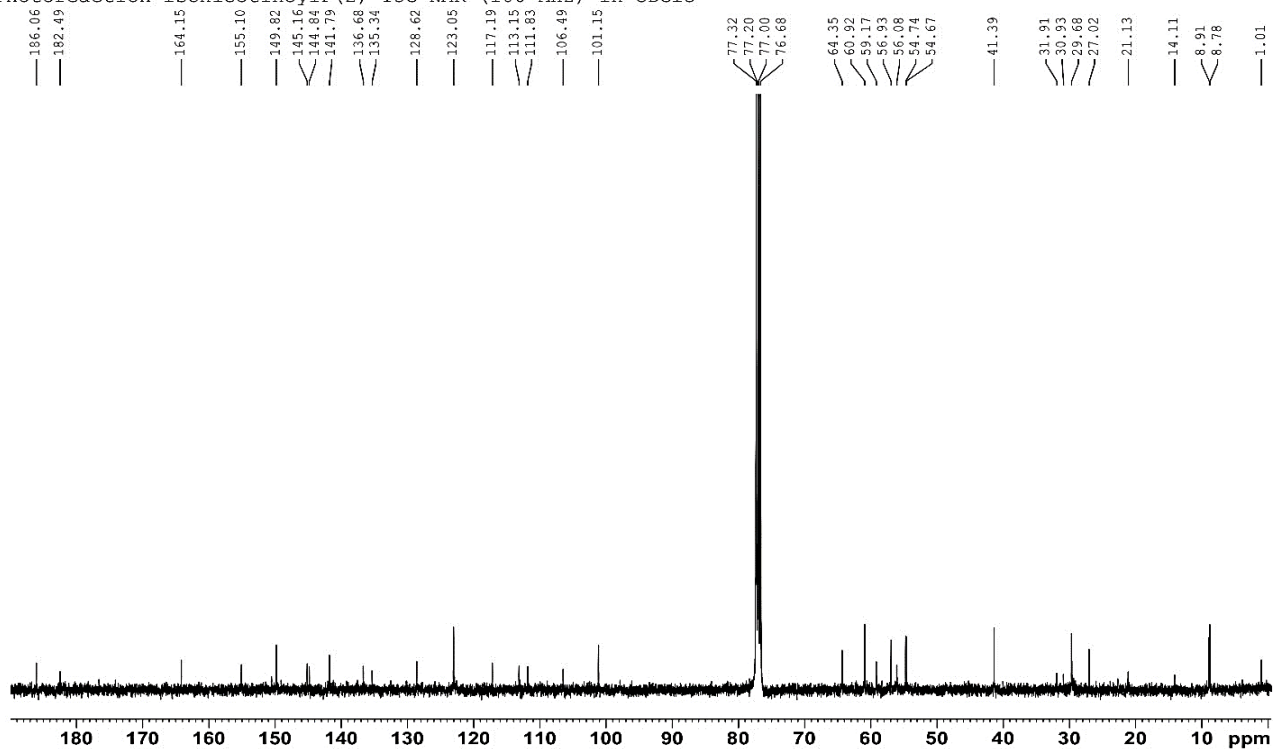
Figure 39 ^{13}C NMR (100 MHz) spectrum of **10** in CDCl$_3$

"Photoreaction isonicotinoylF(2)" 7 1 D:\Supakarn\data\root\nmr

Photoreaction isonicotinoylF(2) COSY in CDCl3
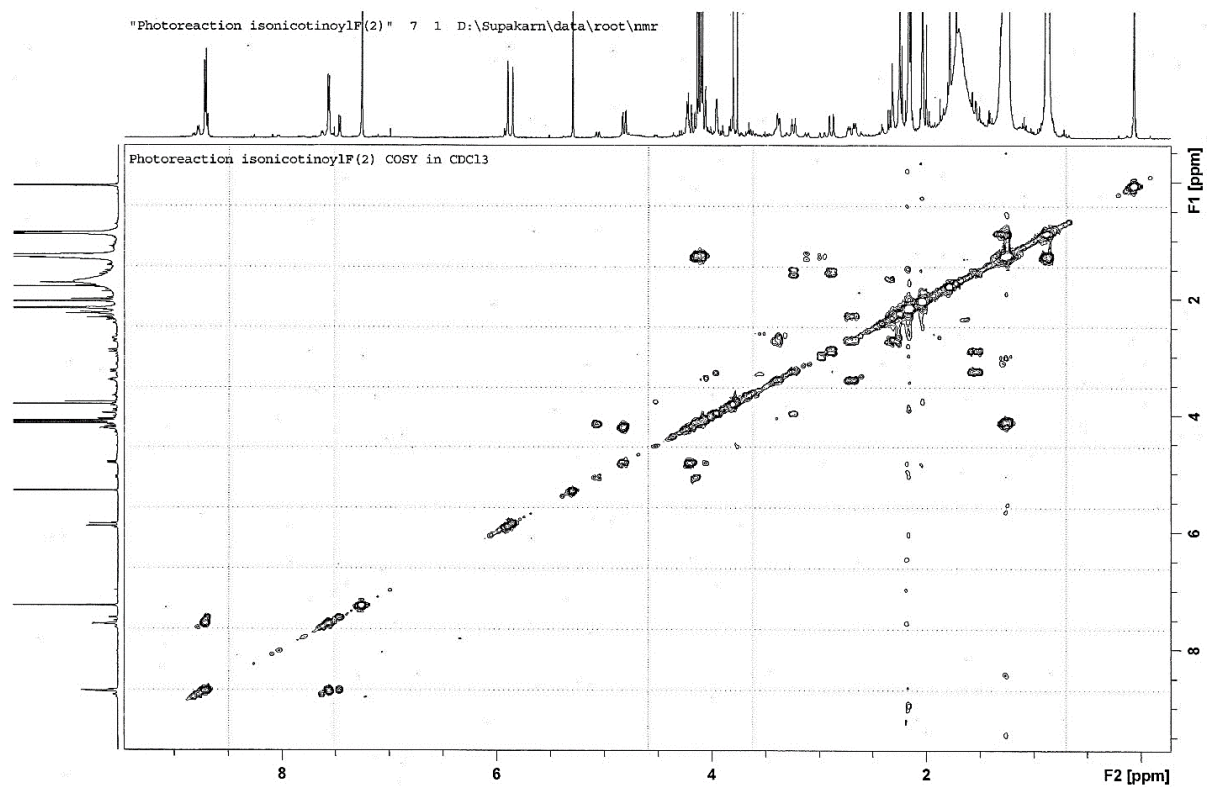
Figure 40 COSY (400 MHz) spectrum of **10** in CDCl₃

"Photoreaction isonicotinoylF(2)" 5 1 D:\Supakarn\data\root\nmr

Photoreaction isonicotinoylF(2) HSQC in CDCl3
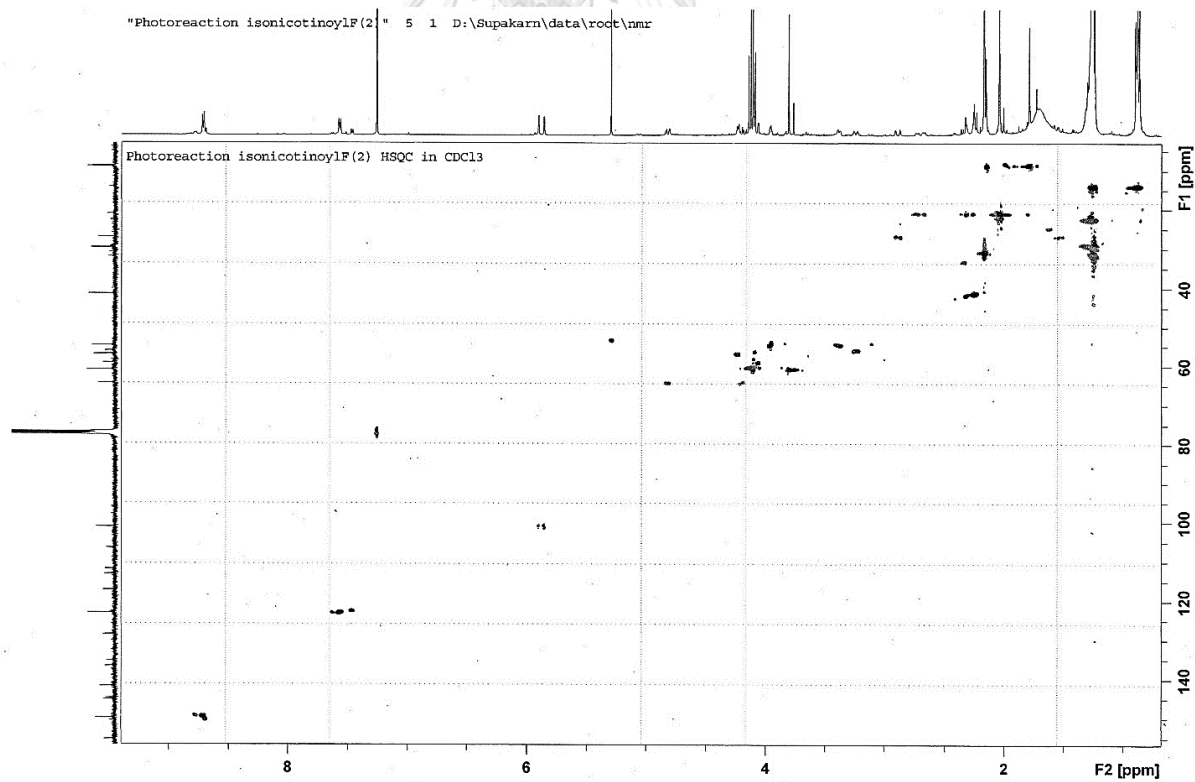
Figure 41 HSQC (400 MHz) spectrum of **10** in CDCl₃

Figure 42 HMBC (400 MHz) spectrum of **10** in CDCl₃
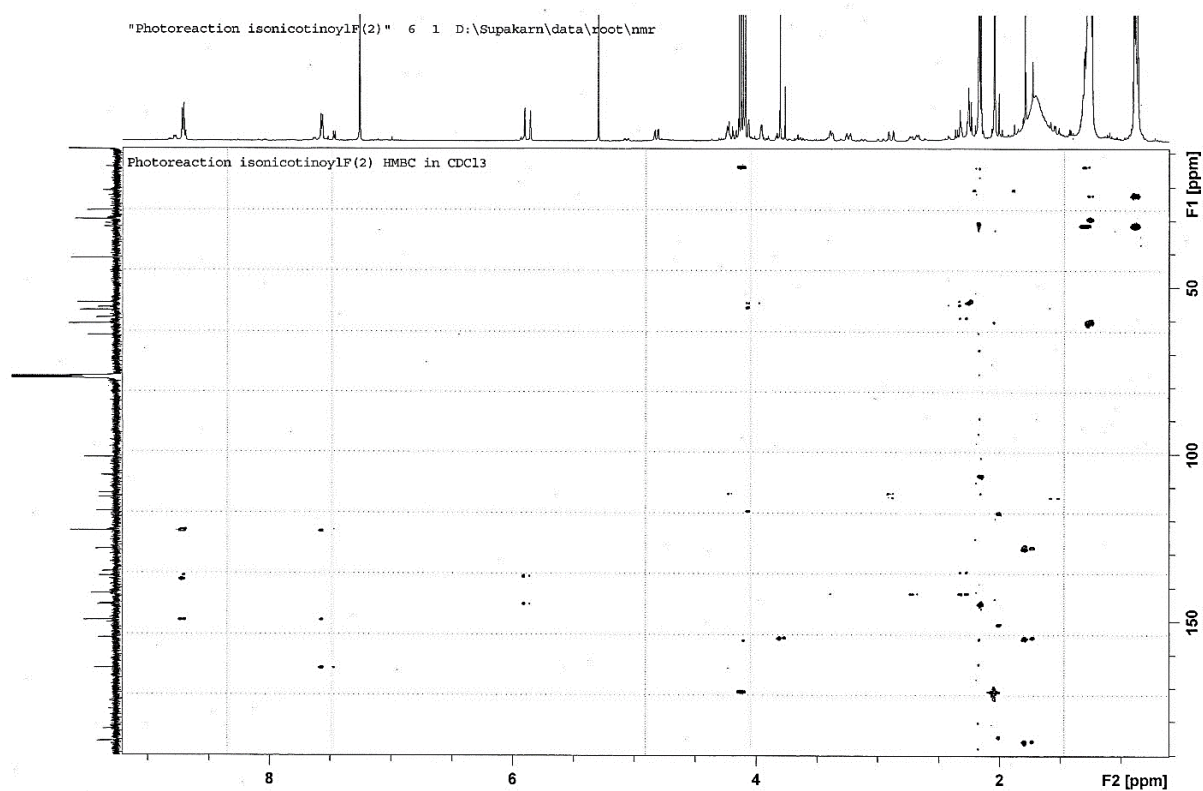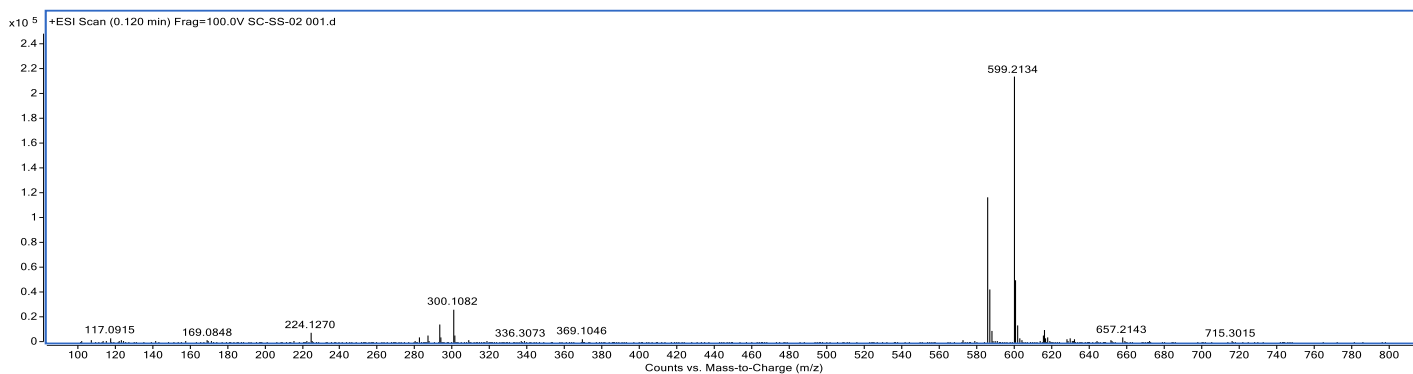
Figure 43 Mass spectrum of **10**
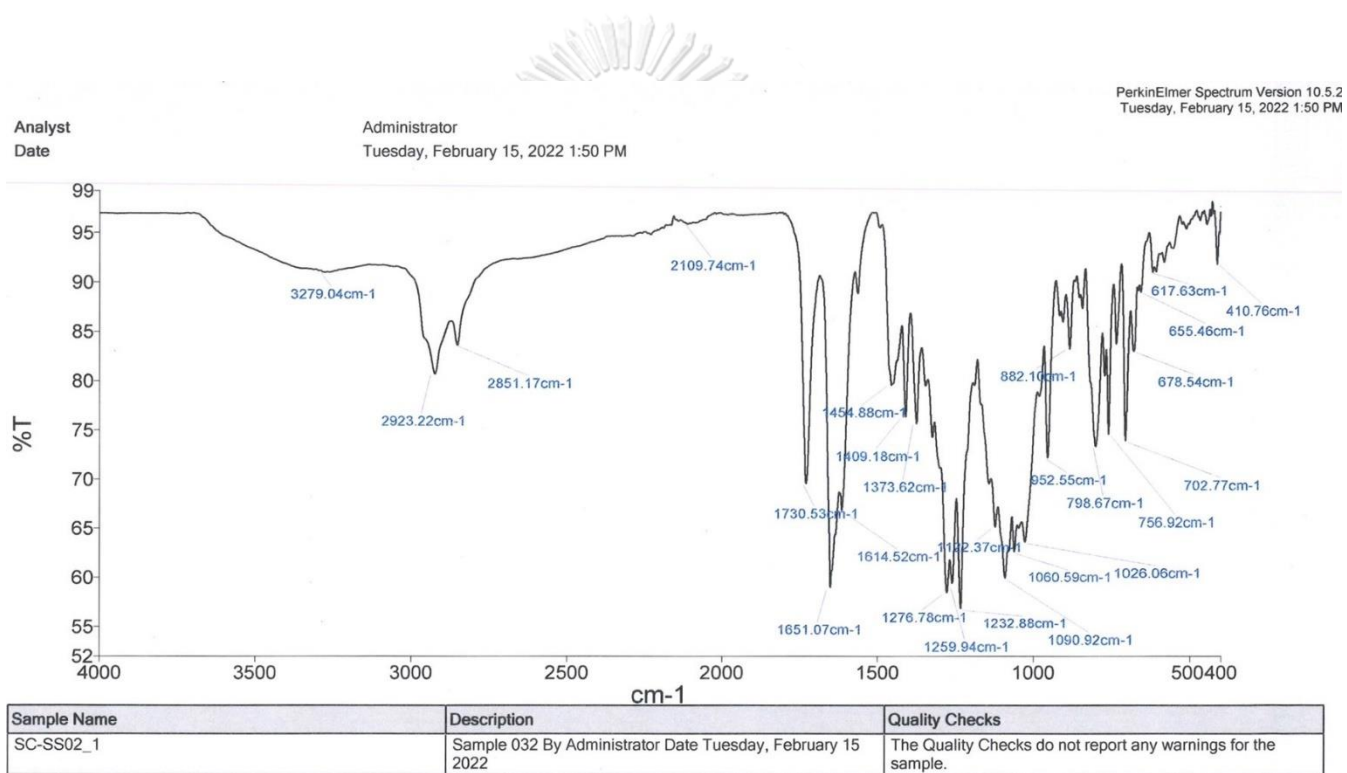
Figure 44 IR spectrum of **10**

Photo 2

[Data Information]
Creation Date   11/7/2565 12:05

[Measurement Information]
Instrument Name   P-2000
Model Name   P-2000
Serial No.   B204761232
Polarizer   Dichrom
Faraday Cell   Flint Glass

Accessory   PTC-262
Accessory S/N   C098461481
  Temperature   25.00 C
  Control Sonsor   Holder
  Monitor Sensor   Holder
  Start Mode   Keep target temperature +/-0.10 C
while 5 seconds
Light Source   Na
Monitor wavelength 589 nm
D.I.T.   10 sec
No. of cycle   3
Cycle interval   0 sec
Temp. Monitor   Holder
Temp. Corr. Factor 0 at 25 C
Aperture(S)   8.0mm
Aperture(L)   Auto
Mode   Specific O.R.
Path Length   10 mm
Concentration   0.37 w/v%
Water content of sample   0 %
Factor   1

[Comment]
Sample name   glucose std
Comment
Username
Division
Organization   CU

		No.	Sample No.	Mode	Calc. Data	Temperature(C)	Blank	Measurement Date	Comment
1	*	1	2-1	Specific O.R.	-20.7027	25.00	0.0048	11/7/2565 12:04	
2	*	2	2-2	Specific O.R.	-20.7027	24.99	0.0048	11/7/2565 12:04	
3	*	3	2-3	Specific O.R.	-19.8919	25.00	0.0048	11/7/2565 12:05	
4	*	4	Avg.		-20.4324				
5		5	S.D		0.4681				
6		6	C.V		2.2911				

Figure 45 Optical rotation report of **10**

REFERENCES

1.   Fang Y, Li H, Ji B, Cheng K, Wu B, Li Z, et al. Renieramycin-type alkaloids from marine-derived organisms: Synthetic chemistry, biological activity and structural modification. European Journal of Medicinal Chemistry. 2021;210(1):1-18.

2.   Saito N. Chemical Research on Antitumor Isoquinoline Marine Natural Products and Related Compounds. Chem Pharm Bull. 2021;69(2):155-77.

3.   D'Incalci M, Galmarini CM. A Review of Trabectedin (ET-743): A Unique Mechanism of Action. Mol Cancer Ther. 2010;9(8):2157-63.

4.   Gordon EM, Sankhala KK, Chawla N, Chawla SP. Trabectedin for Soft Tissue Sarcoma: Current Status and Future Perspectives. Adv Ther. 2016;33(7):1055-71.

5.   Cesne AL, Martín-Broto J, Grignani G. A review of the efficacy of trabectedin as second-line treatment of advanced soft tissue sarcoma. Future Oncol. 2022;18(30s):5-11.

6.   Abate A, Tamburello M, Rossini E, Basnet RM, Ribaudo G, Gianoncelli A, et al. Trabectedin impairs invasiveness and metastasis in adrenocortical carcinoma preclinical models. Endocr Relat Cancer. 2023;30(2):e220273.

7.   Patel S, Petty WJ, Sands JM. An overview of lurbinectedin as a new second-line treatment option for small cell lung cancer. Ther Adv Med Oncol. 2021;13:17588359211020529.

8.   Manzo A, Sforza V, Carillio G, Palumbo G, Montanino A, Sandomenico C, et al. Lurbinectedin in small cell lung cancer. Front Oncol 2022;12.

9.   Frincke JM, Faulkner DJ. Antimicrobial metabolites of the sponge *Reniera* sp. J Am Chem Soc. 1982;104(1):265-9.

10.   He HY, Faulkner DJ. Renieramycins E and F from the sponge *Reniera* sp.: reassignment of the stereochemistry of the renieramycins. J Org Chem. 1989;54(24):5822-4.

11.   Pettit GR, Knight JC, Collins JC, Herald DL, Pettit RK, Boyd MR, et al. Antineoplastic Agents 430. Isolation and Structure of Cribrostatins 3, 4, and 5 from the Republic of Maldives *Cribrochalina* Species. J Nat Prod. 2000;63(6):793-8.

12.   Amnuoypol S, Suwanborirux K, Pummangura S, Kubo A, Tanaka C, Saito N. Chemistry of Renieramycins. Part 5. Structure Elucidation of Renieramycin-Type Derivatives O, Q, R, and S from Thai Marine Sponge Xestospongia Species Pretreated with Potassium Cyanide. Journal of Natural Products. 2004;67(6):1023-8.

13.   Suwanborirux K, Amnuoypol S, Plubrukarn A, Pummangura S, Kubo A, Tanaka C, et al. Chemistry of Renieramycins. Part 3. Isolation and Structure of Stabilized Renieramycin Type Derivatives Possessing Antitumor Activity from Thai Sponge *Xestospongia* Species, Pretreated with Potassium Cyanide. J Nat Prod. 2003;66(11):1441-6.

14.   Nakao Y, Shiroiwa T, Murayama S, Matsunaga S, Goto Y, Matsumoto Y, et al. Identification of Renieramycin A as an Antileishmanial Substance in a Marine Sponge *Neopetrosia* sp. Mar Drugs. 2004;2(2):55-62.

15.   Daikuhara N, Tada Y, Yamaki S, Charupant K, Amnuoypol S, Suwanborirux K, et al. Chemistry of renieramycins. Part 7: Renieramycins T and U, novel renieramycin–ecteinascidin hybrid marine natural products from Thai sponge Xestospongia sp. Tetrahedron Letters. 2009;50(29):4276-8.

16.   Chamni S, Sirimangkalakitti N, Chanvorachote P, Saito N, Suwanborirux K. Chemistry of Renieramycins. 17. A New Generation of Renieramycins: Hydroquinone 5-O-Monoester Analogues of Renieramycin M as Potential Cytotoxic Agents against Non-Small-Cell Lung Cancer Cells. Journal of Natural Products. 2017;80(5):1541-7.

17.   Petsri K, Chamni S, Suwanborirux K, Saito N, Chanvorachote P. Renieramycin T Induces Lung Cancer Cell Apoptosis by Targeting Mcl-1 Degradation: A New Insight in the Mechanism of Action. Marine Drugs. 2019;17(5):301.

18.   Sirimangkalakitti N, Chamni S, Suwanborirux K, Chanvorachote P. Renieramycin M Sensitizes Anoikis-resistant H460 Lung Cancer Cells to Anoikis. Anticancer Res. 2016;36(4):1665-71.

19.   Sirimangkalakitti N, Chamni S, Suwanborirux K, Chanvorachote P. Renieramycin M Attenuates Cancer Stem Cell-like Phenotypes in H460 Lung Cancer Cells. Anticancer Research. 2017;37(2):615-21.

20.   Chantarawong W, Chamni S, Suwanborirux K, Saito N, Chanvorachote P. 5-*O*-Acetyl-Renieramycin T from Blue Sponge *Xestospongia* sp. Induces Lung Cancer Stem

Cell Apoptosis. Mar Drugs. 2019;17(2):109.

21.   Suksamai D, Racha S, Sriratanasak N, Chaotham C, Aphicho K, Lin ACK, et al. 5-*O*-(*N*-Boc-l-Alanine)-Renieramycin T Induces Cancer Stem Cell Apoptosis via Targeting Akt Signaling. Mar Drugs. 2022;20(4):235.

22.   Oo Y, Nealiga JQL, Suwanborirux K, Chamni S, Ecoy GAU, Pongrakhananon V, et al. 22-*O*-(*N*-Boc-l-glycine) ester of renieramycin M inhibits migratory activity and suppresses epithelial–mesenchymal transition in human lung cancer cells. J Nat Med. 2021;75(4):949-66.

23.   Petsri K, Chamni S, Suwanborirux K, Saito N, Chanvorachote P. Renieramycin T Induces Lung Cancer Cell Apoptosis by Targeting Mcl-1 Degradation: A New Insight in the Mechanism of Action. Mar Drugs. 2019;17(5):301.

24.   Halim H, Chunhacha P, Suwanborirux K, Chanvorachote P. Anticancer and Antimetastatic Activities of Renieramycin M, a Marine Tetrahydroisoquinoline Alkaloid, in Human Non-small Cell Lung Cancer Cells. Anticancer Res. 2011;31(1):193-201.

25.   Maiuthed A, Pinkhien T, Chamni S, Suwanborirux K, Saito N, Petpiroon N, et al. Apoptosis-inducing Effect of Hydroquinone 5-*O*-Cinnamoyl Ester Analog of Renieramycin M on Non-small Cell Lung Cancer Cells. Anticancer Res. 2017;37(11):6259-67.

26.   Pinkhien T, Maiuthed A, Chamni S, Suwanborirux K, Saito N, Chanvorachote P. Bishydroquinone Renieramycin M Induces Apoptosis of Human Lung Cancer Cells Through a Mitochondria-dependent Pathway. Anticancer Res. 2016;36(12):6327.

27.   Saito N, Tanaka C, Koizumi Y-i, Suwanborirux K, Amnuoypol S, Pummangura S, et al. Chemistry of renieramycins. Part 6: Transformation of renieramycin M into jorumycin and renieramycin J including oxidative degradation products, mimosamycin, renierone, and renierol acetate. Tetrahedron. 2004;60(17):3873-81.

28.   Charupant K, Daikuhara N, Saito E, Amnuoypol S, Suwanborirux K, Owa T, et al. Chemistry of renieramycins. Part 8: synthesis and cytotoxicity evaluation of renieramycin M-jorunnamycin A analogues. Bioorganic & Medicinal Chemistry. 2009;17(13):4548-58.

29.   Sirimangkalakitti N, Chamni S, Charupant K, Chanvorachote P, Mori N, Saito N, et al. Chemistry of Renieramycins. 15. Synthesis of 22-O-Ester Derivatives of Jorunnamycin A and Their Cytotoxicity against Non-Small-Cell Lung Cancer Cells. Journal of Natural

Products. 2016;79(8):2089-93.

30.	Yokoya M, Yamazaki-Nakai M, Nakai K, Sirimangkalakitti N, Chamni S, Suwanborirux K, et al. Transformation of Renieramycin M into Renieramycins T and S by Intramolecular Photoredox Reaction of 7-Methoxy-6-methyl-1,2,3,4-tetrahydroisoquinoline-5,8-dione Derivatives. J Nat Prod. 2023;86(1):222-31.

31.	Species WRoM. 2021 [cited 2021 Sep 27]. Available from: http://www.marinespecies.org/aphia.php?p=taxdetails&id=131849%20.

32.	Charupant K. Renieramycins from the nudibranch Jorunna funebris and chemical modifications of cytotoxic Renieramycin M from the sponge Xestospongia sp. [dissertation]. Bangkok: Chulalongkorn University; 2006.

33.	Chamni S, Sirimangkalakitti N, Chanvorachote P, Suwanborirux K, Saito N. Chemistry of Renieramycins. Part 19: Semi-Syntheses of 22-O-Amino Ester and Hydroquinone 5-O-Amino Ester Derivatives of Renieramycin M and Their Cytotoxicity against Non-Small-Cell Lung Cancer Cell Lines. Marine Drugs. 2020;18(8):1-14.

34.	Halim H, Chunhacha P, Suwanborirux K, Chanvorachote P. Anticancer and antimetastatic activities of Renieramycin M, a marine tetrahydroisoquinoline alkaloid, in human non-small cell lung cancer cells. Anticancer Research. 2011;31(1):193-201.

35.	Saito N, Yokoya M, Takahashi S. Preparation of Tricyclic Analog as CDE Ring Model of Renieramycin Marine Natural Product by Novel Photo-Induced Transformation of 6-Methoxy-1,2,3,4-Tetrahydroisoquinoline-5,8-dione. Heterocycles. 2019;99(2):1276-303.

36.	He W, Zhang Z, Ma D. A Scalable Total Synthesis of the Antitumor Agents Et-743 and Lurbinectedin. Angewandte Chemie International Edition. 2019;58(12):3972-5.

37.	Cuevas C, Pérez M, Martín MJ, Chicharro JL, Fernández-Rivas C, Flores M, et al. Synthesis of Ecteinascidin ET-743 and Phthalascidin Pt-650 from Cyanosafracin B. Organic Letters. 2000;2(16):2545-8.

38.	Xu S, Wang G, Zhu J, Shen C, Yang Z, Yu J, et al. A Concise and Practical Semisynthesis of Ecteinascidin 743 and (–)-Jorumycin. European Journal of Organic Chemistry. 2017;2017(5):975-83.

39.	Yokoya M, Yamazaki-Nakai M, Nakai K, Sirimangkalakitti N, Chamni S, Suwanborirux K, et al. Transformation of Renieramycin M into Renieramycins T and S by

Intramolecular Photoredox Reaction of 7-Methoxy-6-methyl-1,2,3,4-tetrahydroisoquinoline-5,8-dione Derivatives. Journal of Natural Products. 2023;86(1):222-31.

40. Maiuthed A, Pinkhien T, Chamni S, Suwanborirux K, Saito N, Petpiroon N, et al. Apoptosis-inducing Effect of Hydroquinone 5-O-Cinnamoyl Ester Analog of Renieramycin M on Non-small Cell Lung Cancer Cells. Anticancer Research. 2017;37(11):6259-67.

41. Cheun-Arom T, Chanvorachote P, Sirimangkalakitti N, Chuanasa T, Saito N, Abe I, et al. Replacement of a Quinone by a 5-O-Acetylhydroquinone Abolishes the Accidental Necrosis Inducing Effect while Preserving the Apoptosis-Inducing Effect of Renieramycin M on Lung Cancer Cells. Journal of Natural Products. 2013;76(8):1468-74.

42. Hongwiangchan N, Sriratanasak N, Wichadakul D, Aksorn N, Chamni S, Chanvorachote P. Hydroquinone 5-O-Cinnamoyl Ester of Renieramycin M Suppresses Lung Cancer Stem Cells by Targeting Akt and Destabilizes c-Myc. Pharmaceuticals. 2021;14(11):1112.

43. Yu B, Liang J, Li X, Liu L, Yao J, Chen X, et al. Renieramycin T Inhibits Melanoma B16F10 Cell Metastasis and Invasion via Regulating Nrf2 and STAT3 Signaling Pathways. Molecules. 2022;27(16):5337.

44. Sumkhemthong S, Chamni S, Ecoy GU, Taweecheep P, Suwanborirux K, Prompetchara E, et al. Jorunnamycin A Suppresses Stem-Like Phenotypes and Sensitizes Cisplatin-Induced Apoptosis in Cancer Stem-Like Cell-Enriched Spheroids of Human Lung Cancer Cells. Marine Drugs. 2021;19(5):261.

45. Iksen I, Sinsook S, Wattanathamsan O, Buaban K, Chamni S, Pongrakhananon V. Target Identification of 22-(4-Pyridinecarbonyl) Jorunnamycin A, a Tetrahydroisoquinoline Derivative from the Sponge Xestospongia sp., in Mediating Non-Small-Cell Lung Cancer Cell Apoptosis. Molecules. 2022;27(24):8948.

46. Sung H, Ferlay J, Siegel RL, Laversanne M, Soerjomataram I, Jemal A, et al. Global Cancer Statistics 2020: GLOBOCAN Estimates of Incidence and Mortality Worldwide for 36 Cancers in 185 Countries. CA Cancer J Clin. 2021;71(3):209-49.

47. Siegel RL, Miller KD, Jemal A. Cancer statistics, 2020. CA Cancer J Clin. 2020;70(1):7-30.

48. Dela Cruz CS, Tanoue LT, Matthay RA. Lung cancer: epidemiology, etiology, and

prevention. Clin Chest Med. 2011;32(4):605-44.

49.   Xu Z, Yang Q, Chen X, Zheng L, Zhang L, Yu Y, et al. Clinical associations and prognostic value of site-specific metastases in non-small cell lung cancer: A population-based study. Oncol Lett. 2019;17(6):5590-600.

50.   Riihimäki M, Hemminki A, Fallah M, Thomsen H, Sundquist K, Sundquist J, et al. Metastatic sites and survival in lung cancer. Lung Cancer. 2014;86(1):78-84.

51.   Tamura T, Kurishima K, Nakazawa K, Kagohashi K, Ishikawa H, Satoh H, et al. Specific organ metastases and survival in metastatic non-small-cell lung cancer. Mol Clin Oncol. 2015;3(1):217-21.

52.   Zhu T, Bao X, Chen M, Lin R, Zhuyan J, Zhen T, et al. Mechanisms and Future of Non-Small Cell Lung Cancer Metastasis. Front Oncol. 2020;10:585284.

53.   Ettinger DS, Wood DE, Aisner DL, Akerley W, Bauman JR, Bharat A, et al. Non-Small Cell Lung Cancer, Version 3.2022, NCCN Clinical Practice Guidelines in Oncology. J Natl Compr Canc Netw. 2022;20(5):497-530.

54.   Giaccone G. Clinical impact of novel treatment strategies. Oncogene. 2002;21(45):6970-81.

55.   Chang A. Chemotherapy, chemoresistance and the changing treatment landscape for NSCLC. Lung Cancer. 2011;71(1):3-10.

56.   Huang CY, Ju DT, Chang CF, Muralidhar Reddy P, Velmurugan BK. A review on the effects of current chemotherapy drugs and natural agents in treating non-small cell lung cancer. Biomedicine (Taipei). 2017;7(4):23.

57.   Hammerschmidt S, Wirtz H. Lung cancer: current diagnosis and treatment. Dtsch Arztebl Int. 2009;106(49):809-18; quiz 19-20.

58.   Sandler A, Gray R, Perry MC, Brahmer J, Schiller JH, Dowlati A, et al. Paclitaxel-carboplatin alone or with bevacizumab for non-small-cell lung cancer. N Engl J Med. 2006;355(24):2542-50.

59.   Scagliotti GV, Parikh P, von Pawel J, Biesma B, Vansteenkiste J, Manegold C, et al. Phase III study comparing cisplatin plus gemcitabine with cisplatin plus pemetrexed in chemotherapy-naive patients with advanced-stage non-small-cell lung cancer. J Clin Oncol. 2008;26(21):3543-51.

60.   Scheff RJ, Schneider BJ. Non-small-cell lung cancer: treatment of late stage

disease: chemotherapeutics and new frontiers. Semin Intervent Radiol. 2013;30(2):191-8.

61.   Sharma P, Hu-Lieskovan S, Wargo JA, Ribas A. Primary, Adaptive, and Acquired Resistance to Cancer Immunotherapy. Cell. 2017;168(4):707-23.

62.   Tang B, Xi Y, Cui F, Gao J, Chen H, Yu W, et al. Ionizing radiation induces epithelial-mesenchymal transition in human bronchial epithelial cells. Biosci Rep. 2020;40(8).

63.   Wild-Bode C, Weller M, Rimner A, Dichgans J, Wick W. Sublethal irradiation promotes migration and invasiveness of glioma cells: implications for radiotherapy of human glioblastoma. Cancer Res. 2001;61(6):2744-50.

64.   Marino P, Preatoni A, Cantoni A. Randomized trials of radiotherapy alone versus combined chemotherapy and radiotherapy in stages IIIa and IIIb nonsmall cell lung cancer. A meta-analysis. Cancer. 1995;76(4):593-601.

65.   Organization WH. 2021 [cited 2021 Sep 27]. Available from: https://www.who.int/news-room/fact-sheets/detail/cancer.

66.   Kalemkerian GP, Gadgeel SM. Modern Staging of Small Cell Lung Cancer. Journal of the National Comprehensive Cancer Network. 2013;11(1):99–104.

67.   Society AC. 2021 [cited 2021 Sep 27]. Available from: https://www.cancer.org/cancer/non-small-cell-lung-cancer/about/key-statistics.h.

68.   Society AC. Lung Cancer 2021 [cited 2021 Sep 27]. Available from: https://www.cancer.org/cancer/lung-cancer.html.

69.   Newman D, Cragg G. Marine-Sourced Anti-Cancer and Cancer Pain Control Agents in Clinical and Late Preclinical Development. Marine Drugs. 2014;12(1):255-78.

70.   Thommen C, Neuburger M, Gademann K. Collective Syntheses of Icetexane Natural Products Based on Biogenetic Hypotheses. Chemistry. 2017;23(1):120-7.

71.   Tatsukawa M, Punzalan LLC, Magpantay HDS, Villaseñor IM, Concepcion GP, Suwanborirux K, et al. Chemistry of renieramycins. Part 13: Isolation and structure of stabilized renieramycin type derivatives, renieramycins W–Y, from Philippine blue sponge Xestospongia sp., pretreated with potassium cyanide. Tetrahedron. 2012;68(36):7422-8.

72.   Hydroquinone [MAK Value Documentation, 1998]. The MAK‑Collection for

Occupational Health and Safety2012. p. 114-45.

73.   Steps C. Reactions of Acid Chlorides (ROCl) with Nucleophiles 2023 [cited 2023 July 8]. Available from: https://www.chemistrysteps.com/reactions-of-acid-chlorides-rocl-with-nucleophiles/.

74.   McGeoch IA, Sutherland A, editors. A novel approach to the total synthesis of the piperidine alkaloid (+)-α- conhydrine2009.

75.   Wordpress C. Steglich Esterification 1978 2023 [cited 2023 July 8]. Available from: https://cheminfographic.wordpress.com/2018/04/15/94-steglich-esterification-1978/.

76.   Charupant K, Suwanborirux K, Amnuoypol S, Saito E, Kubo A, Saito N. Jorunnamycins A-C, new stabilized renieramycin-type bistetrahydroisoquinolines isolated from the Thai nudibranch Jorunna funebris. Chem Pharm Bull (Tokyo). 2007;55(1):81-6.

VITA

NAME	Miss Suwimon Sinsook
DATE OF BIRTH	06/10/2540
PLACE OF BIRTH	Phetchaburi Province
INSTITUTIONS ATTENDED	Master's degree in Pharmaceutical Sciences and Technology
HOME ADDRESS	No. 21, Moo 5, Tamru Sub-district, Ban Lat District, Phetchaburi Province 76150
PUBLICATION	

1.   Sinsook S, Yokoya M, Saito N, Suwanborirux K, Chamni S. Renieramycin T from Photochemical Reaction of Renieramycin M and its Cytotoxicity Against Non-Small Cell Lung Cancer (NSCLC) Cell Lines. Poster presentation, e-Asia Joint Symposium on "Marine Biodiversity as a Source of New Chemotypes"; December 9th, 2022; Institute of Marine Science, Burapha University, 2022.

2.   Iksen I, Sinsook S, Wattanathamsan O, Buaban K, Chamni S, Pongrakhananon V. Target Identification of 22-(4-Pyridinecarbonyl) Jorunnamycin A, a Tetrahydroisoquinoline Derivative from the Sponge Xestospongia sp., in Mediating Non-Small-Cell Lung Cancer Cell Apoptosis. Molecules. 2022;27(24):8948.

3.   Sinsook S, Buaban K, Iksen I, Petsri K, Innets B, Chansriniyom C, Suwanborirux K, Yokoya M, Saito N, Pongrakhananon V, Chanvorachote P, Chamni S. Light-Mediated Transformation of Renieramycins and Semisynthesis of 4'-Pyridinecarbonyl-Substituted Renieramycin-Type Derivatives as Potential Cytotoxic Agents against Non-Small-Cell Lung Cancer Cells. Marine

Drugs. 2023;21(7):400.

4.   Buaban K, Innets B, Petsri K, Sinsook S, Chanvorachote P, Chansriniyom C, Suwanborirux K, Yokoya M, Saito N, Chamni S. Semisynthesis of 5-O-Ester Derivatives of Ecteinascidin–Renieramycin Hybrid Alkaloids and Their Cytotoxicity against Non-Small-Cell Lung Cancer Cell Lines. Scientific Reports. 2023.

5.   Iksen I, Seephan S, Limprasutr V, Sinsook S, Buaban K, Chamni S, Pongrakhananon V. Preclinical Characterization of 22-(4'-Pyridinecarbonyl) Jorunnamycin A Against Lung Cancer Cell Invasion and Angiogenesis via AKT/mTOR Signaling. ACS Pharmacology & Translational Science. 2023.

AWARD RECEIVED   นิสิตดีเด่น ระดับบัณฑิตศึกษา คณะเภสัชศาสตร์ ประจำปีการศึกษา 2564